2020

The Effects and Analysis of Implant Type and Surgical Approach in Total Hip Arthroplasty Dislocation Resistance

Brittany Marshall
University of Denver

The Effects and Analysis of Implant Type and Surgical Approach in Total Hip Arthroplasty Dislocation Resistance

Abstract

Total hip arthroplasty (THA) is one of the most successful orthopaedic surgeries performed, in which the hip joint is reconstructed to decrease pain and to improve the functionality to the joint. Although these surgeries are very successful, there still remain areas for improvement, such as failures due to instability and dislocation of the implanted joint. The purpose of this thesis is to investigate the effect of surgical entrance approach on dislocation, the effect of implant type, and the effect of capsule repair and closure. The need to quantify the resistance to dislocation is important in understanding the effect that each of these factors has on the total contribution to minimize the dislocation moment.

Document Type

Thesis

Degree Name

M. S.

Department

Mechanical Engineering

First Advisor

Chadd W. Clary

Second Advisor

Paul Rullkoetter

Third Advisor

Margareta Stefanovic

Keywords

Capsule repair, Dislocation resistance, Dual mobility, Surgical approach, Total hip arthroplasty

Subject Categories

Biomechanical Engineering | Biomechanics and Biotransport | Biomedical Engineering and Bioengineering | Mechanical Engineering

The Effects and Analysis of Implant Type and Surgical Approach in Total Hip Arthroplasty Dislocation Resistance

_____

A Thesis

Presented to

the Faculty of the Daniel Felix Ritchie School of Engineering and Computer Science

University of Denver

_____

In Partial Fulfillment

of the Requirements for the Degree

Master of Science

_____

by

Brittany Marshall

August 2020

Advisor: Dr. Chadd W. Clary, PhD

Author: Brittany Marshall
Title: The Effects and Analysis of Implant Type and Surgical Approach in Total Hip Arthroplasty Dislocation Resistance
Advisor: Dr. Chadd W. Clary, PhD
Degree Date: August 2020

ABSTRACT

Total hip arthroplasty (THA) is one of the most successful orthopaedic surgeries performed, in which the hip joint is reconstructed to decrease pain and to improve the functionality to the joint. Although these surgeries are very successful, there still remain areas for improvement, such as failures due to instability and dislocation of the implanted joint. The purpose of this thesis is to investigate the effect of surgical entrance approach on dislocation, the effect of implant type, and the effect of capsule repair and closure. The need to quantify the resistance to dislocation is important in understanding the effect that each of these factors has on the total contribution to minimize the dislocation moment.

ACKNOWLEDGEMENTS

I would like to sincerely thank my advisor, Dr. Chadd Clary, for his guidance and support. I would like to thank my thesis defense committee members, Dr. Paul Rullkoetter and my committee chair member Dr. Margareta Stefanovic.

I would like to thank all of my peers in the Center for Orthopaedic Biomechanics for their support and assistance, specifically Yashar Behnam for his exceptional knowledge on operating the lab equipment and advice to running successful tests and Luke Storer for introducing me to the world of hip testing. I would like to thank Michael Scinto for his assistance and countless hours of testing a dozen hips with me and performing all the necessary registration work to make testing possible in the final work of this thesis. I would also like to thank all other members of the lab group for consistently taking time to answer questions and assist me with troubleshooting a wide variety of issues that were encountered.

I would next like to thank DePuy Synthes for sponsoring all of this work and Ethicon for their sponsorship for a part of this work, specifically Ryan Keefer and Dan Huff. Thank you to Dr. Bohannon Mason, MD for performing surgeries for a portion of this work and for his guidance.

TABLE OF CONTENTS

ABSTRACT ii

CHAPTER ONE: Introductory Remarks 1
1.1 Introduction 1
1.2 Objectives 2
1.3 Thesis Overview 3

CHAPTER TWO: Review of Pertinent Literature 4
2.1 Total Hip Arthroplasty 4
2.1.1 General Hip Information 4
2.1.2 Hip and Capsule Anatomy 6
2.2 Implant Types: 9
2.2.1 Traditional Implant 9
2.2.2 Dual Mobility Implant 10
2.3 Surgical Approaches 14
2.3.1 Posterior Approach 14
2.3.2 Direct Anterior Approach 15
2.3.3 Other Approaches 16
2.3.4 Capsule Repair 18

CHAPTER THREE: The Effect of Patient BMI on Bearing Kinematics in Dual Mobility Total Hip Arthroplasty 22
3.1 Introduction 22
3.2 Methodology 23
3.3 Results 26
3.4 Discussion 28

CHAPTER FOUR: A Pilot Study on Posterior Dislocation Simulations in THA-Implanted Hips 31
4.1 Introduction 31
4.2 Methodology 32
4.3 Results 35
4.4 Discussion 39

CHAPTER FIVE: The Role of Capsular Repair on the Stability of Total Hip Arthroplasty using the Direct Anterior Approach 42
5.1 Introduction: 42
5.2 Methods: 44
5.3 Results: 50
5.4 Discussion: 53

CHAPTER SIX: Dual Mobility Dislocation Resistance Comparing Approach and Capsule Repair through Laxity and Dislocation Simulations 58
6.1 Introduction 58
6.2 Methodology 59
6.2.1 Impingement Analysis 60
6.2.2 Experimental Testing 61
6.3 Proposed Results 66

CHAPTER SEVEN: Concluding Remarks 68
7.1 Final Remarks 68
7.2 Future Work 69
7.3 Key Takeaways 70

REFERENCES 71

APPENDIX 77
A.1: Conference Abstracts 77
A.2: Upcoming Journal Submissions 77
A.3: Additional Figures Associated with Chapter Three 78
A.4: Additional Figures Associated with Chapter Four 85
A.5: Additional Figures Associated with Chapter Five 92
A.6: Additional Information Associated with Chapter Six 104

LIST OF FIGURES

Figure 1: Natural hip joint (left), osteoarthritic hip (middle), implanted hip joint (right) (mayoclinic.org) 6
Figure 2: Ligaments surround the hip that make up the hip capsule. Left: anterior view, Right: posterior view (Wagner et al., 2018) 8
Figure 3: From left to right, a natural hip outlining the important bony geometries, an exploded view of the components of a traditional hip implant, an assembled view of the hip implant, and finally the component implanted into the pelvis bone (orthoinfo.aaos.org) 9
Figure 4: Standard cup (A and C) vs dual mobility cup (B and D). The dashed lines in A and B symbolize articulating surfaces. This image demonstrates the ability for the dual mobility cup to achieve a greater range of motion before component on component impingement occurs (C vs. D) (De Martino et al., 2014). 13
Figure 5: Dual mobility articulating surfaces demonstrated at different orientations (orthoaxis) 13
Figure 6: The incision line for the Posterior approach (left), Lateral approach (middle), and Anterior approach (right) (holycrossleonecenter.com) 18
Figure 7: Stratafix suture - example of continuous, barbed, knotless suture (Ethicon) 20
Figure 8: Concept and application of the knotless, continuous suture, Stratafix (Ethicon) 21

Figure 9: Computer model of experimental set-up defining the axes of rotation and direction of force and translation. 23
Figure 10: Experimental set-up showing the 3D-printed bone geometries mounted into the VIVO and the DIC target markers placed on the periphery of the DM bearing and acetabular shell. This figure also shows the normal cup position on the left and the anterior cup position on the right. 24
Figure 11: Loading profile for compressive load showing Low BMI (dashed), Mean BMI (solid), and High BMI (dotted) for one stair descent cycle and one gait cycle. 25
Figure 12: Change in Angle of the Liner during Gait for the two cup positions 27
Figure 13: Change in Angle of the Liner during Stair Descent for both cup positions 28

Figure 14: Segmented pelvis model formed to fixture for anatomical alignment 34
Figure 15: Fixturing set up using CT scanned bone geometries with custom fixturing to mount femoral head center in the VIVO rotation center. The VIVO flexion arm is in black. Left: Anterior view. Middle: Isometric view. Right: Medial view 35
Figure 16: Posterior approach matched-pair hips demonstrating the capsule contribution and suture contribution to dislocation resistance 36

Figure 17: Anterior approach hips tested via posterior dislocation tests comparing the natural intact posterior capsule compared to the posterior cut contribution in the maroon, and the resected capsule contribution in the gold. 37
Figure 18: A typical resistive moment curve with increasing knee flexion with the sutures intact, after removal of the sutures, and after removal of all soft tissue for three adduction angles at a constant internal rotation of 5 degrees. 37
Figure 19: Right side hip total peak moment with components vs different internal rotations at different adduction angles demonstrating the breakdown of the angle components. 38
Figure 20: Left side hip, total peak moment with the moment components for a wider variety of internal rotation and adduction to increase moment response demonstrating the breakdown of the angle components. 38
Figure 21:From 90 degrees flexion of the hip to 120 degrees flexion of the hip, the lateral band of the iliofemoral ligament does not increase in length, thus not tightening the capsule more as flexion is increased. 41

Figure 22: #2 VICRYL interrupted suture repair (left) and STRATAFIX barbed continuous suture repair (right). Dashed red lines indicate the location of the capsular arthrotomy and the black lines indicate suture locations. 45
Figure 23: Segmented bony anatomy was used to ensure specimen were accurately mounted into the VIVO simulator. Custom fixtures were 3D printed to center the femoral head at the intersection of the F-E, Ad-Ab, and I-E axis of the simulator and align the specimen's anatomic axis with the simulator coordinate system. 46
Figure 24: Step-by-step animation of the IE rotation laxity test, the ADAB laxity assessment, and the anterior dislocation simulation by hyperextending and externally rotating. Kinematics captured the exact location of the bones at every point in time. 47
Figure 25: Definition of capsule contribution and suture contribution from the three set of tests that were performed. 49
Figure 26:Breakdown of moment components for the Internal and External Rotation laxity assessment. 52
Figure 27: Breakdown of moment components for the Adduction and Abduction Rotation laxity assessments. 52
Figure 28: Breakdown of moment components for Anterior Dislocation simulation by hyper-extending and externally rotating. 53

CHAPTER ONE: Introductory Remarks

1.1 Introduction

Total joint replacements are most commonly a solution for osteoarthritis to eliminate pain and improve function in the joint (Jones et al., 2007). The American Academy for Orthopaedic Surgeons found from the National Inpatient Sample that in 2014 there were 370,770 total hip replacements and 680,150 total knee replacements (Riley and Ip, 2018). They also predict that by 2030, there will be a 171% increase in primary total hip arthroplasty (THA) surgeries and a 189% increase in primary total knee arthroplasty (TKA) surgeries (Riley and Ip, 2018). Due to the large number of people affected each year from a total joint replacement, it is imperative to continue to increase the success rate of these surgeries.

Failure of total hip arthroplasty is most commonly due to aseptic loosening, instability or dislocations, infections, wear, or periprosthetic fractures. In regard to a total hip arthroplasty surgery, it has been found that instability or dislocation is one of the primary reasons for revision surgeries, accounting for 22.5% of all revision surgeries (Bozic et al., 2009). If the failures due to dislocation can be minimized, thousands of patients will avoid having to receive an additional surgery to revise the implant and achieve a more successful outcome.

The cause of hip dislocation is multifactorial, including implant design, surgical technique, and patient factors. Different implants might have varying effects on

dislocation resistance. The dual mobility implant is an alternative implant that has been designed to decrease the dislocation rate. This implant includes an additional moving interface to simulate having a larger femoral head through a polyethylene bearing between the femoral head and acetabular liner. The larger femoral head correlates to a larger jump distance, or the distance the femoral head needs to egress out of the socket prior to dislocating. A femoral head smaller than the original, native femoral head, has been found to leave the surround capsule looser, hindering the capsule's stability (Logishetty et al., 2019).

It is currently unknown if repairing the capsule post-THA surgery provides an additional resistive moment to dislocation and if the repair is more effective in one surgical approach over others. Different suture types might also contribute to the resistive moment differently, whether they are the traditional, interrupted, knotted sutures or a newer barbed, continuous suture type.

The purpose of this thesis is to investigate the effects of implant type, surgical approach, and capsule repair on dislocation resistance.

1.2 Objectives

The objectives of this thesis are to:

1. Determine the movement of the bearing in a dual mobility total hip arthroplasty implant to establish if additional wear is a concern with this implant type in high-risk patients.
2. Quantify and measure the resistive moment to dislocation in THA-implanted hips.

3. Quantify and measure the contribution that the capsule and sutures provide to dislocation resistance and the contribution of each during laxity assessments.

1.3 Thesis Overview

Each chapter of this thesis is a study that serves to provide original content to contribute to the field of orthopaedic biomechanics with each chapter falling into the chronological order in which they were performed. Chapter Two provides an insightful review of previous, pertinent literature to assist in the demonstration of current published papers for background information. Chapter Three describes a study that quantifies the relative motion of a dual mobility THA implant between the two moving interfaces. Chapter Four provides detail on a study to determine how to quantify the resistive moment that the capsule and capsule repair each contribute during dislocation for posterior approach hips. Chapter Five is the most comprehensive study in this thesis to further investigate and expand the quantification of resistive moments on anterior approach THA-implanted hips. Chapter Six provides the introduction and methods corresponding to the most recent and largest ongoing study presented in this thesis. Chapter Seven concludes with final remarks and summarizes the conclusions of each study. This is all followed by references and appendices with additional figures and graphs for more detail on each study.

CHAPTER TWO: Review of Pertinent Literature

2.1 Total Hip Arthroplasty

The purpose of this section is to introduce total hip arthroplasty, why it is used, and areas of current study. This chapter will then transition to basic information on the hip joint anatomy. By the conclusion of this section, the goal is that a strong base of understanding is presented to provide a foundation to proceed to more specific and specialized topics relevant to this thesis project.

2.1.1 General Hip Information

Total hip arthroplasty (THA) is the gold standard for the treatment of patients with osteoarthritis in the hip and is regarded as one of the most successful elective surgeries. Osteoarthritis occurs when the articular cartilage within the joint degrades, which then promotes the growth of osteophytes (Pfleger and Woolf, 2003), resulting in pain within the joint (Kumar et al., 2019, Liberman et al., 1997, Pfleger and Woolf, 2003). With approximately 10% of all men and 18% of all women suffering from osteoarthritis (Pfleger and Woolf, 2003), total knee and total hip replacements are found to significantly improve the quality of life of people suffering from this joint degradation disease (March et al., 1999, Liberman et al., 1997). Out of all the people who filed for disability in 1990, 2.8% of the cases were due to people with osteoarthritis who were

unable to work to their full capability, which significantly impacts the overall economic burden throughout the world (Pfleger et al., 2003). THA is also commonly used to treat rheumatoid arthritis, trauma related injuries and avascular necrosis (Kumar et al., 2019, Liberman et al., 1997). Other conditions such as hip dysplasia and ankylosing spondylitis make up a smaller percentage of conditions that THA is used to treat (Kumar et al., 2019, Liberman et al., 1997).

There were approximately 2.55 million total hip replacements performed in the United States prior to 2010, with a growing percentage each year (Kremers et al., 2014, Riley and Ip, 2018). With the increasing number of surgeries each year, it is important to keep improving THA's success rate. Kurtz et al. (2007) projected that there will be a growth of 174% in surgeries performed each year, reaching approximately 5.72 million THA's in the United States by 2030 (Kurtz et al., 2007). Riley and Ip also predict a drastic increase in surgeries, forecasting a 171% increase in THAs by the year 2030 (Riley and Ip, 2018).

Instability or dislocation is a primary cause for a revision surgery in THA (Bozic et al., 2009, Dobzyniak et al., 2006, Goldman et al., 2019). Other reasons for revision surgeries include aseptic loosening, periprosthetic fractures, wear-related failures, and infection, with infections being the largest cause for arthrotomy and removal of the implant (Bozic et al., 2009, Dobzyniak et al., 2006, Crowe et al., 2003). Revision surgeries commonly lead to extended hospital stays, bone loss that could result in a bone graft, and an increased risk of complications (Bozic et al., 2009, Crowe et al., 2003). They also introduce added costs, with a total hip revision surgery hospital cost, as

published in 2003, ranging from $10,000 to $45,000 (Crowe et al., 2003). With over 51,000 revision surgeries between October 2005 to the end of December 2006 (Bozic et al., 2009), the economic burden should be minimized. Knowing all the associated economical and health-related costs to a revision surgery and understanding that instability and dislocations are a primary cause for revision in THA, we can conclude that it is important to investigate and understand dislocation mechanisms to minimize their prevalence.

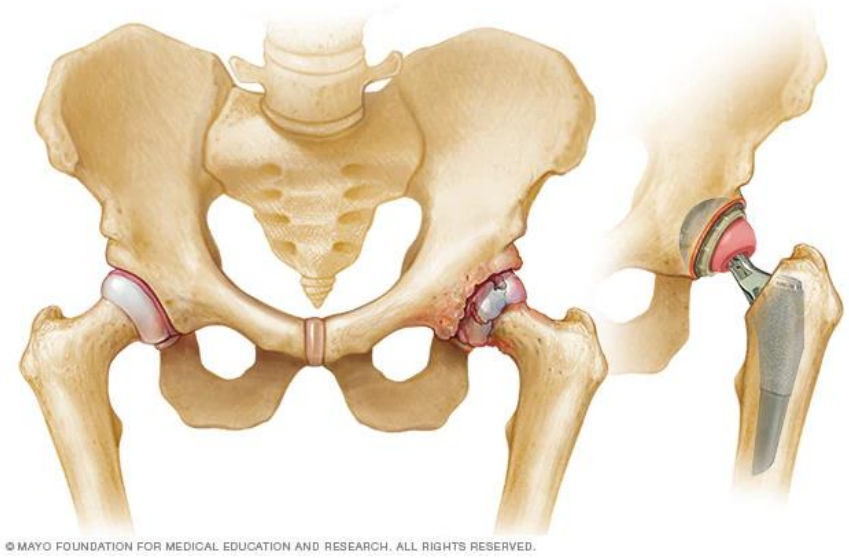

Figure 1: Natural hip joint (left), osteoarthritic hip (middle), implanted hip joint (right) (mayoclinic.org)

2.1.2 Hip and Capsule Anatomy

The hip joint is a ball and socket joint that prioritizes both stability and mobility (Martin et al., 2008). The major stabilizers of the hip joint are the three primary ligaments that surround it: the iliofemoral ligament, pubofemoral ligament, and the ischiofemoral ligament. These ligaments are made up of a very dense, fibrous tissue that have been

found to exhibit an ultimate strength of 6.16 MPa and a failure load of each ligament exceeding 300 N (Stewart et al., 2002).

Through a series of magnetic resonance arthrography performed in a study by Wagner et al., the attachments of each ligament can be described as follows with supporting visualization in Figure 2 (Wagner et al., 2012). The iliofemoral ligament (ILFL) can be found supporting the anterior aspect of the joint with two distinctive bands: the superior band and the inferior band. Both originate in the anterior inferior iliac spine, attaching to the upper and lower intertrochanteric line, respectively, to resist motion in external rotation and extension (Martin et al., 2008). The pubofemoral ligament (PBFL) was found to primarily resist abduction and secondarily resist external rotation during full extension, as it originates from the superior ramus of the pubic bone and crosses the inferior portion of the articular capsule. The ischiofemoral ligament (ISFL) originates on the ischial circumference of the acetabular rim and splits into superior and inferior bands. The superior band joins with the zona orbicularis (ZO) on the femoral neck at the base of the greater trochanter, and the inferior band joins on the posteroinferior portion of the ZO. The ischiofemoral ligament is found to primarily restrict internal rotation (Martin et al., 2008). The purpose of the zona orbicularis is also found to be a hip stabilizer, creating a ring around the neck of the femur (Wagner et al., 2012), with its fiber oriented circumferentially. Alternatively, the ILFL, PBFL, and ISFL all have their fibers oriented longitudinally (Martin et al., 2008). It is important to note that the ligaments that surround the hip are commonly referenced collectively as the hip capsule because they integrate to form a continuous soft tissue structure around the hip.

The purpose of the uninterrupted hip capsule is to create a strong, encompassing sleeve-like structure to promote stability within the joint (Martin et al., 2008). The capsule also helps to regulate the joints' synovial fluid (Martin et al., 2008, Ng et al., 2019). It has been found that the posterior capsule is weaker than the anterior portion of the capsule (Steward et al., 2002); therefore, the zona orbicularis is more prominent in the posterior aspect of the capsule to compensate for the weaker support on the posterior portion (Ng et al., 2012). Understanding the anatomy and ligaments that surround the hip is important, as this structure needs to be breached to access the hip joint in order to perform a total hip replacement surgery.

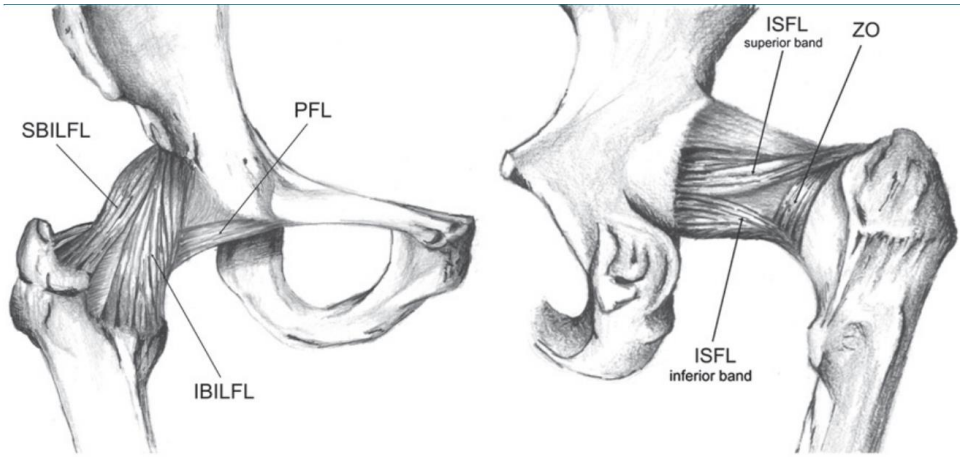

Figure 2: Ligaments surround the hip that make up the hip capsule. Left: anterior view, Right: posterior view (Wagner et al., 2018)

2.2 Implant Types:

The goal of this section is to briefly explain the traditional THA implant and to go into a detailed explanation of what a dual mobility bearing is, its uses, benefits, and disadvantages.

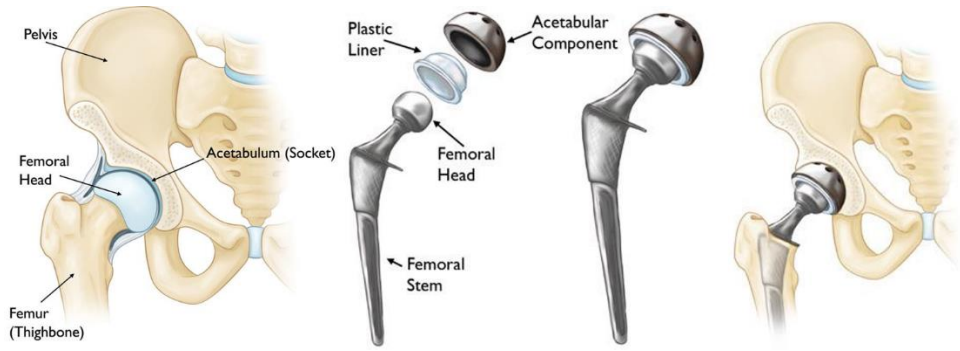

Figure 3: From left to right, a natural hip outlining the important bony geometries, an exploded view of the components of a traditional hip implant, an assembled view of the hip implant, and finally the component implanted into the pelvis bone (orthoinfo.aaos.org)

2.2.1 Traditional Implant

A traditional implant is composed of four main components: the femoral stem, the femoral head, the acetabular shell, and the acetabular liner, as seen in Figure 3. The femoral stem is impacted into the cavity of the femur to provide an anchor for the femoral head. The head of the femur is secured to the stem using a Morse taper. The stem of the femur is usually made of a metal, such as cobalt chromium, with the head of the femur being either a metal or ceramic material. The stem and backside of the acetabular shell are frequently coated with an additional layer of material, such as hydroxyapatite, to promote bony ingrowth of the implant into the bone for long-term fixation. The acetabulum is then reamed to allow for the acetabular shell to be placed. The acetabular

shell is usually screwed into the back of the acetabulum to allow for a secure fixation. The liner is then press-fit into the acetabular shell, which is most commonly made of polyethylene for a smooth, low wear articulation with the femur head. With the combination of these four components, the total hip arthroplasty design is able to mimic the natural hip joint as best as possible, with a plethora of sizes designed to match the needs of all patients.

2.2.2 Dual Mobility Implant

Hip instability is one of the major causes for revision surgeries in THA (Bozic et al., 2009, Dobzyniak et al., 2006, Goldman et al., 2019). The dual mobility cup was developed by a French professor and a French engineer, who teamed up with the goal of creating a stable bearing to allow for the greatest range of motion (De Martino, 2014). This increased range of motion can be seen in Figure 4, where the standard cup has less rotation compared to the dual mobility implant, before component on component impingement occurs. To achieve this goal, two articulating surfaces were created to allow for a larger femoral head to articulate within the acetabular shell. This will reduce the likelihood of component on component impingement, or when the femoral neck contacts either the acetabular shell, liner, or mobile bearing. Impingement is a mechanism for dislocation, creating a moment arm for the femoral head to egress from the acetabulum. Dual mobility systems were introduced to be used as a primary THA option for patients that were subject to dislocations (De Martino, 2014). Currently, there is more use for them as a revision THA for patients that experienced instability in their primary THA, as

well as at-risk patients, such as elderly and obese, to increase stability in the joint and try to decrease the risk of dislocation.

Heffernan et al. studied various dual mobility designs with a range of head sizes to identify the leading factors on "posterior horizontal dislocation distance" during activities of daily living (Heffernan et al., 2014). The posterior horizontal dislocation distance can be described as the "minimum translational distance in the coronal plane measured from the center of the acetabular component to the center of the femoral head" (Heffernan et al., 2014). Implant design was found to be the leading factor in reducing dislocation, with the anatomic dual mobility cup performing better than the modular dual mobility cup, the hemispherical fixed bearing, and the subhemispheric dual mobility cup. A larger head size was also found to decrease posterior horizontal dislocation distance in all implant types. From this study, we can determine that the dual mobility bearing does in fact provide greater dislocation resistance compared to a conventional, fixed bearing THA implant (Heffernan et al., 2014).

In a systematic review performed by Jonker et al., 549 dual mobility cups and 649 unipolar cups were utilized. Only one dislocation was reported in the dual mobility cups, yielding a dislocation rate of 0.2%, yet 46 dislocations were reported in the unipolar or standard cups, for a dislocation rate of 7.1% (Jonker et al., 2020). The revision rate in this same study, comparing the dual mobility group and the unipolar group, was 1.6% and 6.0%, respectively (Jonker et al., 2020). The major cause for revision in the unipolar group was due to instability (30 out of 39), and no reported causes of revision were due to instability in the dual mobility group, but other causes lead to revisions (Jonker et al,

2020). Fabry et al. found that there was a lower hospital readmission rate for the dual mobility implant than the traditional fixed bearing implant in the first 90 days post-surgery (Dubin et al., 2020). There were no dual mobility implant dislocations in this cohort study of 664, with two dislocations in the fixed bearing group of 218, yielding a p-value of 0.06 (Dubin et al., 2020).

A primary concern with dual mobility implants is that there are two moving interfaces, increasing the potential for wear to occur on the implant. Fabry et al. conducted an experiment measuring the frictional torque and self-centering torque between eccentric and concentric dual mobility designs (Fabry et al., 2014). This study found that in the eccentric dual mobility cup design, during activities of daily living, the smaller interface between the femoral head and the polyethylene bearing provided the majority of the motion (Fabry et al., 2014). Schmalrized et al. found that "wear is a function of use, not time" for conventional THA bearings, emphasizing the importance of understanding wear mechanisms. From dual mobility bearing retrieval studies, Adam et al. did not find additional wear despite the two interfaces. Loving et al. found that the average wear rate of dual mobility implants was actually less than the wear rates of the conventional THA bearings.

Despite these positive findings on the relationship between wear and dual mobility bearings, there is still a hesitation to use them as primary implants for the at-risk elderly and obese patients. While wear has been measured through analyzing retrieval implant's volumetric wear and wear rate, no studies analyze the actual motion of the dual mobility liner relative to the acetabular cup and femoral head during activities of daily

living to determine the source of wear. There is also no prior research evaluating how a patient's body mass index may affect bearing kinematics, or if there is increased bearing friction with additional weight applied.

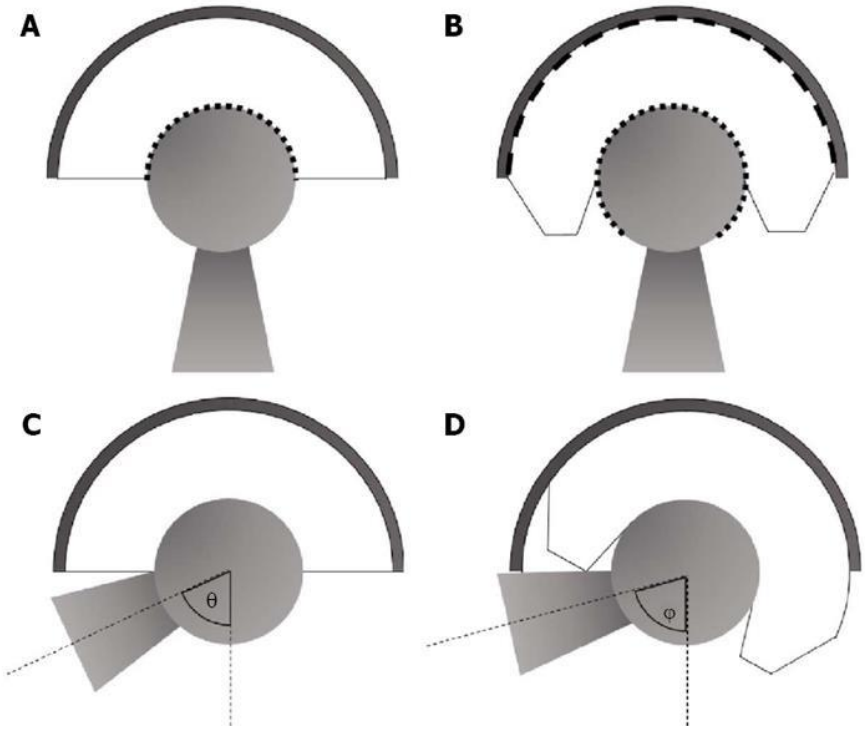

Figure 4: Standard cup (A and C) vs dual mobility cup (B and D). The dashed lines in A and B symbolize articulating surfaces. This image demonstrates the ability for the dual mobility cup to achieve a greater range of motion before component on component impingement occurs (C vs. D) (De Martino et al., 2014).

Figure 5: Dual mobility articulating surfaces demonstrated at different orientations (orthoaxis)

2.3 Surgical Approaches

This section on surgical approach will explain the methods in which a surgeon resects the hip capsule and the associated benefits, challenges, and influences on dislocation rates. There are many approaches to THA that are popular, giving the spectrum from posterior approach, to posterolateral, to lateral, to anterolateral, and finally to the direct anterior approach. This section will conclude by investigating the idea of suturing closed the hip capsule at the conclusion of surgery, also commonly referred to as capsule repair, stating previous outcomes and findings.

2.3.1 Posterior Approach

The posterior approach historically has been the most popular surgical approach for performing total hip replacement surgeries, especially in North America. Surgeons in North America perform the posterior approach 69% of the time, as compared to only 36% of surgeries in Europe are posterior approaches (Chechik et al., 2013). Although Canada falls under the North American statistics, only about 36% of their THA's are posterior approaches (Petis et al., 2015), which shows the dominance of posterior approach used in the United States.

The posterior surgical approach is performed by cutting through the fasciae latae and gluteus maximus muscles, then incising the piriformis at the insertion point into the greater trochanter. Once at the joint capsule, the posterior aspect of the capsule is cut, exposing the femoral head and acetabulum (Petis et al., 2015). Due to the large visibility of the hip joint at this angle, and as the primary approach used in the United States

specifically, the posterior approach has been found to be significantly shorter in surgical time than the anterior approach (Petis et al., 2015).

2.3.2 Direct Anterior Approach

The direct anterior approach has grown in popularity in the United States since its debut in Europe. The anterior approach has been found to be the most direct entrance and access point to the hip joint (Kennon et al., 2004). The most compelling reason to use the anterior approach is because it minimizes the number of muscles which must be cut, with a few specific techniques on how to best accomplish this goal: Smith-Peterson approach, Heuter approach, and Muscle Sparing Approach (MSA™). The technique used to access the hip joint via the direct anterior approach, is to dissect between the sartorius and tensor fasciae latae, splitting between femoral nerves (Kennon et al., 2004, Petis et al., 2014). By coming in between these two muscles, the hope is to have less muscle impact to promote faster healing.

Many benefits to the anterior approach have led to its increase in popularity due to its ability to cut between muscles, instead of directly through them. As a result, benefits are found to include decreased pain, faster recovery, and improved hip stability (Higgins et al., 2014). One advantage that the anterior approach has over all the other approaches is that the patient is lying flat in a supine position on the table. This allows for the use of fluoroscopy intraoperatively to optimize component placement (Higgins et al., 2014). A shorter incision is also used in an anterior approach (Kennon et al., 2004, Wang et al., 2018). In Higgins et al., a systematic review and meta-analysis used 17 previous studies and found that the anterior approach was statistically significantly favored over the

posterior approach in: 6-week Harris Hip Score (HSS), 3-month Hip disability and Osteoarthritis Outcome Score (HOOS), 2-month Merele d'Aubigne and Postel ability to walk score, Western Ontario and McMaster Universities Osteoarthritis Index (WOMAC) stiffness score, 2-week Visual Analogue Score (VAS), postoperative hospital length of stay, and postoperative dislocations (Higgins et al., 2014). Although listed here are possible advantages of the anterior approach over other approaches, it needs to be made clear that at this time there are no far-superior advantages of one approach over others, but only small differences that have been found.

The anterior approach has challenges associated with it; one of the primary disadvantages is its lack of visibility. One of the ways this challenge has been overcome is with the assistance of a specialized table to ease in maneuverability and traction of the joint, such as the Hana® Table, but this requires an operator or additional person in the operating room. If a specialized table is not used, then fluoroscopy is usually used to compensate for the lack of visibility and accessibility to the joint to ensure proper component placement (Higgins et al., 2014, den Daas et al., 2019). Surgeons are trying to find the balance between the lack of visibility in the anterior approach and sacrificing the capsule to achieve this additional visibility.

2.3.3 Other Approaches

With the two most popular approaches being covered (posterior approach and anterior approach), there is a spectrum that exists between these two approaches that are commonly used. The anterolateral approach is common due to its minimally invasive nature and is commonly referred to as the Watson-Jones approach in literature. The

dissection is made between the tensor fasciae latae and the gluteus medius with the anterior portion of the capsule needing to be cut along the line of the femoral neck. The articular capsule is also cut along the upper edge of the acetabulum and base of femoral neck to create an “H”-shaped capsule incision (Lu et al., 2019).

The direct lateral approach has the advantage that it is associated with a small dislocation rate relative to the other approaches (Kwon et al., 2006, Petis et al., 2014), which makes it quite attractive and explains the reason it is the second most common approach as of 2011 (Chechik et al., 2013). 60% of all THA’s in Canada were performed via the direct lateral approach (Petis et al., 2014). In this approach, the fascia between the tensor facia latae and gluteus maximum is cut, along with the underlying gluteus medius to access the hip capsule (Petis et al., 2014).

Comparing various studies and meta-analyses, no conclusive results on a superior approach are found in regard to the dislocation rate alone. In a study of 268 direct anterior and 184 posterior approach surgeries, only one dislocation occurred in each group, yielding dislocation percentages of 0.4% and 0.5%, respectively (Malek et al., 2006). In the systematic review and meta-analysis by Higgins et al., the percentage of dislocations is significantly less in the anterior approach group than in the posterior approach group (Higgins et al., 2014). One study looked at 1891 posterior approach THA’s and found a dislocation rate of 1.2% (Hernandez et al., 2018). In a study comparing different approaches and reporting their dislocation rates with a fully repaired capsule, they were 0.70%, 0.43%, and 1.01%, corresponding to the anterolateral, direct lateral, and posterior approaches, respectively (Kwon et al., 2006). All dislocation rates

between the approaches are comparable, ranging from 0.4% to 1.2%, with anterior approaches having slightly less dislocations than posterior approach surgeries.

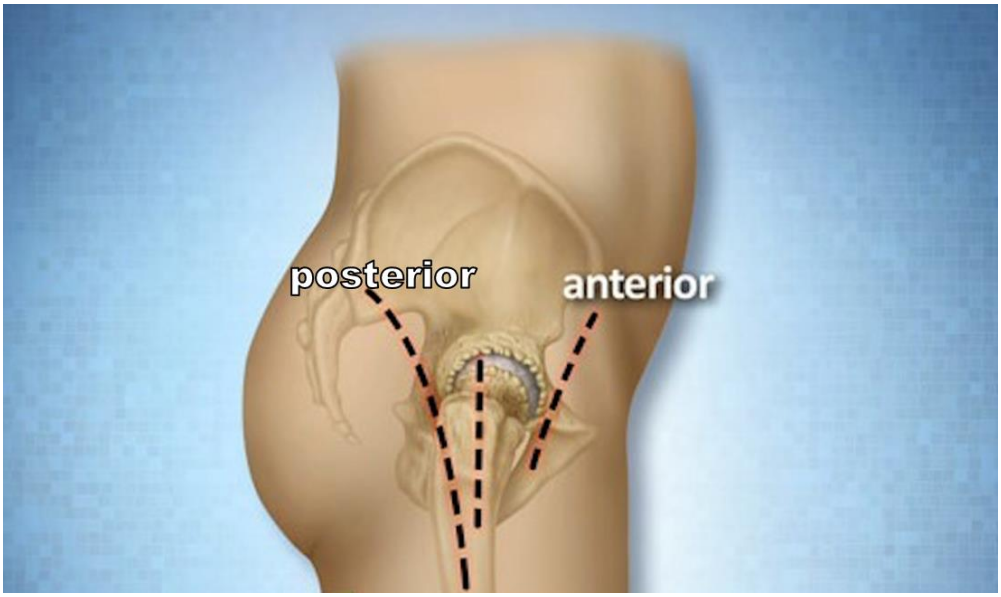

Figure 6: The incision line for the Posterior approach (left), Lateral approach (middle), and Anterior approach (right) (holycrossleonecenter.com)

2.3.4 Capsule Repair

The clinical value of capsule repair, specifically in anterior approach THA, is controversial. Some surgeons perform a complete capsulectomy to improve surgical access to the hip, while others preserve and repair the capsule. Evidence is continuing to grow to conclude that repairing the capsule leads to lower dislocation rates than capsules left unrepaired for posterior approach surgeries (Hernández et al., 2018, Kwon et al., 2006, Mihalko et al., 2004), anterolateral approach (Lu et al., 2019, Kwon et al., 2006,), and lateral approach (Hughes et al., 2015, Kwon et al., 2006,). Bolia et al. (2019) revealed the importance of capsule repair even during hip arthroscopy. No previous literature was found regarding capsule repair for anterior approach hip surgeries.

The findings of these studies can be summarized to provide evidence for capsule repair. Kwon et al. (2006), analyzed the dislocation rates for the posterior approach and found, with 2467 hips that did not get repaired, there were 110 dislocations, resulting in a 4.46% incidence rate, compared to only 8 hip dislocations out of 1648 in the repaired-capsule group, for a dislocation rate of 0.49%. Mihalko measured the maximum angle during internal and external rotation after a posterior approach THA, cutting and repairing the external rotators and the posterior capsule, and found that there was more rotation in the non-repaired group compared to the repaired group to achieve the same, constant 2 Nm torque value. They then found a significantly lower torque was needed to dislocate the hip in the non-repaired group compared to the repaired capsule group (Mihalko et al., 2004). Lu et al. (2019), using an anterolateral approach, found that one subject from the repair group suffered a dislocation, out of a cohort of 137, resulting in a 0.7% dislocation rate. In the non-repair group, 13 subjects suffered a dislocation out of a group of 248 patients, for a 5.2% dislocation rate. Hughes et al. studied the angle and torque of dislocation for a hip hemiarthroplasty using a direct lateral approach and found significant results favoring repair of the capsule (Hughes et al., 2015). Previous literature supporting hip capsule repair has started accumulating, yet no studies have provided evidence for the repair of the capsule in anterior approach hips.

With capsule repair in THA becoming more prevalent, alternative suture types to the traditional interrupted sutures are being explored. Traditional sutures refer to the interrupted suture, requiring knots to connect the two tissue halves, such as Vicryl. A continuous, knotless, barbed suture was first patented in 1964, which lead to a series of

surgeons further developing patents around the idea (Ruff, 2013). As of 2013 when Ruff published his paper, only two FDA-approved barbed sutures were on the market (Quill and V-Loc). Now multiple companies have a barbed suture on the market, one being Stratafix by Ethicon. There continues to be developing research around using barbed, knotless sutures in joint arthroplasty surgeries, with many promising results starting to be published (Borzio et al., 2016, Li et al., 2018).

As barbed sutures have grown in popularity in the field of arthroplasty, many advantages have been found; barbed sutures could assist in infection reduction, with there being a decrease in wound ooze (Knapper et al., 2019) and lower superficial infection rate (Thacher et al., 2019). It was also concluded that surgical time can be reduced using barbed sutures over the traditional interrupted sutures (Li et al. 2018, Borzio et al., 2015, Lin et al., 2016). Although there is a higher market cost to the barbed suture, the saved time outweighs the per-unit cost, ultimately being a cost-saving solution (Li et al. 2018). Furthermore, the barbed suture may be more effective at restoring the mechanical strength and wound-holding strength of the repair (Ruff, 2013).

Figure 7: Stratafix suture - example of continuous, barbed, knotless suture (Ethicon)

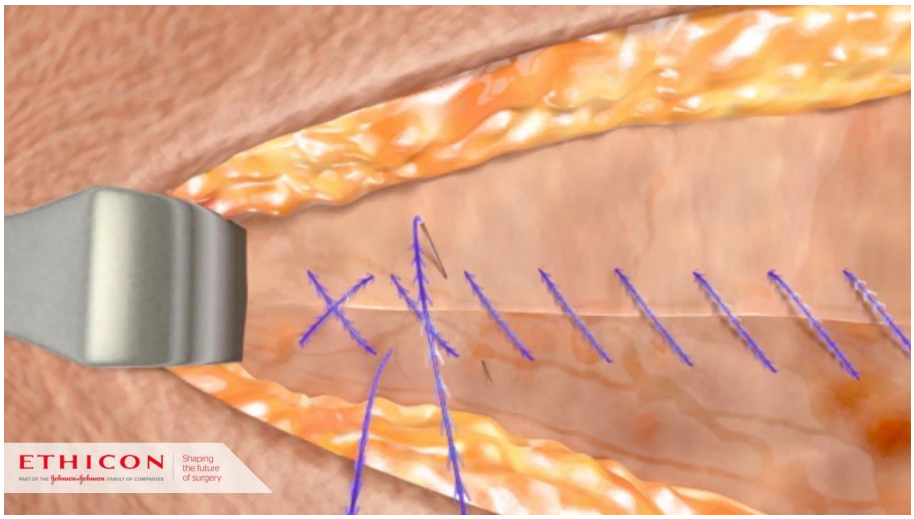

Figure 8: Concept and application of the knotless, continuous suture, Stratafix (Ethicon)

CHAPTER THREE: The Effect of Patient BMI on Bearing Kinematics in Dual Mobility Total Hip Arthroplasty

3.1 Introduction

Dual mobility total hip arthroplasty (DM-THA) implants offer improved dislocation resistance without the increased risk of femoral neck impingement, by gaining a larger range of motion compared to the traditional implant. This increased range of motion might benefit certain at-risk patients. Despite clinical evidence of successful outcomes, reports indicate bearing mobility may become restricted due to increased bearing friction. It is currently unknown how differences in patients' body mass index (BMI) may affect bearing kinematics.

The purpose of this study was to experimentally evaluate bearing kinematics during gait, stair descent, and sit-to-stand activities, simulating both high and low levels of loading, simulating BMI, with the DM-THA. The first objective was to determine and quantify the movement that occurs between the polyethylene liner and the acetabular cup. The second objective was to determine if BMI impacts the movement of the polyethylene liner. Our hypothesis was that increased hip compression, or BMI, would result in increased frictional resistance between the bearing and cup, reducing bearing motion.

3.2 Methodology

A dual mobility THA acetabular shell and liner were cemented into a three-dimensional (3D) printed pelvis geometry and a femur stem, head, and dual mobility bearing were fixated into a 3D-printed femur, as seen in Figure 9. The pelvis and femur were then mounted into the AMTI VIVO Joint Simulator. Superficial target markers were placed on the periphery of the dual mobility bearing and the rim of the acetabular component, as seen in Figure 10, to enable bearing tracking using Digital Image Correlation (DIC, Aramis, GOM). The DIC system allows for precise tracking of the target markers through time to track relative motions.

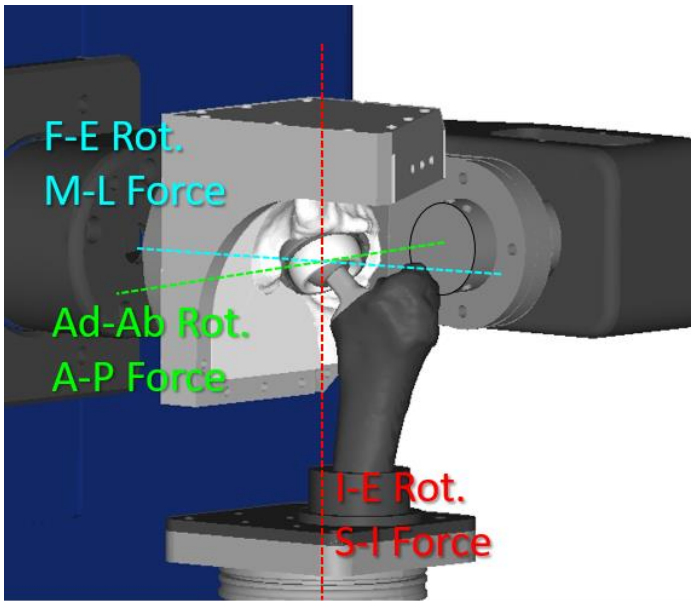

Figure 9: Computer model of experimental set-up defining the axes of rotation and direction of force and translation.

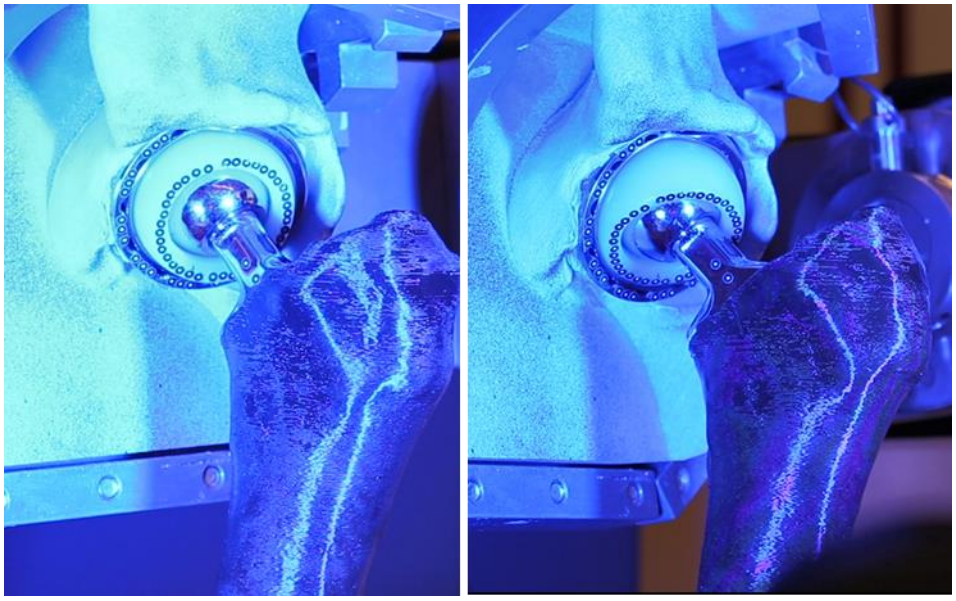

Figure 10: Experimental set-up showing the 3D-printed bone geometries mounted into the VIVO and the DIC target markers placed on the periphery of the DM bearing and acetabular shell. This figure also shows the normal cup position on the left and the anterior cup position on the right.

Loading conditions representing gait, stair descent, and sit-to-stand were developed. For each of these activities of daily living (ADLs), the kinetic data was downloaded from the OrthoLoad database. The average from each subject on the database, for each of the activities, was found at every point throughout the time. This kinetic data was coupled with kinematic data that the University of Denver Human Dynamics Laboratory collected for the respective ADLs. The kinetic data and kinematic data were synchronized to match the two cycle's together. Three different kinetic loading profiles were developed based on the average of the OrthoLoad data, and the hip loads were varied by ± 1 standard deviation to represent low, average, and high-BMI patients. Figure 11 presents the kinetic data for the three BMI's for the gait and stair descent activities. Consistent kinematics were used despite the change in kinetic data. In combination with the three ADLs and three compressive loads, two different dual

mobility initial bearing positions were used. For each simulation, the bearing was positioned in either a neutral (bearing plane parallel to acetabular shell plane) or anterior (bearing at the anterior limit) initial position, as seen in Figure 10. The purpose of this change in the initial position was to observe if the bearing movement was dependent on orientation.

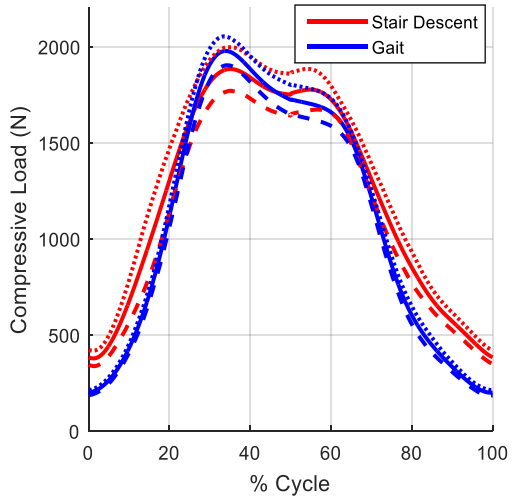

Figure 11: Loading profile for compressive load showing Low BMI (dashed), Mean BMI (solid), and High BMI (dotted) for one stair descent cycle and one gait cycle.

Articulating surfaces between the acetabular liner and the polyethylene bearing were lubricated with fetal bovine serum to simulate the presence of joint synovial fluid. Five activity cycles were run with the pelvis and femur segments set-up in the VIVO to pre-condition the components. The bearing kinematics were recorded and measured during the subsequent cycles using the DIC. Simulations were repeated three times for each loading condition and bearing position.

Bearing kinematics were calculated by registering models of the shell and bearing to the target positions recorded by the DIC and synced with the kinematic feedback from the simulator. The relative angle between the normal vectors of the cup and bearing were

calculated and projected onto the anatomic planes of the pelvis using custom MATLAB scripts. The motion of these vectors was broken up into internal/external, abduction/adduction, and flexion/extension rotations.

ANOVA two-way post-hoc tests were performed between the BMI loading condition and the initial orientation of the polyethylene bearing.

3.3 Results

During the gait activity, no bearing motion relative to the acetabular component was observed during the stance phase for any of the compressive loads and for the different initial bearing positions. Bearing motions were consistently observed only during the swing phase of gait, with overall motions ranging from 0.5°± 0.1° to 6.0 °± 1.2° (Figure 12). For the normal cup position, the total motion ranged from 3.8°± 1.6° to 3.8°± 3.5° to 3.9°± 0.9° for low, mean, and high BMI's, respectively. For the anterior initial cup position, the total motion of the bearing relative to the acetabular cup for the low compressive load was 6.0°± 1.2°, for the mean compressive load was 0.5°± 0.1°, and for the high compressive load was 0.7°± 0.4°. Statistical significance was not found in the total angle of motion, but only in the angle components.

During the stair descent activity, the overall bearing motion relative to the acetabular motion ranged from 1.7° ± 1.1° to 7.3° ± 4.6° (Figure 13). For the normal cup initial position, the low compressive load was 7.3° ± 4.6°, the mean compressive load was 2.2° ± 1.2°, and the high compressive load was 2.7° ± 1.8°. For the anterior initial cup position, the loads were 1.7° ± 1.1°, 4.1° ± 2.5°, and 6.9° ± 3.7°, for the low, mean,

and high compressive loads, respectively. No statistical differences were found through an ANOVA two-way test.

Bearing motion consistently occurred suddenly, corresponding to the point of minimal hip compressive load applied in the cycle. As previous literature might have suspected, the movement of the bearing was not a result of neck and bearing impingement. The rotation of the bearing was consistently in the internal rotation and flexion directions, corresponding to the sliding direction at the contact surface between the femoral head and bearing at the time the rotation occurred.

The visibility and tracking of the markers in the sit-to-stand data was not of high enough quality to produce comprehensive results to report.

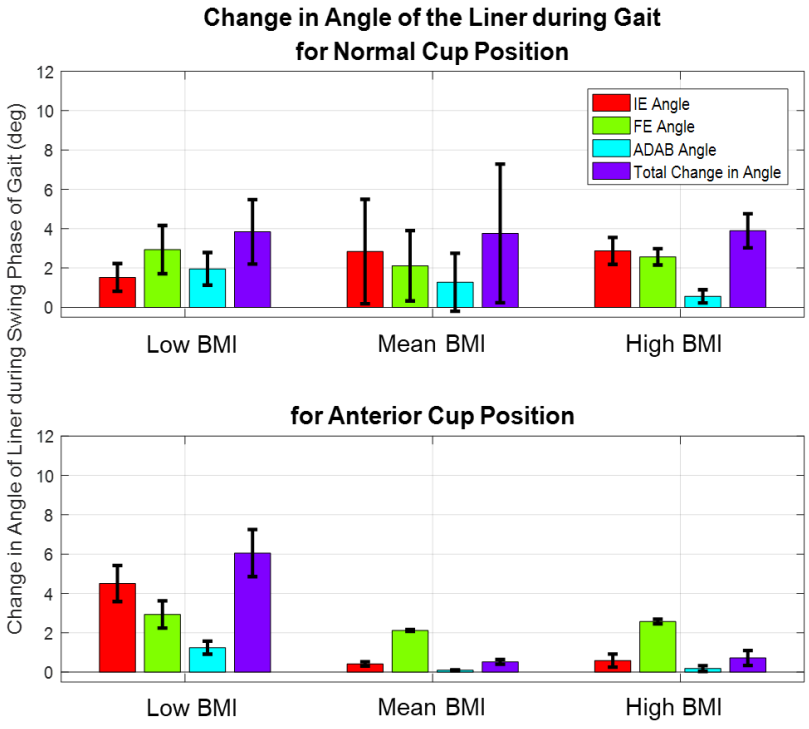

Figure 12: Change in Angle of the Liner during Gait for the two cup positions

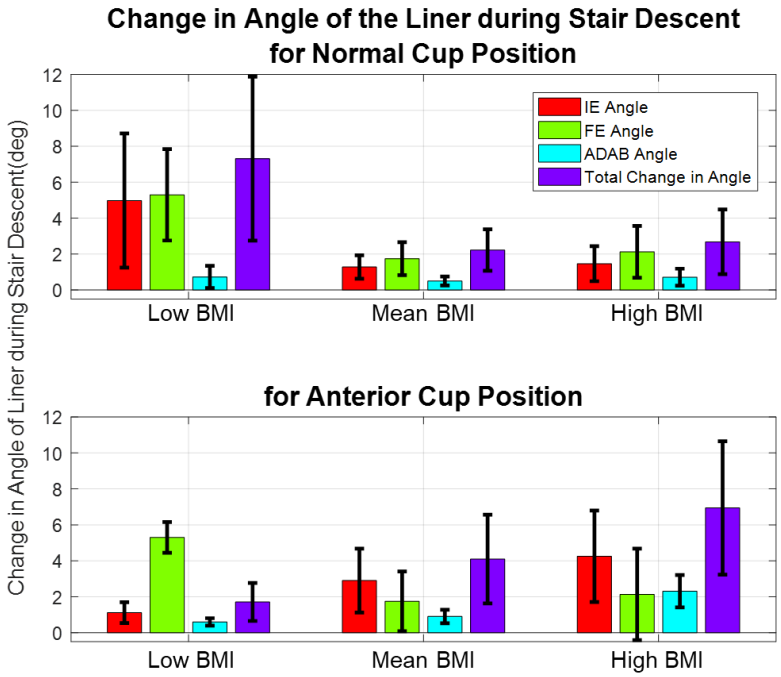

Figure 13: Change in Angle of the Liner during Stair Descent for both cup positions

3.4 Discussion

No consistent changes in motion patterns were seen due to increasing the compressive load or initial bearing position. The results suggest that under modest compressive loads, the friction at the bearing and acetabulum interface overcomes friction at the bearing and femoral head interface to prevent bearing motion. Bearing motions occurred consistently during the swing phase of an activity when hip compression was minimal. One reason conclusive results might not have been seen is when comparing the different BMI's loading profile curves, the difference in load between the three compressive loads is a very small percent of the difference between when the peak force is applied, and the minimal force in the loading curves.

The compressive load, however, was found to have a larger effect on the motion of the bearing than the initial cup position. The position of the dual mobility bearing was set before the bearing contacted the acetabular cup. This was done since the activity would start as soon as the two components contacted each other. This introduced an error because on occasion, when the bearing would contact the acetabular liner, the bearing would shift its position away from the initial position that it was set at. This could sway the results away from a consistent initial bearing position.

One of the goals of this study was to determine if wear was a concern in the dual mobility bearing. Due to the minimal motion that occurred during the ADL's, there exists a reduced wear potential for the device. This study focused on resolving our hypothesis that was aimed at studying the high-loading behavior, rather than the low loading section of the profile curve. Because we found that motion only occurred in the time of low loading, our study was not designed to focus on this section of the loading profile. If we were to repeat this study, we would focus on observing the motion that occurs during swing-phase, or the low-loading mechanics of a cycle.

The collection of the sit-to-stand data presented challenges due to the loss of visibility of the target markers used to track relative motion by the DIC. The loss in visibility occurs when the subject is in the seated position, then leans forward to gain momentum to bring them to an upright position. This excessive flexion, prior to a full extension motion, made the field of view for the DIC cameras hard to capture for the whole cycle.

A major limitation was the fact that this study occurred on 3D printed bone instead of implanted into a cadaveric specimen. The reason for this decision was to maximize the visibility of the implant to be able to use DIC to measure the relative motion between the two components. The visibility of the implant was still limited, so in a future iteration of the study, a better way to capture consistent data will be needed. Fetal bovine serum is the current standard for simulating synovial joint fluid, but this is not a perfect solution found in the joint.

We hypothesized that with increased compressive loading there would be increased bearing friction, thus decreased motion of the polyethylene liner relative to the acetabular shell. We were able to meet our first objective by developing the methods necessary for quantifying bearing motion relative to the acetabular shell. Our second objective to determine how BMI affects bearing motion was not so clearly answered, but from the set-up of our study, we can conclude that BMI should not have an effect on bearing motion due to the small difference in compressive load at the time of peak loading.

CHAPTER FOUR: A Pilot Study on Posterior Dislocation Simulations in THA-Implanted Hips

4.1 Introduction

Total hip arthroplasty (THA) has been proven to be one of the most successful surgeries. Dislocation or instability of the hip joint is one of the leading causes for revision surgery (Bozic et al., 2009, Dobzyniak et al., 2006, Goldman et al., 2019). If the dislocation torque, also referred to as the resistive moment to dislocation, can be calculated for a variety of conditions, then a better understanding of how to minimize dislocations might be found. There is preliminary evidence for repairing the capsule in posterior approach THA's and for this study the hopes are to validate this fact with the pilot study methods presented. By learning that repairing the capsule could be a valuable aspect to a successful THA surgery, the next question is to determine if suture type affects the resistive torque since barbed sutures are gaining in popularity in the field of orthopaedics.

The purpose of this study was to perform posterior dislocation simulations on THA implanted hips, to understand the mechanism for dislocation, and to measure the resistive moment of dislocation. This study was in part designed as a pilot study of methods for future studies.

4.2 Methodology

Two specimen, four hips, underwent a total hip replacement and were implanted with a dual-mobility hip implant design during a surgeon design lab hosted at the University of Denver. One specimen underwent a posterior approach THA and the second specimen underwent an anterior approach THA. The capsule was repaired with a traditional, interrupted suture pattern on the first hip, Vicryl #1 (Ethicon) and the contralateral hip capsule was repaired with a continuous-style Stratafix repair (Ethicon).

To test the resistive moment to dislocation, the hips were mounted into the AMTI VIVO joint simulator via custom specimen-specific fixtures that were created from computerized tomography (CT) scans, as shown in Figure 14. These custom fixtures centered the hip joint with the VIVO center of rotation and allowed for the hips to be mounted in an anatomical configuration, as seen in Figure 15.

Consistent posterior dislocation tests were created to allow the joint simulator to perform the simulations on each hip. The posterior dislocation assessments consisted of the combination of hip hyper-flexion, coupled with constant adduction and internal rotation angles. This combination of motions has been previously shown to cause posterior dislocation in vivo (Nadzadi et al., 2003). The initial position for each test was 75° flexion with neutral adduction (AD) and internal (Int) rotations. A 25N medially directed load was applied at the hip-joint center in addition to a 100N compressive load. A trapezoidal waveform was run from 75 degrees flexion to 105 degrees flexion, holding a constant adduction and internal femoral rotation angle. Flexion profiles were performed at nine combinations of internal rotation and adduction angles, each ranging from 0 to 15

degrees at 5-degree increments. Anterior and posterior movements were allowed to fulfill a zero-load force-controlled condition. If the hip did not dislocate in any of the nine internal rotation and adduction angle assessments, the testing waveform ramped to 120 degrees of flexion, or if needed, 135 degrees with a condition of 0 degrees adduction and 5 degrees internal rotation to try to keep the test as anatomically feasible as possible.

Each component of the moment (flexion-extension moment, internal-external moment, and adduction-abduction moment) were measured directly from the VIVO load cell. The sum of the squares for each moment contribution was taken to find the total resistive moment contribution.

The peak moments were calculated at the time of dislocation, or if the hip did not dislocate, it was calculated at the time of peak flexion. The sutures were then removed, and the waveforms were repeated to quantify the contribution of the sutures. Because one specimen was performed using the anterior approach, the posterior capsule was intact during the initial simulation. Instead of cutting the sutures on the anterior aspect of the capsule, an incision was made on the posterior aspect of the capsule to replicate the posterior incision made during a posterior approach THA surgery. The effect of the anterior approach during these posterior dislocation simulations was assumed to be negligible since that aspect of the capsule is not stressed during posterior dislocation. Finally, all the surrounding tissue and capsule were cut, and dislocation profiles were re-run to quantify the contribution of the remaining capsular structures. With no tissue surrounding the implant, both bone and implant impingement were able to be visually seen and noted to determine the cause of dislocation.

To measure the suture contribution, the difference at every increment during the loading waveform between the sutures intact test and the sutures cut tests were assessed. The differences between the sutures cut moment curve and the full capsule resected moment curve were calculated to find the total capsule contribution. This subtraction of curves allows for a clear distinction to understand the contribution that repairing the capsule provides in the resistive moment to dislocation.

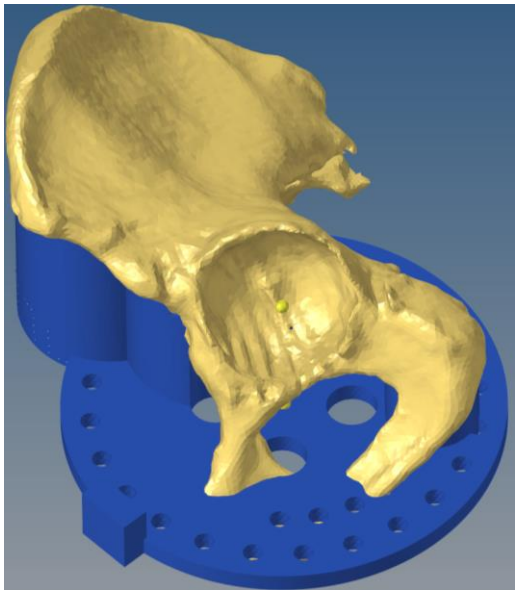

Figure 14: Segmented pelvis model formed to fixture for anatomical alignment

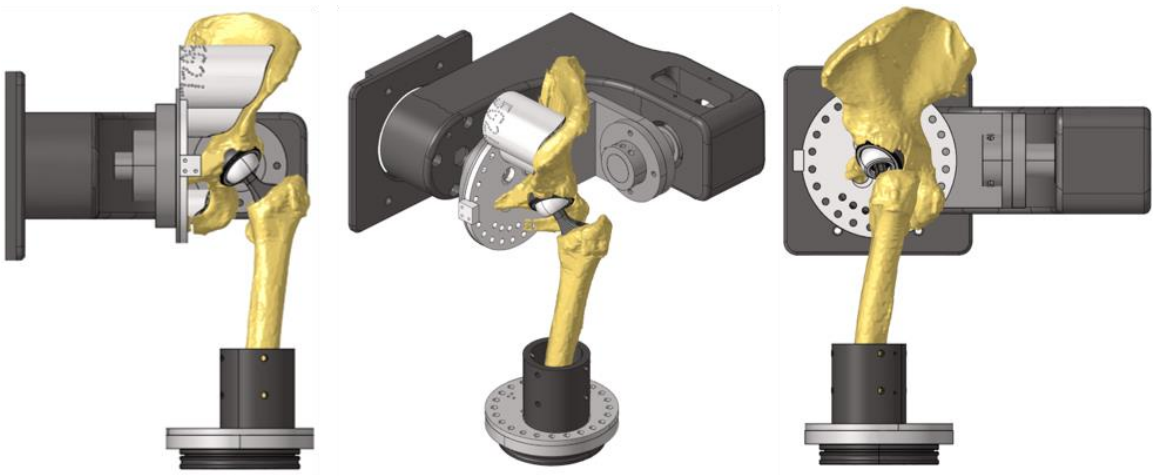

Figure 15: Fixturing set up using CT scanned bone geometries with custom fixturing to mount femoral head center in the VIVO rotation center. The VIVO flexion arm is in black. Left: Anterior view. Middle: Isometric view. Right: Medial view

4.3 Results

During the posterior dislocation tests, the capsule provides a resistive moment that initially increases with flexion, but plateaus at approximately 90° flexion and frequently reduces with increasing flexion, unless an additional impingement event occurs (Figure 19). In this way, the peak resistive moment is not necessarily maximum at the extreme range of motion, or maximum flexion. The peak resistive moment provided by the sutured capsule repair was highly variable between specimen and generally increased with increasing internal rotation and adduction of the femur, indicating these femoral motions stressed the capsule repair. In three of the four specimens, the capsule repair contributed significantly to the overall dislocation resistance of the hip. Figures 17 and 18 show the total resistive moment to dislocation, breaking up the suture contribution and the capsule contribution. The adduction and the internal rotation angles for the different trials are shown with the peak moment seen before impingement occurred. Figure 20

demonstrates the breakdown of angle component contributions at the total peak moment, for one hip, at each of the nine posterior dislocation tests. Figure 21 demonstrates the contralateral side hip that was found to be more resistant to dislocation from the start. To allow the most data to be collected, the low angle adduction and internal rotations were neglected, and only higher-angle adduction and internal rotation tests were performed to attempt at dislocating the hip. Higher levels of flexion were also performed to accomplish this task.

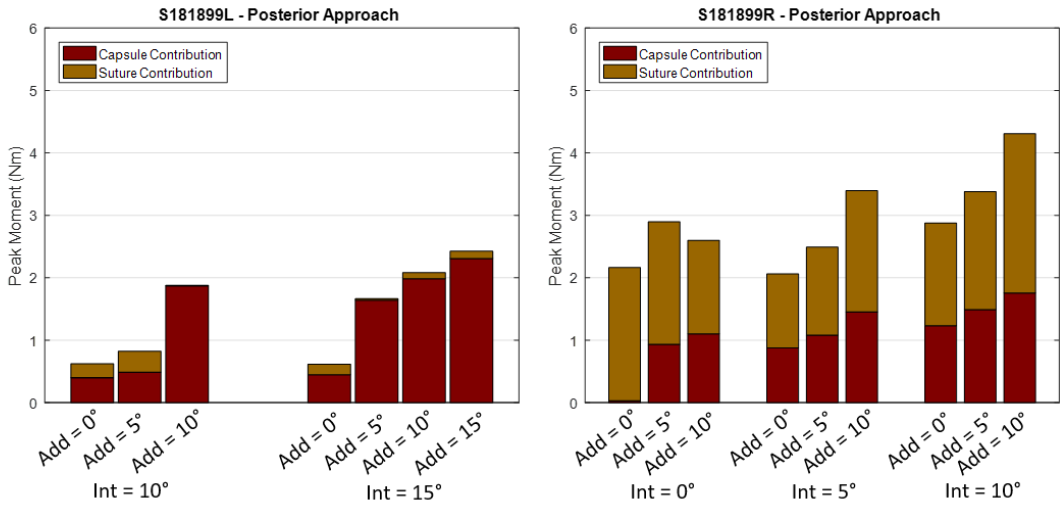

Figure 16: Posterior approach matched-pair hips demonstrating the capsule contribution and suture contribution to dislocation resistance

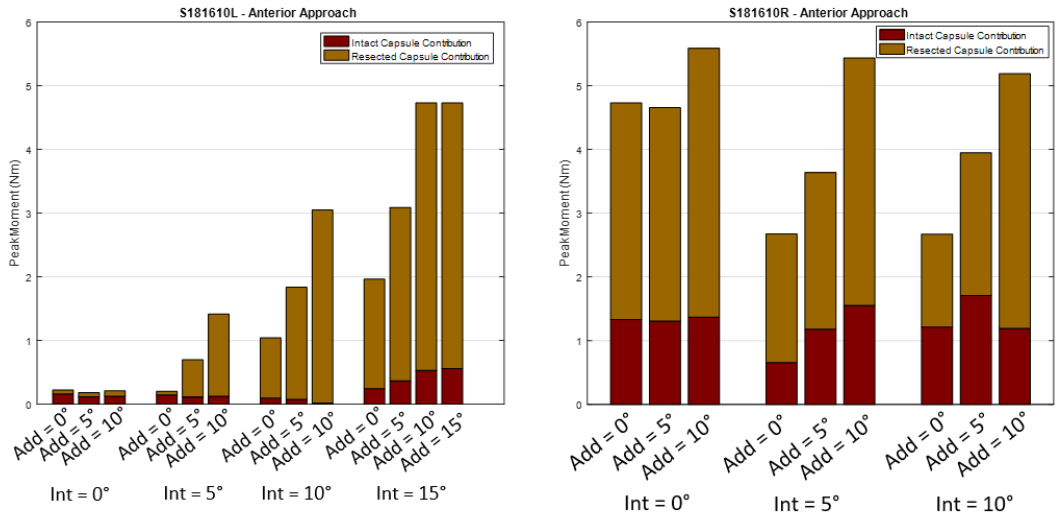

Figure 17: Anterior approach hips tested via posterior dislocation tests comparing the natural intact posterior capsule compared to the posterior cut contribution in the maroon, and the resected capsule contribution in the gold.

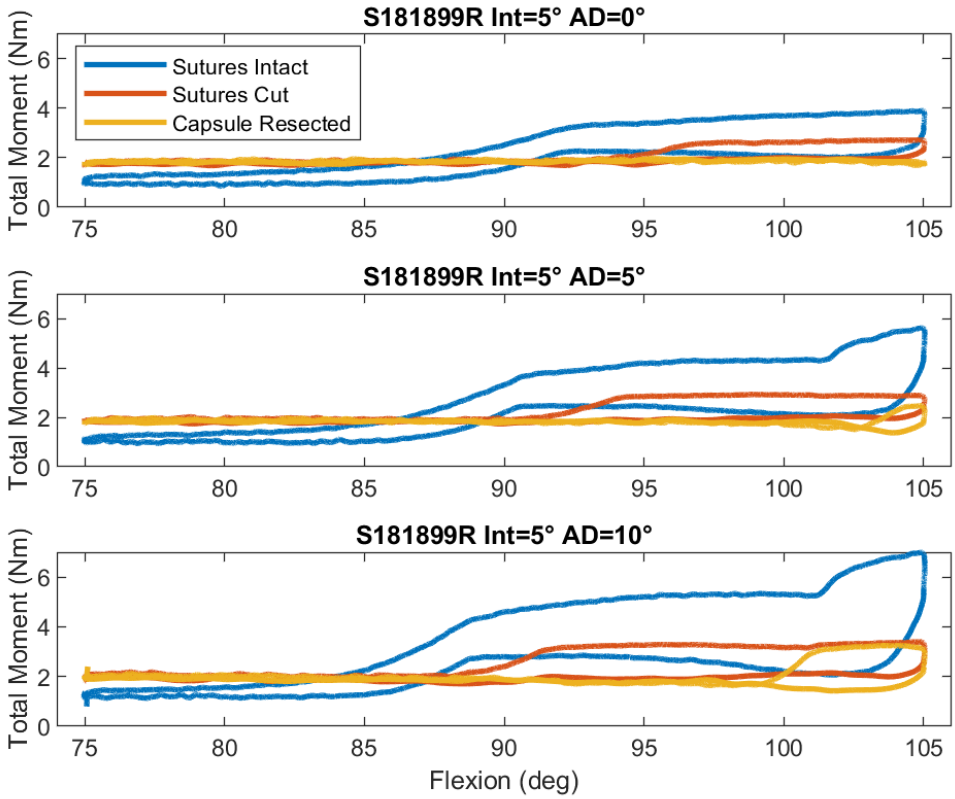

Figure 18: A typical resistive moment curve with increasing knee flexion with the sutures intact, after removal of the sutures, and after removal of all soft tissue for three adduction angles at a constant internal rotation of 5 degrees.

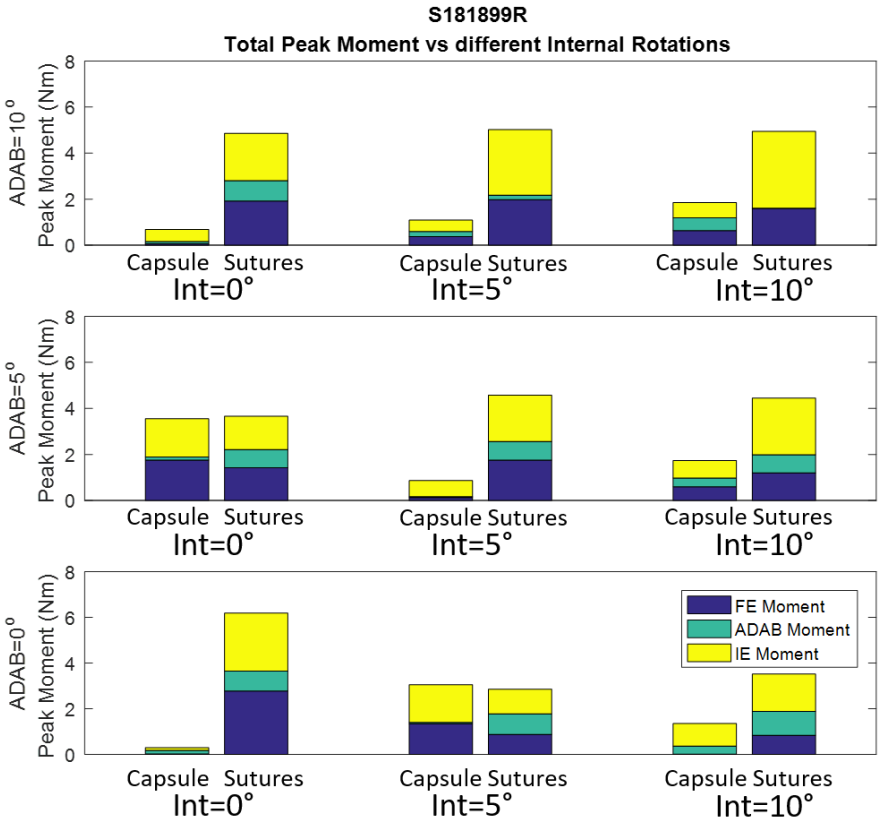

Figure 19: Right side hip total peak moment with components vs different internal rotations at different adduction angles demonstrating the breakdown of the angle components.

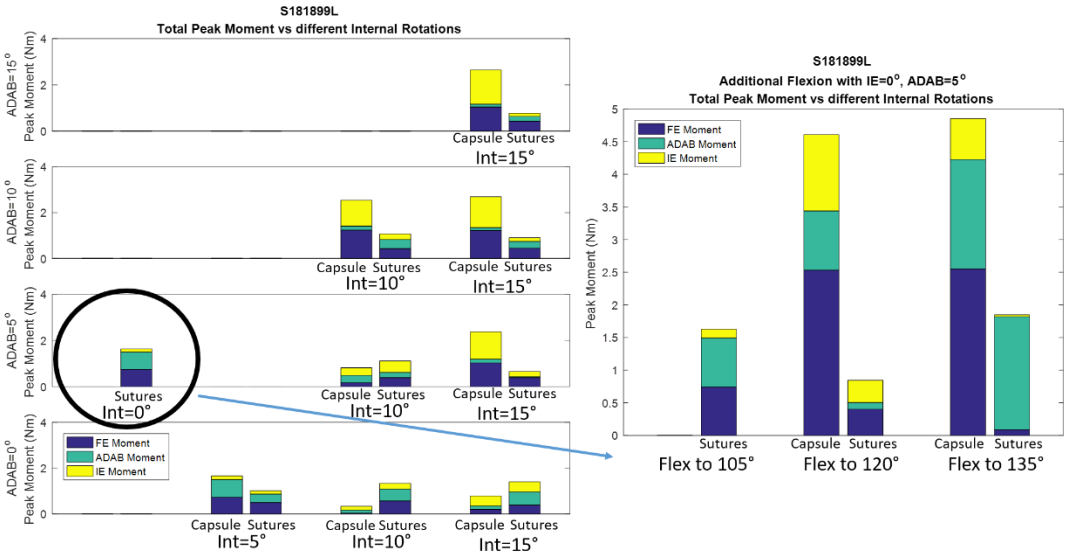

Figure 20: Left side hip, total peak moment with the moment components for a wider variety of internal rotation and adduction to increase moment response demonstrating the breakdown of the angle components.

4.4 Discussion

As internal rotation and adduction increase, the flexion angle at which the hip reaches its peak moment decreases, then levels off and maintains that peak moment value through the duration of the flexion waveform. This might be attributed to the tissue around the hip joint center maintaining its peak distance across the center of the hip as it flexes, and not needing to elongate due to the constant diameter rotation. In Figure 21, the blue line represents the lateral band of the iliofemoral ligament as it attaches to the greater trochanter and the superior aspect of the acetabulum; this ligament model can be seen to not increase as the hip is hyper-flexed from 90° to 120°. Also, as internal rotation and adduction increase, the total moment increases as the capsule and surrounding tissue try to keep the hip from dislocating posteriorly. When the posterior incision was made on an anterior approach hip, one hip dislocated seven out of nine tests, whereas when the capsule was fully intact, it was able to produce a counter-torque exceeding 14 Nm before the test was ended to prevent sensor damage.

Impingement is when contact occurs between either the bone or implanted components between the femur and pelvis. When impingement occurs, there is a sudden increase in the slope of the moment-rotation curve, which then levels off to maintain a constant torque, as seen in Figure 14. Because interest lies in the contribution of the tissue in this test, versus the contribution of impingement that occurred, the value of the moment right before impingement occurred was used to isolate just the tissue and capsule contribution.

Having both anterior and posterior approach hips allowed for a direct comparison between the integrity of the natural posterior aspect of the capsule, a suture-repaired capsule, and an unrepaired capsule. Unfortunately, with only having two specimen, no distinctive conclusions could be made.

Based on the results of this pilot study, when no impingement occurred, there was no inherent force causing the hip to dislocate. Whether impingement occurred was heavily dependent on how the implants were positioned in the pelvis and femur. Variability in the resistive moment provided by the repair was likely due to surgeon-to-surgeon differences in repair technique and the overall tension in the capsule resulting from the implant positioning and the femoral head-offset used.

For a future experiment, we will perform an analysis using CT scans of the implanted specimen to determine the exact position of the pelvis where impingement occurs and leverage this impingement event to drive dislocation of the hip. By increasing the influence of impingement, we will be able to more clearly see the contribution of the implant design to the overall dislocation moment.

In this study we were able to learn ways in which to improve our methods and also validate current methods. The new fixturing system that was proposed and used in this study, which allowed for a better anatomical alignment in the AMTI VIVO joint simulator, successfully met the needs and usability requirements to perform this study. We were also able to effectively measure and quantify the resistive moment experience during laxity assessments as well as dislocation simulations. In being able to measure the resistive moment, we were able to break it down to identify the contribution of the

moment toward the capsule and toward the suture. The methods in this study present an easy and effective way to separate these contributions while also providing the ability to separate the moment induced by impingement.

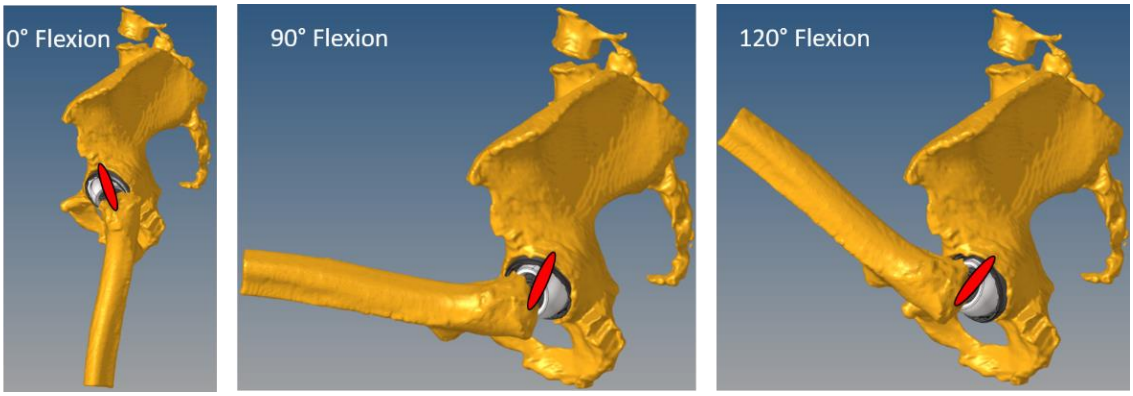

Figure 21:From 90 degrees flexion of the hip to 120 degrees flexion of the hip, the lateral band of the iliofemoral ligament does not increase in length, thus not tightening the capsule more as flexion is increased.

CHAPTER FIVE: The Role of Capsular Repair on the Stability of Total Hip Arthroplasty using the Direct Anterior Approach

5.1 Introduction:

Total hip arthroplasty (THA) is a widely practiced treatment for hip arthritis with the number of surgeries performed growing annually (Bozic et al., 2009). THA is frequently performed through a posterior approach (PA) or direct lateral approach to enable access to the hip joint. More recently, THAs performed using the direct anterior approach (DAA) have become commonplace due to reported reductions in muscle trauma and faster recovery rates (Maldonado et al., 2019).

Hip dislocations and revisions due to instability are common complications with both PA and DAA techniques (Goldman et al., 2019, Bozic et al., 2009, Dobzyniak et al., 2006). A recent retrospective study by Angerame et al found equivalent short-term revision rates between PA (1.39%) and DAA (1.69%), but the etiology of revisions differed. Excluding infection, instability was the primary cause of revision for PA (32.2% of revisions, incidence rate of 0.49%). Instability accounted for 14.6% of revisions in the DAA cohort for an overall incidence rate of 0.25%. Other retrospective studies have reported higher incidences of hip instability for DAA ranging from 0.4% to 1.3% (Sali et al., 2019, Malek et al., 2016, Aggarwal et al., 2019) and 0.5% to 0.8% for PA (Malek et

al., 2016, Aggarwal et al., 2019). Revisions rates for instability likely underestimate overall hip dislocation rates, with only recurrent dislocation leading to revision surgery.

Studies that quantify the risk of instability in THA rarely control the capsular repair technique used. Multiple studies have demonstrated that capsular repair leads to lower dislocation rates when using the PA (Hernández et al., 2018, Kwon et al., 2006, Mihalko et al., 2004), direct lateral approach (Hughes et al., 2015, Kwon et al., 2006), and anterolateral approach (Lu et al., 2019, Kwon et al., 2006). Using the anterior lateral approach, Lu et al. (2019) observed a 5.2% dislocation rate when not repairing the capsule, compared to 0.7% when repaired. The clinical value of capsular repair in DAA is more controversial. Some surgeons perform an anterior capsulectomy to gain better access to the joint while others strive to retain and repair the iliofemoral ligament. Understanding the contribution of the capsular repair to the resistive moments at the hip during movements known to cause dislocation may offer insight into the value of the capsule in preventing dislocation.

Efforts to increase operating room (OR) efficiency require careful consideration for each step of the surgical process. Barbed sutures have experienced increased use during joint arthroplasty procedures due to reduced surgical times compared with traditional interrupted sutures (Li et al. 2018, Borzio et al., 2015, Lin et al., 2016). Use of barbed sutures have also been associated with decreased wound ooze (Knapper et al., 2019) and lower superficial infection rates (Thacher et al., 2019). It is unclear how the use of barbed sutures affects the repair strength and function after joint arthroplasty,

especially for repair of the anterior capsule in DAA. Improved hip stability with capsular repair would help justify the increased surgical time required to perform the repair.

The purpose of this study was to quantify the contribution of capsular repair to the stability of the hip during DAA THA and determine if the type of suture used influenced capsule function. We hypothesized that capsular repairs would increase the constraint provided to the hip during motions known to cause anterior dislocation and that use of barbed suture would increase hip stability over a traditional interrupted repair.

5.2 Methods:

Six fresh-frozen pelvis-to-toe cadaveric specimen (12 hips) underwent DAA THA using a Hana® table (Mizuho OSI, Union City, CA), performed by a board certified orthopaedic surgeon experienced with DAA. CORAIL® femoral stems and PINNACLE® acetabular components with 32-mm head and +1mm offset were implanted into all specimens (DePuy Synthes, Warsaw, IN). After implantation, two alternate types of capsule repair were performed on contralateral hips. The first hip of each specimen was repaired using three interrupted #2 VICRYL® (Ethicon, Somerville, NJ) sutures and the second side repaired with continuous barbed suture (STRATAFIX™ Symmetric, Ethicon, Somerville, NJ) (Figure 22). The side of the specimen receiving each repair type was randomized prior to surgery.

After surgery, the hips were dissected from the specimen with care taken to preserve the capsular attachments. Custom fixtures were designed and 3D-printed for each hip to enable mounting and alignment into an AMTI VIVO joint simulator (AMTI, Watertown, MA) (Figure 23). Fixtures were designed based on CT-reconstructions of the

pelvis to interface with the unique curvature on the medial face of the ilium and position the pelvis such that the center of curvature for the acetabulum was coincident with the rotational degrees-of-freedom (DoF) of the simulator. The fixtures also enabled the accurate definition and registration of the pelvis' anatomic coordinate system derived from CT-landmarks to the flexion-extension (F-E), adduction-abduction (Ad-Ab), and internal-external (I-E) rotational axes of the VIVO. Hip resistive moments during simulations were measured through a 6 degree-of-freedom load cell at the base of the femur. Loads from the load cell were transformed into moments about the head center in the pelvic coordinate system. A head center calibration was performed with the specimen in the VIVO whereby a 1000-N compressive load was applied to the hip in full extension and the head center location adjusted to balance out any residual moments. In this way,

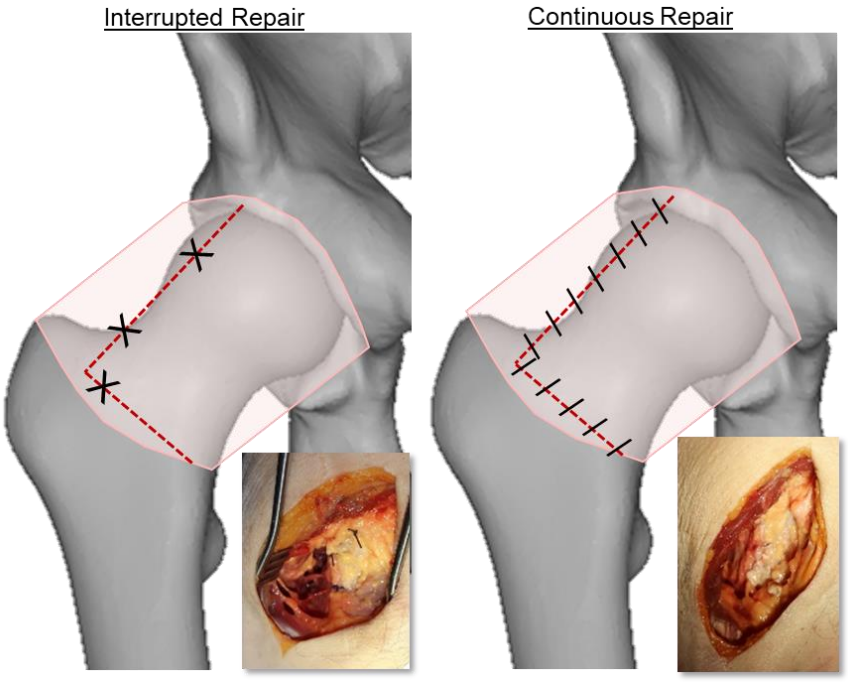

Figure 22: #2 VICRYL interrupted suture repair (left) and STRATAFIX barbed continuous suture repair (right). Dashed red lines indicate the location of the capsular arthrotomy and the black lines indicate suture locations.

controlled rotations could be applied directly to the hip joint using the VIVO's integrated control system while the resulting hip resistive moments were accurately measured.

An auxiliary optical tracking system (Optotrak Certus™, NDI, Ontario, Canada) was used to track rigid arrays mounted directly to the pelvis and femur. After testing, the bony and implant geometries were digitized and registered to the CT-reconstructions of the bones and implant models provided by the manufacturer. 6-DoF kinematics of the hip were calculated using the ISB-recommended definitions (International Society of Biomechanics, 2002). Use of the auxiliary optical tracking system to directly measure hip kinematics reduced errors associated with compliance of the loading rig and the associate fixturing.

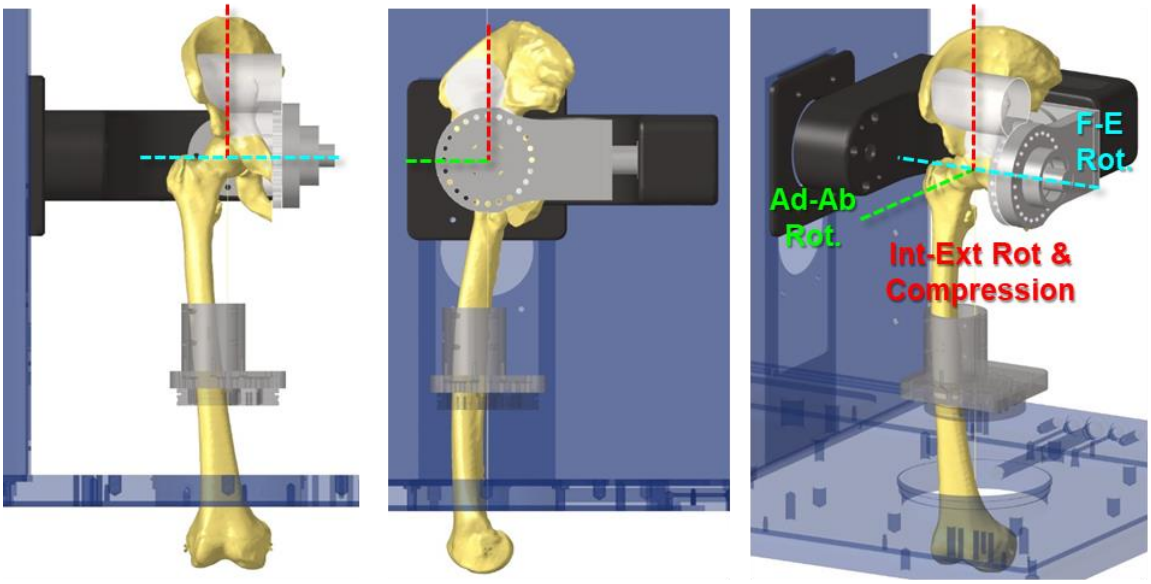

Figure 23: Segmented bony anatomy was used to ensure specimen were accurately mounted into the VIVO simulator. Custom fixtures were 3D printed to center the femoral head at the intersection of the F-E, Ad-Ab, and I-E axis of the simulator and align the specimen's anatomic axis with the simulator coordinate system.

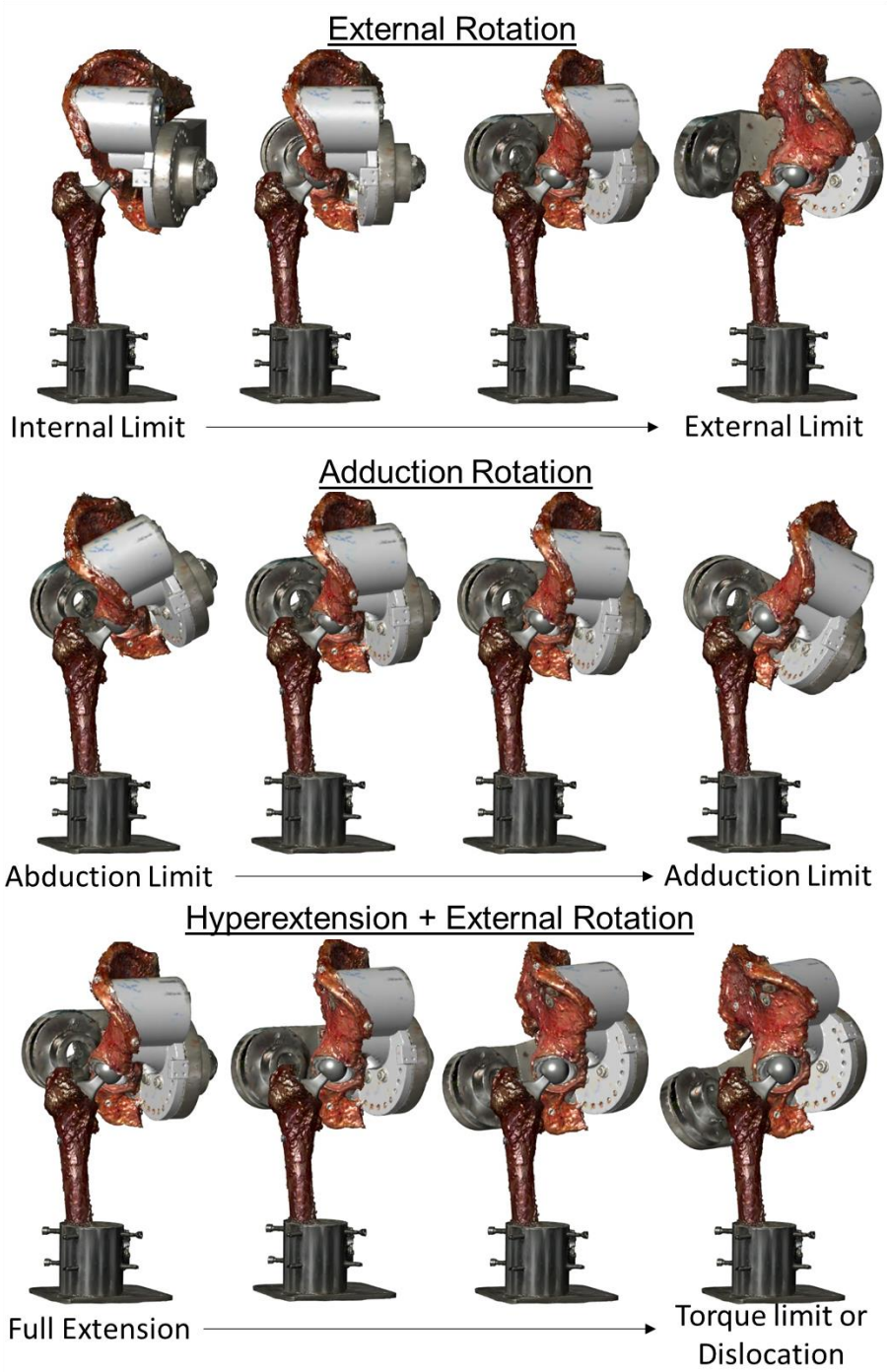

Figure 24: Step-by-step animation of the IE rotation laxity test, the ADAB laxity assessment, and the anterior dislocation simulation by hyperextending and externally rotating. Kinematics captured the exact location of the bones at every point in time.

The hips were subjected to loading profiles that assess capsular function during movements associated with anterior dislocation, specifically turning the upper body away from the operated hip from the standing position (Nazadi et al., 2003). This maneuver induces external, adduction, and extension rotations at the hip which are also known to stress the anterior capsule. To recreate this motion, three loading profiles were applied: an isolated internal to external rotation, an isolated abduction to adduction rotation, and combined hyper-extension with external rotation (Figure 24). The simulations started from an initial position with the hip fully extended and with a 100-N compressive load and 25-N medial load applied to the femur. I-E and Ab-Ad loading profiles initially ramped to the internal/abduction rotational limit, then rotated to the external/adduction limit following a trapezoidal waveform over the time of 140 seconds. Rotation limits were set to generate approximately 5 N-m moments at the hip for the isolated rotations. In a similar fashion, the extension with external rotation simulation started from the full extension position and ramped with into hyper extension with 1° of external rotation per 1° of extension until dislocation or until the peak resistive moment approached 10 N-m. Resistive moments were recorded about the F-E, Ad-Ab, and I-E axes throughout the simulation and a total resistive moment was calculated as the square root of the summed squares of the rotational moment components.

Following characterization of the repaired capsule, the sutures were removed, and the mechanical tests were repeated to quantify the contribution of the sutures to the total resistive moments at the hip. In the final iteration, all of the remaining capsular soft tissue surrounding the hip was removed and the mechanical tests were repeated, providing the ability to observe any bone and/or implant impingement at the extreme ranges of motion.

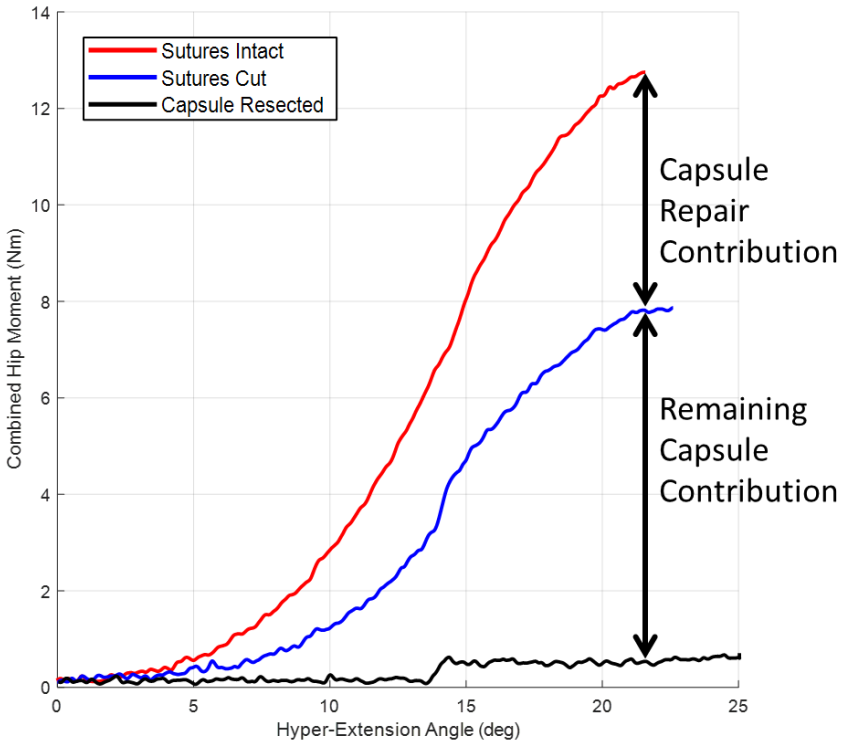

Figure 25: Definition of capsule contribution and suture contribution from the three set of tests that were performed.

The overall contribution of the capsular suture repair to the total hip resistive moment for each activity was calculated as the difference in measured moments between corresponding trials with the sutures intact and after the sutures were removed. Likewise, the contribution of the remaining hip capsule was calculated as the difference in measured moments between corresponding trials with the sutures removed and the completely resected hip capsule (Figure 25). To normalize the relative contribution of the

sutures and the remaining capsule, the moment contribution of each structure was divided by the peak moment observed during the trial. The resistive hip moments for each suture type and each activity were averaged across specimen and a 2-way analysis of variance (ANOVA) with Tukey post-hoc tests performed to detect statistically significant differences ($p < 0.05$).

5.3 Results:

The capsular repair increased the resistive moment of the hip for all specimens during all activities and with both suture types, however, the magnitude of the increased resistive moment varied between specimens. During the external rotation movement, the suture repair provided 38.3 ± 24% of the total resistive moment (3.1 ± 2.6 Nm for intact sutures versus 1.9 ± 1.5 Nm after suture removal). Due to the complex nature of the capsule, the applied external femoral rotation induced coupled flexion and adduction moments along with an internal moment of the hip. Of the coupled moments, the sutures contributed primarily to the flexion moment (40.3 ± 42%) and to a lesser extent the adduction (25.2 ± 41%) and internal resistive moments (42.6 ± 25%). Figure 26 shows the breakdown of the moment component contributions for internal-external rotation laxity assessments.

During the adduction movement, Figure 27, the suture repair provided 27.5 ± 30% of the total resistive moment (3.9 ± 2.3 Nm for intact sutures versus 2.9 ± 2.2 Nm after suture removal). Similar to external rotation, the adduction rotation induced coupled flexion and internal moments of the hip. Unlike the external rotation, the sutures

contributed equally to all components of the coupled moments (29.5 ± 33% for flexion, 26.7 ± 31% for adduction 17.3 ± 37% internal moments).

The suture repair provided 23.7% ± 19% of the total resistive moment during the hyper-extension and external rotation movement (5.8 ± 2.1 Nm for intact sutures versus 4.5 ± 2.0 Nm after suture removal), the lowest relative contribution of the three activities, as observed in Figure 28. For the coupled moments, the sutures primarily contributed to the flexion and internal components of the resistive moment (27.0 ± 17% and 28.8 ± 23%, respectively) compared to 22.1 ± 27% for the adduction moment. Capsular repair contributions to internal and abduction femoral rotations were negligible.

No statistically significant differences were observed based on the type of suture used (continuous versus interrupted) for any of the activities. During external rotation, the interrupted suture contributed 33.5 ± 32% while the continuous suture contributed 42.9 ± 15%. During adduction, the interrupted suture contributed 27.7 ± 27% while the continuous suture contributed 27.5 ± 35%. During the hyperextension and external rotation movement, the interrupted suture contributed 26.4 ± 17% while the continuous suture contributed 20.9 ± 21%.

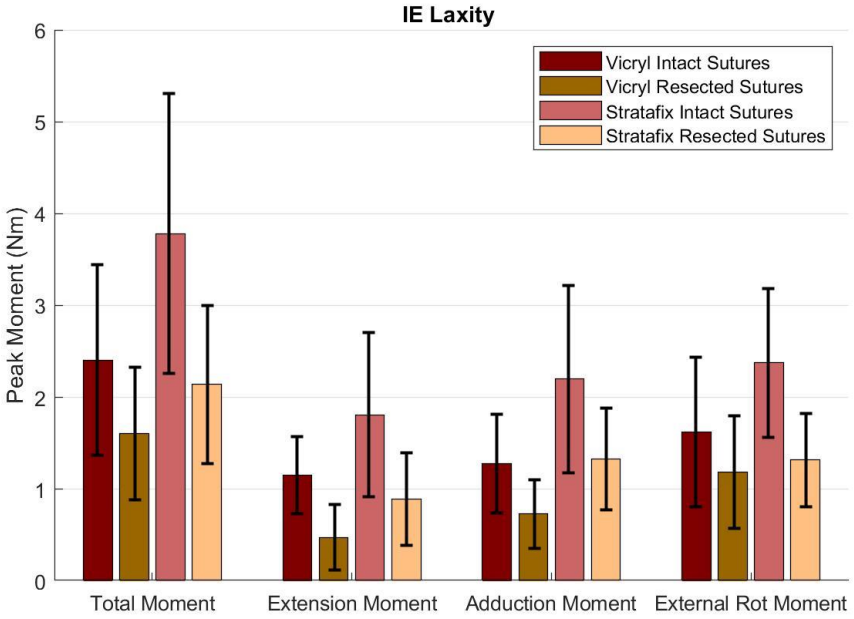

Figure 26:Breakdown of moment components for the Internal and External Rotation laxity assessment.

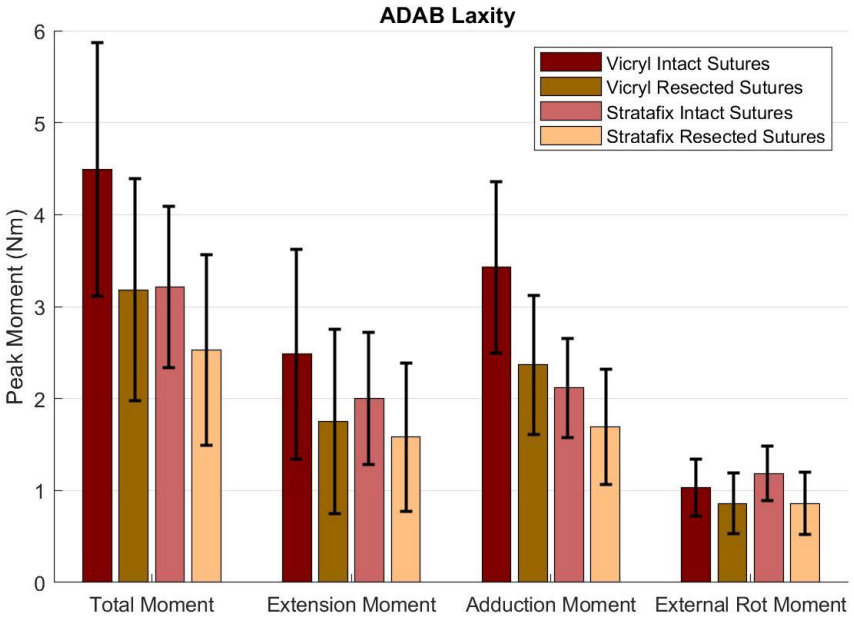

Figure 27: Breakdown of moment components for the Adduction and Abduction Rotation laxity assessments.

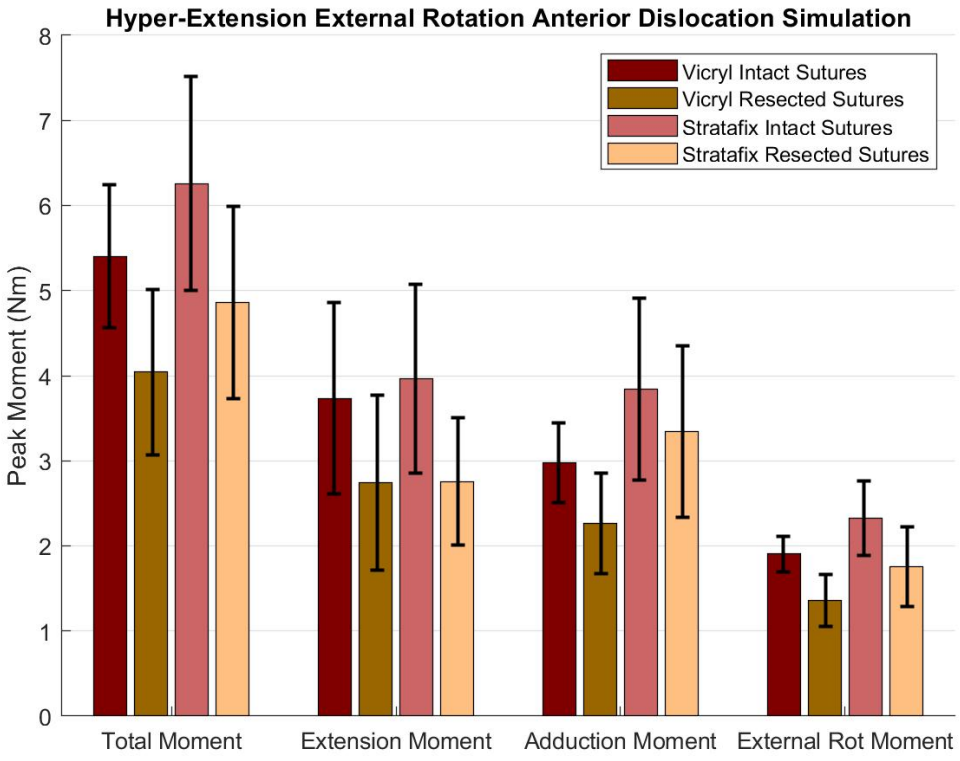

Figure 28: Breakdown of moment components for Anterior Dislocation simulation by hyper-extending and externally rotating.

5.4 Discussion:

Repair of the anterior capsule after DAA-THA contributed between 24% and 38% to the total resistive moments at the hip during motions that are known to induce anterior dislocation, including external rotation, adduction, and hyperextension.

The iliofemoral ligament (IFL) spans the anterior aspect of the hip, originating proximal to the superior aspect of the acetabular rim with a medial arm that transverses distally to the distal intertrochanteric line and a lateral arm that transverses distal and laterally to the greater trochanteric crest (Martin et al., 2008). Previous biomechanical investigations have shown that the IFL resists external rotation of the extended hip and

hyperextension (Martin et al., 2008, Myers et al., 2015) and observed increased external range of motion after arthroscopic capsulectomy and hip resurfacing (Bayne et al., 2014). Our results are consistent with the previous literature, showing that the capsular repair had the highest contribution to external rotation (38.2 ± 24%), followed by adduction (27.5 ± 30%), and hyperextension (23.7 ± 19%) with negligible contributions to abduction and internal rotations at neutral hip extension.

The biomechanics of anterior hip dislocation are not well understood, and descriptions are primarily based on anecdotal observations of patients performing an axial twisting motion in the extended hip position. Previous studies of hip dislocation highlight the role of implant or bony impingement on initiating a dislocation event. Depending on the alignment of the cup and combined version of the femur, external femoral rotation of the extended hip can induce impingement between the femoral neck and the distal posterior quadrant of the acetabular component. This impingement is more pronounced with hyperextension of the hip and likely contributes to anterior dislocation events. Component-component impingement was frequently observed in our study during the hyperextension and external rotation motion and was detectable by a sudden increase in hip moments.

Previous studies have focused on isolated changes in hip laxity associated with capsular resection, but none have documented the individual moment components of the overall reaction moment at the hip. The results from the current study highlight the complex function of the capsular structures in the form of the coupled moments about the hip's rotational degrees of freedom. We observed that during external hip rotation with an

intact capsular repair, 44.9 ± 16.1% of the moment was in the internal direction, 31.0 ± 11% was in adduction, and 24.1 ± 15% was in flexion. Removal of the capsule sutures experienced the same flexion percentage (22.5 ± 14%) of the total moment, yet the internal rotation and adduction components of the moments flipped in dominance (35.2 ± 13% and 42.3± 17% reduction, respectively. Without the sutures, the primary moment resisting external hip rotation was in the adduction direction (42.3 ± 17% of total moment). It is known that the healthy capsule works as an integrated structure to prevent the hip moving into vulnerable positions, so the loss of coupling between these moment components could increase susceptibility to dislocation, primarily when moving into external rotation.

Previous reports have shown that continuous sutures provide greater wound closure forces and greater pull out strength compared to interrupted repairs (Khair et al., 2017). The capsulotomy used for DAA-THA runs parallel to the fibers of the lateral arm of the IFL from the proximal rim of the acetabulum to the anterior crest of the greater trochanter, then traverses distally and medially along the intertrochanteric line through the fibers of the medial IFL. The stress applied to the IFL during the hyperextension movement was primarily parallel to the incision and did not stress the capsular repair perpendicular to the incision. This may be why we did not observe significant differences based on continuous or interrupted sutures.

Despite the contribution of these structures to the stability of the hip, it is common practice for many surgeons to not repair these structures after THA. Our results do indicate that the residual components of the IFL and the remainder of the capsule

contribute significantly to the resistive moments of the extended hip and may be sufficient to stabilize the hip. During dissection and testing, the continuous repair technique was more robust while the interrupted sutures would occasionally untie with stress. The continuous suture type was able to connect the two sides of the capsule where it was difficult to find where the suture repair was done.

It is important to note that the objective of the laxity assessments was not to dislocate the hip but to simply bring the hip to a range of motion in which the hip capsule exhibited a torque response. The simulated anterior dislocation, through hyper-extension and external rotation, found the absolute maximum torque the anterior capsule and sutures are able to resist prior to dislocation.

The results of this study demonstrate that while capsule repair increases the resistive moments at the hip in full extension, the remaining capsule also provides substantial resistance to external, adduction, and hyperextension rotations. The latent contribution of the remaining capsule and scarring of the capsule during recovery may help explain clinically observed low dislocation rates during anterior approach THA even when the capsule was not repaired.

The limitations of this study include the fact that the cadaveric hips used were dissected and the skin and surrounding muscles were removed from around the pelvis and femur. The pelvis was separated into the left and right sides at the sacroiliac joint so they could be tested independently of each other. Despite the anatomically aligned fixtures, it was difficult to perfectly orient the pelvis and femur, therefore introducing a small error in alignment. For future studies, we have developed a more structured method and rig to

be able to secure and align the bones to their fixture with more precision. The direct strength of the suture was not measured. A final limitation is all surgeries were performed by one surgeon.

In conclusion, the results of this study highlight the benefits of surgical capsule repair during anterior approach total hip arthroplasty due to the added resistive moment the sutures provide in resisting dislocation.

CHAPTER SIX: Dual Mobility Dislocation Resistance Comparing Approach and Capsule Repair through Laxity and Dislocation Simulations

6.1 Introduction

Total hip arthroplasty (THA) is one of the most successful orthopaedic surgical procedures with the leading cause for THA failure as instability and dislocation in the joint (Bozic et al., 2009, Dobzyniak et al., 2006, Goldman et al., 2019). To attempt to solve this problem, the concept of the dual mobility implant was founded, creating two articulating surfaces. With these two moving interfaces, the implant allows for more range of motion before impingement between the femoral stem and acetabular cup occurs. The larger head size that the dual mobility implant provides, also increases the jump distance, to minimize the dislocation risk.

Dual mobility hip implants have been proven to reduce dislocation, as both a primary implant and as a revision implant (Dubin et al., 2020, Jonker et al., 2020). Quantifying the resistive torque that the hip provides during a dislocation simulation is important in understanding how to prevent dislocations from occurring.

The purpose of this study was to quantify the effects of surgical technique in dual mobility implants on dislocation resistance and to determine and understand the points and modes of impingement. By keeping all of the soft tissue and skin intact, this allows a more realistic look at impingement analysis and mechanisms by introducing soft tissue

and skin impingement conditions that computational models have not explored. In the future, this data will be used to further develop computational models of the hip. A secondary purpose to this study was to determine the ranges of motion at which impingement occurs, its relationship to surgical approach, and to compare the dislocation resistance of a dual mobility implant to a conventional implant.

6.2 Methodology

Six fresh-frozen specimen were implanted with dual mobility THA components. Twelve different surgeons performed the surgeries, representing a wide range of skill and techniques.

Each specimen had anterior approach and posterior approach surgical techniques performed on contralateral hips, with the approach side randomized. All anterior approach hips were implanted with Corail stems (DePuy Synthes) and four posterior approach hips were implanted with the Summit stem (DePuy Synthes) and the remaining two posterior approach hips were implanted with Corail stems. Both anterior and posterior approach hips were implanted with Pinnacle shells (DePuy Synthes) and SERF dual-mobility heads, as a part of the Bi-Mentum implant system by DePuy Synthes. Table 1 in the appendix provides specimen and implant information.

After surgery, the pelvis was extracted from the specimen and separated into hemi-pelvi at the pubic synthesis and sacroiliac joints, while the femur was sectioned mid-shaft. The capsule structures surrounding the hip, the soft tissue, and the skin, were preserved.

6.2.1 Impingement Analysis

Computerize tomography (CT) scans were performed pre- and post-surgery on each hip to identify bone geometry and implant placement. The pre- and post-surgical scans were segmented to create three-dimensional computerized models using ScanIP (Synopsis Inc., Mountain View, CA). The three-dimensional (3D) component models of the pelvis, femur, acetabular components, and femoral stems were aligned to their segmented geometries. The pre-operation models were brought into an anatomic Grood and Suntay coordinate system (Grood and Suntay, 1983). The post-surgical scan was then aligned to the pre-surgical scan. Implant alignments were determined, noting the acetabular cup inclination angle, anteversion angle, and femur anteversion angle relative to the hip anatomic coordinate systems. Dynamic movements of the computerized solid models were then applied using a custom MATLAB script. Each hip model was brought through a full range of motion in adduction, abduction, internal, and external rotations at full extension, 30° flexion, 60° flexion, and 90° flexion, while keeping other degrees of freedom in a neutral position. A second set of tests was performed applying flexion and extension while keeping the remaining degrees of freedom in the neutral position. A final set of tests were performed to simulate both an anterior and posterior dislocation. The anterior dislocation simulation used a combination of hyper-extension and external rotation, increasing at an equal rate. The posterior dislocation simulation started at 90° flexion, internally rotating and flexing, while adducting at half the rate. These dynamic simulations were run until impingement occurred, and the mechanism for impingement was noted as either bone-on-bone, bone-on-component, or component-on-component

impingement. Analyses comparing surgical approach, anteversion and inclination angle, and impingement angle were performed to determine similarities between these variables as part of another graduate student's research.

6.2.2 Experimental Testing

After the impingement analyses were complete, the experimental testing aspect occurred using the six fresh-frozen specimen. Custom specimen-specific mounting fixtures, which conformed to the internal face of the iliac crest, were fabricated to mount each hip into the AMTI VIVO joint simulator. These fixtures incorporated the anatomic coordinate system of the pelvis to ensure the hip joint center was oriented at the machine center. Once the hip was mounted in the VIVO, a calibration procedure was performed to ensure that the virtual hip center, about which moments are calculated, was coincident with the femoral head center of the THA implant. This operation reduced erroneous moments measured by the VIVO associated with changes in the head center after the THA surgery was performed. This procedure isolated the contribution of the implant and soft tissue to the dislocation resistance by zeroing all artificial moments.

Using our impingement analysis data based off the CT scans and computer models, VIVO loading profiles were developed. To validate our impingement methods and understand the motion of each hip, adduction, abduction, internal, and external rotation tests were performed at the four flexion angles: full extension, 30° flexion, 60° flexion, and 90° flexion. The purpose of these laxity assessments was to determine the point of impingement in order compare with pre-testing predictions. Given the VIVO mechanical limits, the tests were planned accordingly to make sure a torque response,

either from the contribution of the capsule or due to impingement, was produced. The improved fixturing design allowed for increased internal and external rotations in increments of 15° and a 30° increment for adduction and abduction to address previous limitations on the VIVO range of motion. The starting point for each test was determined by hand, choosing the rotation when a slight resistance in torque could be felt in the direction of interest. This ensured the full torque-rotation curve for the specimen could be collected prior to encountering the physical limits of the VIVO.

Each of the four rotations (adduction, abduction, internal, and external rotation) were performed for the four flexion angles (0° flexion, 30° flexion, 60° flexion, and 90° flexion). Each test was run in force-control with the angle of interest run at a trapezoidal waveform ramping up to 5Nm. The flexion angle was held constant and the off-directional rotation was held constant in displacement control. The compressive load applied was 50N, with its purpose of keeping the femur in the acetabular cup. There was a 10N load applied medially to keep the femur head in the pelvic cup. A load controlled 0N anterior-posterior constant was applied to allow for the anterior-posterior motion to occur. Rotations and loads were measured across the waveform.

Following the laxity assessments, dislocation simulation tests were performed. Despite the surgical approach of the hip, both the anterior and posterior dislocation simulations were performed, with focus on the dislocation profile associated with the surgical approach (e.g. posterior dislocation for posterior-approach specimen). Due to the necessary incision into the capsule, the dislocation profile correlating to the surgical

approach is more likely to dislocate due to the lack of integrity in that aspect of the capsule.

The purpose of the anterior dislocation test was to create a movement where the anterior capsule was fully exposed, allowing the head of the femur to leave the pelvic acetabular cup. For the anterior approach dislocation simulation, hyper-extension and external rotations was applied using a displacement-controlled profile. The hip started at full extension, then would hyper-extend and externally rotate at a constant rate up to 30° of hyper-extension and 30° of external rotation. If a dislocation did not occur during this simulation as indicated by a drop in the resistive moment, then it was noted that the hip was not able to dislocate. Any movement past this point was deemed unphysiological. During the simulation, the abduction-adduction axis was displacement-controlled in the neutral position. Anterior-posterior translations maintained 0N using load-control with a mild compressive and a 25N medial load applied to stabilize the hip joint. Realtime loading feedback from the VIVO was monitored to prevent excessive loading of the hip and determine if dislocation had occurred. Maximum torques limits were instated to ensure capsule and soft tissue damage or sensor damage did not occur (12 Nm for anterior-approach hips and 6 Nm for posterior-approach hips).

The posterior dislocation simulation was performed in a similar fashion, but the hip started at 90° flexion and flexed into maximal flexion. The hip was internally rotated at the same rate that flexion occurred and adducted at half the rate of flexion. With all three of these rotations in displacement control following a ramp function, compressive and medial loads were applied to keep the femur head in place, while setting anterior-

posterior in a 0N load-controlled state. The combination of hyperflexion, internal rotation, and adduction created an impingement event that induced a posterior dislocation through the posterior aspect of the capsule. If the torque response during the dislocation simulation exceeded 12Nm for posterior approach hips or 6Nm for anterior approach hips the test was aborted. All tests were run at a quasi-static rate of 66 degrees per second, or one cycle per 140 seconds, to reduce hysteresis within the soft tissue.

For each dislocation simulation, three different compressive loads were applied: 50N, 100N, and 200N. Varying the compressive load will enable isolating the resistance to dislocation provided by the soft tissue, which remains constant with increasing compressive load, from the resistance provided by the implant, which increases with increasing compressive load. Although these compressive loads are less than physiological values, they enable differentiation without inducing excessive artificial moments from alignment of the VIVO head center and the specimen head center.

After completion of all 22 tests (adduction, abduction, internal, external laxity assessments for flexion angles of 0°, 30°, 60°, 90°, with three anterior dislocation tests and three posterior dislocation tests), the sutures were removed from the arthrotomy. The same battery of tests were repeated to quantify the contribution of the sutures to the resistive moments.

In the third iteration, all soft tissue on the hip, such as the skin, fat, musculature, and the hip capsule were removed leaving only the bone and implants. Selected simulations were performed, including the dislocation simulations and laxity assessments where impingement was predicted within the physiological range of movement. The

purpose of these tests were not to evaluate laxity, but to validate our pre-testing predictions for the angle of impingement. Since there was no tissue surrounding the hip to cause impingement that was not accounted for in the computerized model, we were able to determine clearly the point of impingement via bone and component mechanisms.

For the final iteration, the dual mobility liner and head were extracted from the pelvis and femur, respectively, and a conventional THA head and liner were implanted in their place. The purpose of implanting a conventional THA implant was to be able to directly compare the dislocation resistance to the dual mobility implant. For this condition, the anterior and posterior dislocation simulations were run at all three compressive loads.

To accurately track the motions of the pelvis and femur, in addition to the AMTI VIVO feedback, we used an active marker tracking system (Optotrak Certus, NDI). Two marker clusters were attached to the femur to allow visibility in extreme external and internal rotations, a marker cluster was attached to the pelvis, and a cluster was attached to the flexion arm of the VIVO. Because the pelvis and femur were assumed to be rigid bodies, we could determine the location of all points on the pelvis and femur throughout the cycle with these marker clusters.

With the femur and pelvis soft tissue fully resected, the bone and implant geometry were white-light scanned using the Artec Space Spider. These three-dimensional scans were converted into solid models which were overlaid with the CT scan model geometries. Using this information coupled with the motion tracking data, we

were able to recreate the exact dynamic motions that the hip underwent in the VIVO simulator to determine the points at which either bony or implant impingement occurred.

6.3 Proposed Results

In future work, this data will be analyzed to calculate the moment contribution of the sutures, capsule, and implant to dislocation resistance. Unlike previous studies, the point of impingement will be quantified and used to interpret the moment data collected by the VIVO. The post-testing impingement analysis will be used to verify the pre-testing impingement predictions. Specifically, the following analysis will be performed:

- The dislocation data will be analyzed between the three dual mobility tests to determine the mode of dislocation, the contributions of the sutures and capsule, and the impingement mechanism that forced the dislocation. In cases where a dislocation did not occur, there will be an investigation into what allowed the femoral head to stay in the acetabular liner.
- The dual mobility implant and the conventional implant will be analyzed between the six dislocation tests that occurred, to determine if the dual mobility implant improved the dislocation resistance compared to the conventional implant, despite not having the contribution of the capsule and surrounding soft tissue.
- Range of motion during the laxity assessments will be compared to variations in body mass index (BMI) for the subjects. We hypothesize that a greater BMI will lead to less range of motion due to the excess fat around the hip, allowing greater opportunity for soft tissue impingement to occur.

- The component placement, including the version and inclination angles of the acetabular component, and the version of the femur will be compared to the impingement free range of motion. This will allow an investigation into the surgical techniques, comparing the effect the surgical approach had on the placement of the components. This will also allow the opportunity to validate the surgical safe-zone component guidelines.

During the testing procedures, an area of improvement was found; despite best efforts to fixture the specimen at the exact anatomical position, due to machine limits and inherent variability in the fixturing process, specimens are not fixated in their exact anatomical position, thus not impinging at the exact angles expected. To compensate for this, the Optotrak kinematic data will be used to determine the exact position. This position will then be run back through the impingement analysis to compare the actual impingement value with the predicted values in the custom impingement MATLAB scripts.

This comprehensive study will allow for a thorough analysis comparing the effects of implant type, surgical approach, and capsule repair on dislocation resistance while addressing many of the limitations from previous studies.

CHAPTER SEVEN: Concluding Remarks

7.1 Final Remarks

The work presented in this thesis demonstrates a variety of complementary studies focused around total hip arthroplasty (THA) performance and a novel approach to measuring the resistive moment seen during dislocation for cadaveric THA-implanted hips. The methods established in this thesis created the opportunity to break down the resistive moment into the contribution of the capsular structures and the contribution of the capsular repair via sutures. The review of current published literature in Chapter Two provides insight to studies that have been performed and the research gap that this study is trying to fill.

From the work outlined in Chapter Three on dual mobility THA bearing motion, we concluded that there is no significant correlation between body mass index (BMI) and bearing motion. This conclusion provides evidence for the continued use of dual mobility implant types in high risk patients, such as the obese, without an increased risk of implant wear due to the limited bearing motion during ADLs.

The methods used in Chapters Four and Five were able to produce novel measurements enabling a new analytical method for understanding hip dislocation. Calculating the resistive moment to dislocation allows surgeons and engineers to better understand the mechanism of dislocation. From the separation of the capsule contribution

and suture contribution, we can conclude that repairing the capsule is an imperative step to increase the resistive moment in dislocations and lower the patient's risk of dislocation post-THA surgery. The methods section outlined in Chapter Six demonstrates the next generation of the testing protocol, that will address the limitations in our previous studies.

7.2 Future Work

The continuation of the testing and analysis as explained in Chapter Six would be the most impactful way to expand this thesis. Due to an unexpected pandemic that closed all facilities for a significant period of time, this work was not finished within the timeframe to be included in this thesis. The methodology of Chapter Six attempts to answer many questions that have been presented through the work and fulfill the major gaps that are seen in literature. These questions focus on the difference in dislocation resistance between a conventional THA implant and a dual mobility THA implant, quantifying the contribution of capsular and suture to dislocation resistance, comparing the most extreme of the surgical approaches, and understanding impingement mechanisms and effects.

With more resources, a future study could branch off this work to understand impingement mechanisms in a greater detail. To investigate this idea more, each layer from the fully intact skin, fat, muscle, and capsule, would be dissected individually, with a testing session between the dissection of each layer. This would provide the ability to capture the contribution of each of the supporting layers in dislocation resistance and their contributions to impingement and support of the hip joint.

7.3 Key Takeaways

This thesis provides evidence that the risks associated with the dual mobility implant does not increase with BMI to allow the implant to be used in high-risk, obese patients. We can also conclude that the capsule should be repaired after implantation of the THA components to increase the resistive torque necessary for dislocation prevention, thus adding to the dislocation resistance. With these findings presented, we have hopes to provide evidence to support in the research and risk mitigation associated with total hip arthroplasty surgeries.

REFERENCES

Adam, P., Farizon, F., & Fessy, M. H. (2014). Dual mobility retentive acetabular liners and wear: Surface analysis of 40 retrieved polyethylene implants. In *Orthopaedics and Traumatology: Surgery and Research* (Vol. 100, Issue 1, pp. 85–91). https://doi.org/10.1016/j.otsr.2013.12.011

Bayne CO, Stanley R, Simon P, Espinoza-Orias A, Salata MJ, Bush-Joseph CA, et al. (2014). Effect of capsulotomy on hip stability-a consideration during hip arthroscopy. *Am J Orthop.* Apr;43(4):160-5.

Bolia, I. K., Fagotti, L., Briggs, K. K., & Philippon, M. J. (2019). Midterm Outcomes Following Repair of Capsulotomy Versus Nonrepair in Patients Undergoing Hip Arthroscopy for Femoroacetabular Impingement With Labral Repair. *Arthroscopy - Journal of Arthroscopic and Related Surgery*, *35*(6), 1828–1834. https://doi.org/10.1016/j.arthro.2019.01.033

Borzio, R. W., Pivec, R., Kapadia, B. H., Jauregui, J. J., & Maheshwari, A. V. (2016). Barbed sutures in total hip and knee arthroplasty: what is the evidence? A meta-analysis. *International Orthopaedics*, *40*(2), 225–231. https://doi.org/10.1007/s00264-015-3049-3

Bozic, K. J., Kurtz, S. M., Lau, E., Ong, K., Vail, D. T. P., & Berry, D. J. (2009). The epidemiology of revision total hip arthroplasty in the united states. *Journal of Bone and Joint Surgery - Series A*, *91*(1), 128–133. https://doi.org/10.2106/JBJS.H.00155

Chechik, O., Khashan, M., Lador, R., Salai, M., & Amar, E. (2013). Surgical approach and prosthesis fixation in hip arthroplasty world wide. *Archives of Orthopaedic and Trauma Surgery*, *133*(11), 1595–1600. https://doi.org/10.1007/s00402-013-1828-0

Crowe, J. F., Sculco, T. P., & Kahn, B. (2003). Revision Total Hip Arthroplasty: Hospital Cost and Reimbursement Analysis. *Clinical Orthopaedics and Related Research*, *413*, 175–182. https://doi.org/10.1097/01.blo.0000072469.32680.b6

De Martino, I., Triantafyllopoulos, G. K., Sculco, P. K., & Sculco, T. P. (2014). Dual mobility cups in total hip arthroplasty. *World Journal of Orthopaedics*, *5*(3), 180–187. https://doi.org/10.5312/wjo.v5.i3.180

den Daas, A., Reitsma, E. A., Knobben, B. A. S., Ten Have, B. L. E. F., & Somford, M. P. (2019). Patient satisfaction in different approaches for total hip arthroplasty. *Orthopaedics and Traumatology: Surgery and Research*, *105*(7), 1277–1282. https://doi.org/10.1016/j.otsr.2019.08.003

Dobzyniak, M., Fehring, T. K., & Odum, S. (2006). Early failure in total hip arthroplasty. *Clinical Orthopaedics and Related Research*, *447*, 76–78. https://doi.org/10.1097/01.blo.0000203484.90711.52

Dubin, J. A., & Westrich, G. H. (2020). Lack of early dislocation for dual mobility vs. fixed bearing total hip arthroplasty: A multi-center analysis of comparable cohorts. *Journal of Orthopaedics*, *21*(February), 1–5. https://doi.org/10.1016/j.jor.2020.02.006

Fabry, C., Woernle, C., & Bader, R. (2014). Self-centering dual-mobility total hip systems: Prediction of relative movements and realignment of different intermediate components. *Proceedings of the Institution of Mechanical Engineers, Part H: Journal of Engineering in Medicine*, *228*(5), 477–485. https://doi.org/10.1177/0954411914531116

Goldman, A. H., Sierra, R. J., Trousdale, R. T., Lewallen, D. G., Berry, D. J., & Abdel, M. P. (2019). The Lawrence D. Dorr Surgical Techniques & Technologies Award: Why Are Contemporary Revision Total Hip Arthroplasties Failing? An Analysis of 2500 Cases. *Journal of Arthroplasty*, *34*(7), S11–S16. https://doi.org/10.1016/j.arth.2019.01.031

Grood ES, Suntay WJ. A joint coordinate system for the clinical description of three-dimensional motions: application to the knee. (1983) *J Biomech Eng*. 105(2):136-144. doi:10.1115/1.3138397

Heffernan, C., Banerjee, S., Nevelos, J., Macintyre, J., Issa, K., Markel, D. C., & Mont, M. A. (2014). Does dual-mobility cup geometry affect posterior horizontal dislocation distance? *Clinical Orthopaedics and Related Research*, *472*(5), 1535–1544. https://doi.org/10.1007/s11999-014-3469-1

Hernández, A., Nuñez, J. H., Mimendia, I., Barro, V., & Azorin, L. (2018). Early dislocation in primary total hip arthroplasty using a posterior approach with repair of capsule and external rotators. *Revista Española de Cirugía Ortopédica y Traumatología (English Edition)*. https://doi.org/10.1016/j.recote.2018.11.001

Hernández, A., Nuñez, J. H., Mimendia, I., Barro, V., & Azorin, L. (2018). Early dislocation in primary total hip arthroplasty using a posterior approach with repair of capsule and external rotators. *Revista Española de Cirugía Ortopédica y Traumatología (English Edition)*. https://doi.org/10.1016/j.recote.2018.11.001

Higgins, B. T., Barlow, D. R., Heagerty, N. E., & Lin, T. J. (2015). Anterior vs. Posterior Approach for Total Hip Arthroplasty, a Systematic Review and Meta-analysis. *Journal of Arthroplasty*, *30*(3), 419–434. https://doi.org/10.1016/j.arth.2014.10.020

Hughes, A. W., Clark, D., Carlino, W., Gosling, O., & Spencer, R. F. (2015). Capsule reapair may reduce dislocation following hip hemiarthroplasty through a direct lateral appraoch. *Bone and Joint Journal*, *97-B*(1), 115–120.

International Society of Biomechanics, "Standards Documents". https://isbweb.org/about-us/29-standards-documents?layout=

Jones, C. A., Beaupre, L. A., Johnston, D. W. C., & Suarez-Almazor, M. E. (2007). Total Joint Arthroplasties: Current Concepts of Patient Outcomes after Surgery. *Rheumatic Disease Clinics of North America*, *33*(1), 71–86. https://doi.org/10.1016/j.rdc.2006.12.008

Jonker, R. C., Loes W.A.H. van Beers, Bart C.H. van der Wal, H. Charles Vogely, Sebastien Parrattec, René M. Casteleina, R. W. P. (2019). Can dual mobility cups prevent dislocation without increasing revision rates in primary total hip arthroplasty? A systematic review. *Orthopaedics & Traumatology: Surgery & Research*. https://doi.org/10.1016/j.otsr.2019.12.019

Kennon, R. E., Keggi, J. M., & Keggi, K. J. (2004). The anterior approach to hip arthroplasty: The short, single minimally invasive incision. *Operative Techniques in Orthopaedics*, *14*(2), 85–93. https://doi.org/10.1053/j.oto.2004.03.003

Khair MM, Grzybowski JS, Kuhns BD, Wuerz TH, Shewman E, Nho SJ. The Effect of Capsulotomy and Capsular Repair on Hip Distraction: A Cadaveric Investigation (2017). *Arthroscopy : the journal of arthroscopic & related surgery*. 2017 Mar;v33(3):559-65. doi: 10.1007/s12178-019-09567-1

Knapper, T. D., Dahill, M., Eastaugh-Waring, S., Baker, R. P., Webb, J. C. J., Blom, A. W., & Whitehouse, M. R. (2019). Barbed sutures versus staples for closure in total hip arthroplasty using wound ooze as a primary outcome measure: A prospective study. *Journal of Orthopaedic Surgery*, *27*(2), 1–5. https://doi.org/10.1177/2309499019857166

Kremers, H. M., Larson, D. R., Crowson, C. S., Kremers, W. K., Washington, R. E., Steiner, C. A., Jiranek, W. A., & Berry, D. J. (2014). Prevalence of total hip and knee replacement in the United States. *Journal of Bone and Joint Surgery - American Volume*, *97*(17), 1386–1397. https://doi.org/10.2106/JBJS.N.01141

Kumar, P., Sen, R. K., Aggarwal, S., & Jindal, K. (2020). Common hip conditions requiring primary total hip arthroplasty and comparison of their post-operative functional outcomes. *Journal of Clinical Orthopaedics and Trauma*, *11*, S192–S195. https://doi.org/10.1016/j.jcot.2019.02.009

Kurtz S, Ong K, Lau E, Mowat F, Halpern M. (2007). Projections of primary and revision hip and knee arthroplasty in the United States from 2005 to 2030. *J Bone Joint Surg Am*. 89(4):780-785. doi:10.2106/JBJS.F.00222

Kwon, M. S., Kuskowski, M., Mulhall, K. J., Macaulay, W., Brown, T. E., & Saleh, K. J. (2006). Does surgical approach affect total hip arthroplasty dislocation rates? *Clinical Orthopaedics and Related Research*, *447*, 34–38. https://doi.org/10.1097/01.blo.0000218746.84494.df

Li, R., Ni, M., Zhao, J., Li, X., Zhang, Z., Ren, P., Xu, C., & Chen, J. Y. (2018). A modified strategy using barbed sutures for wound closure in total joint arthroplasty: A prospective, randomized, double-blind, self-controlled clinical trial. *Medical Science Monitor*, *24*, 8401–8407. https://doi.org/10.12659/MSM.912854

Lieberman, J. R., Dorey, F., Shekelle, P., Schumacher, L., Kilgus, D. J., Thomas, B. J., & Finerman, G. A. (1997). Outcome after total hip arthroplasty: Comparison of a traditional disease-specific and a quality-of-life measurement of outcome. *Journal of Arthroplasty*, *12*(6), 639–645. https://doi.org/10.1016/S0883-5403(97)90136-4

Lin, Y., Lai, S., Huang, J., & Du, L. (2016). The Efficacy and Safety of Knotless Barbed Sutures in the Surgical Field: A Systematic Review and Meta-analysis of Randomized Controlled Trials. *Scientific Reports*, *6*(March), 1–8. https://doi.org/10.1038/srep23425

Logishetty, K., van Arkel, R. J., Ng, K. C. G., Muirhead-Allwood, S. K., Cobb, J. P., & Jeffers, J. R. T. (2019). Hip capsule biomechanics after arthroplasty: the effect of implant, approach, and surgical repair. *The Bone & Joint Journal*, *101-B*(4), 426–434. https://doi.org/10.1302/0301-620X.101B4.BJJ-2018-1321.R1

Loving, L. Q., Lee, R. K. F., Herrera, L., Essner, A. P., & Nevelos, J. E. (2013). Wear performance evaluation of a contemporary dual mobility hip bearing using multiple hip simulator testing conditions. *Journal of Arthroplasty*, *28*(6), 1041–1046. https://doi.org/10.1016/j.arth.2012.09.011

Lu, Y., Wu, Z., Tang, X., Gu, M., & Hou, B. (2019). Effect of articular capsule repair on postoperative dislocation after primary total hip replacement by the anterolateral approach. *Journal of International Medical Research*, *47*(10), 4787–4797. https://doi.org/10.1177/0300060519863526

Malek, I. A., Royce, G., Bhatti, S. U., Whittaker, J. P., Phillips, S. P., Wilson, I. R. B., Wootton, J. R., & Starks, I. (2016). A comparison between the direct anterior and posterior approaches for total hip arthroplasty: The role of an “enhanced recovery” pathway. *Bone and Joint Journal*, *98-B*(6), 754–760. https://doi.org/10.1302/0301-620X.98B6.36608

March, L. M., Cross, M. J., Lapsley, H., Brnabic, A. J. M., Tribe, K. L., Bachmeier, C. J. M., Courtenay, B. G., & Brooks, P. M. (1999). Outcomes after hip or knee replacement surgery for osteoarthritis. A prospective cohort study comparing patients' quality of life before and after surgery with age-related population norms. *Medical Journal of Australia*, *171*(5), 235–238. https://doi.org/10.5694/j.1326-5377.1999.tb123628.x

Martin, H. D., Savage, A., Braly, B. A., Palmer, I. J., Beall, D. P., & Kelly, B. (2008). The Function of the Hip Capsular Ligaments: A Quantitative Report. *Arthroscopy - Journal of Arthroscopic and Related Surgery*, *24*(2), 188–195. https://doi.org/10.1016/j.arthro.2007.08.024

Mihalko, W. M., & Whiteside, L. A. (2004). Hip Mechanics after Posterior Structure Repair in Total Hip Arthroplasty. *Clinical Orthopaedics and Related Research*, *420*, 194–198. https://doi.org/10.1097/00003086-200403000-00027

Myers CA, Register BC, Lertwanich P, Ejnisman L, Pennington WW, Giphart JE, et al. (2015). Role of the acetabular labrum and the iliofemoral ligament in hip stability: an in vitro biplane fluoroscopy study. *Am J Sports Med.* 2011 Jul; 39 Suppl:85S-91S. https://doi.org/10.1177/0363546511412161

Nadzadi, M. E., Pedersen, D. R., Yack, H. J., Callaghan, J. J., & Brown, T. D. (2003). Kinematics, kinetics, and finite element analysis of commonplace maneuvers at risk for total hip dislocation. *Journal of Biomechanics*, *36*(4), 577–591. https://doi.org/10.1016/S0021-9290(02)00232-4

Ng, K. C. G., Jeffers, J. R. T., & Beaulé, P. E. (2019). Hip Joint Capsular Anatomy, Mechanics, and Surgical Management. *The Journal of Bone and Joint Surgery*, *0*, 1. https://doi.org/10.2106/jbjs.19.00346

Petis, S., Howard, J. L., Lanting, B. L., & Vasarhelyi, E. M. (2015). Surgical approach in primary total hip arthroplasty: Anatomy, technique and clinical outcomes. *Canadian Journal of Surgery*, *58*(2), 128–139. https://doi.org/10.1503/cjs.007214

Pfleger, A. D., and Woolf, B. (2003). Burden of major musculoskeletal conditions. *European Journal for Church and State Research*, *11*(03), 1–6. https://doi.org/10.2143/EJCS.11.0.2029488

Riley, L. P., & Ip, K. (2018). Projected volume of primary and revision total joint replacement in the U.S. 2030 to 2060. *J Am Acad Orthop Surg*. http://aaos-annualmeeting-presskit.org/2018/research-news/sloan_tjr/

Ruff, G. L. (2013). The history of barbed sutures. In *Aesthetic surgery journal / the American Society for Aesthetic Plastic surgery* (Vol. 33, Issue 3 Suppl). https://doi.org/10.1177/1090820X13498505

Schmalzried, T. P., Shepherd, E. F., Dorey, F. J., Jackson, W. O., Dela Rosa, M., Fa'vae, F., McKellop, H. A., McClung, C. D., Martell, J., Moreland, J. R., & Amstutz, H. C. (2000). Wear is a function of use, not time. *Clinical Orthopaedics and Related Research*, *381*, 36–46. https://doi.org/10.1097/00003086-200012000-00005

Stewart, K. J., Edmonds-Wilson, R. H., Brand, R. A., & Brown, T. D. (2002). Spatial distribution of hip capsule structural and material properties. *Journal of Biomechanics*, *35*(11), 1491–1498. https://doi.org/10.1016/S0021-9290(02)00091-X

Thacher, R. R., Herndon, C. L., Jennings, E. L., Sarpong, N. O., & Geller, J. A. (2019). The Impact of Running, Monofilament Barbed Suture for Subcutaneous Tissue Closure on Infection Rates in Total Hip Arthroplasty: A Retrospective Cohort Analysis. *Journal of Arthroplasty*. https://doi.org/10.1016/j.arth.2019.05.001

Wagner, F. V., Negrão, J. R., MD Juliana Campos, MD Samuel R. Ward, PT, PhD Parviz Haghighi, MD Debra J. Trudell, RA Donald Resnick, M., Getty, D. J., Jacobson, F. L., Steigner, M., & Pan, J. J. (2012). capsular ligaments of the hip: Anatomic, Histologic, and Positional Study in Cadaveric Specimens with MR Arthrography. *Radiology*, *263*(1), 346–362. https://doi.org/10.1148/radiol

Wang, Z., Hou, J. zhao, Wu, C. hua, Zhou, Y. jiang, Gu, X. ming, Wang, H. hong, Feng, W., Cheng, Y. xiao, Sheng, X., & Bao, H. wei. (2018). A systematic review and meta-analysis of direct anterior approach versus posterior approach in total hip arthroplasty. *Journal of Orthopaedic Surgery and Research*, *13*(1), 1–11. https://doi.org/10.1186/s13018-018-0929-4

APPENDIX

A.1: Conference Abstracts

Marshall, B., Storer, L., Myers, C., Keefer, R., Clary, C. The Effect of Patient BMI on Bearing Kinematics in Dual Mobility Total Hip Arthroplasty. International Society for Technology in Arthroplasty Annual Meeting 2019. Podium Presentation.

Marshall, B., Behnam, Y., Dalury, D., Fisher, D., Clary, C. Experimental Assessment of PCL Forces with Different Implant Systems and the Effect of Tibial Fixation. Orthopaedic Research Society Annual Meeting 2020. Poster.

Marshall, B., Huff, D., Clary, C., Mason, J.B. Repairing the Capsule during Anterior Approach THR Improved Dislocation Resistance. Orthopaedic Research Society Annual Meeting 2020. Podium Presentation.

Chen, X., Marshall, B., Fritz., B., DeWall, R., Clary, C., Rullkoetter, P. Validation Of A Finite Element Model Of A Fixation Construct For Vancouver Type B Periprosthetic Femoral Fracture. Orthopaedic Research Society Annual Meeting 2020. Poster.

A.2: Upcoming Journal Submissions

Marshall, B., Huff, D., Clary, C., Mason, J.B. The Role of Capsular Repair on the Stability of Total Hip Arthroplasty using the Direct Anterior Approach.

A.3: Additional Figures Associated with Chapter Three

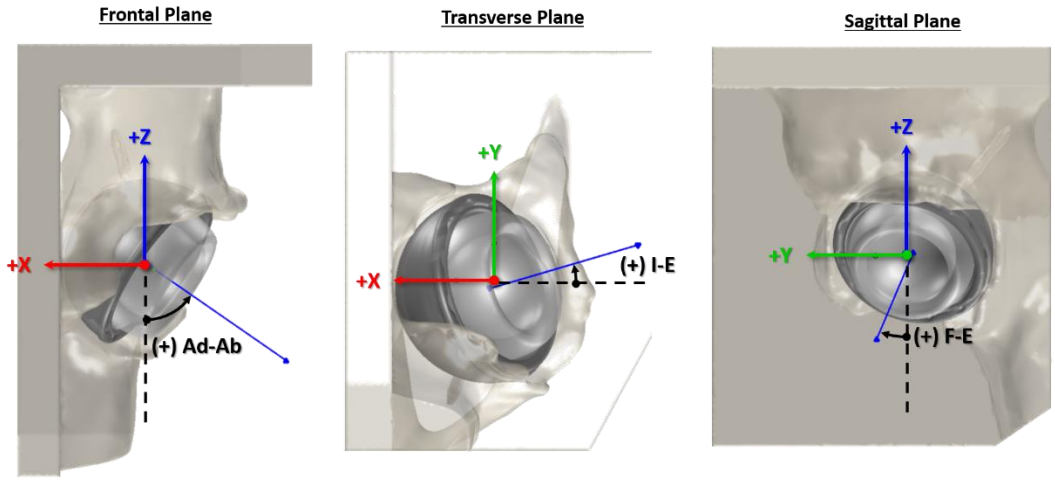

Figure A 1: The coordinate system used to define the angles of motion

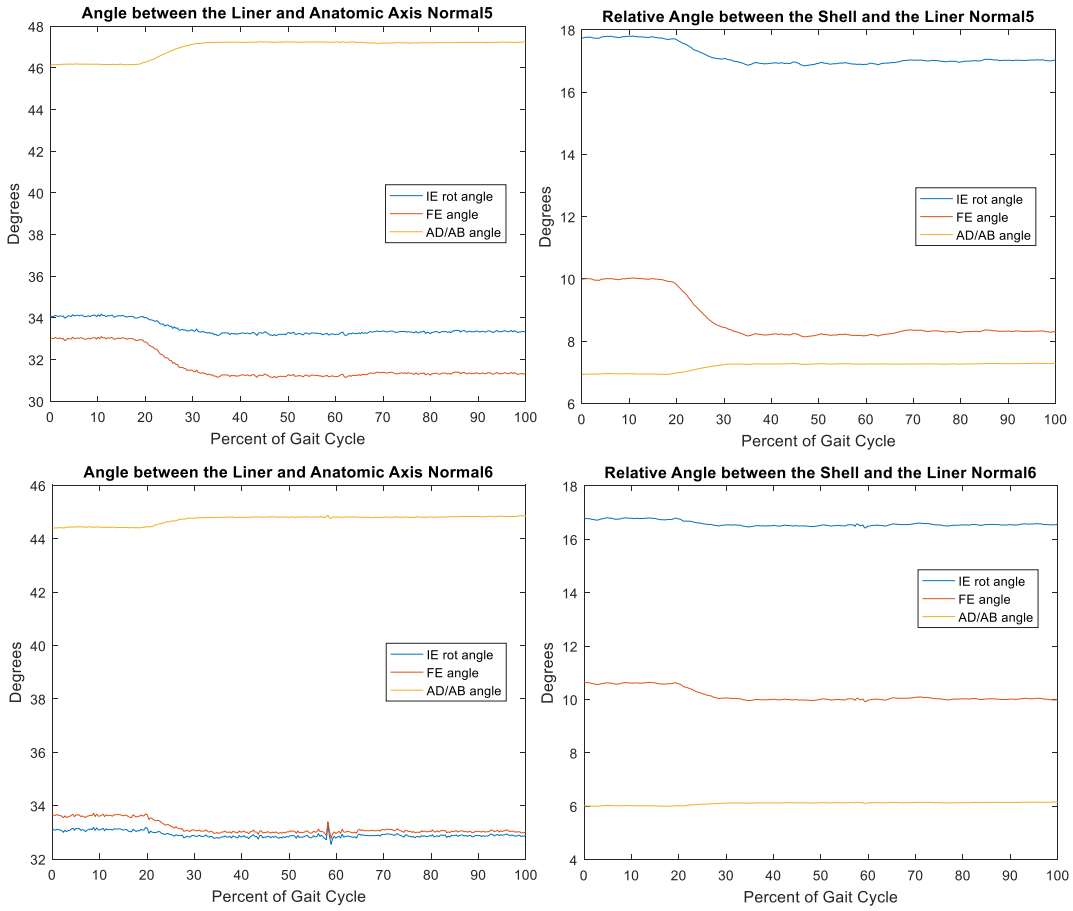

Figure A 2: Motion of the liner during on trial of a gait cycle, at 1- standard deviation compressive loading, with a normal initial cup position. Two trials are shown (rows) with tow angles measured (columns) with the angle between the liner and the cup shown on the left with the relative angle between the shell and the liner calculated on the right.

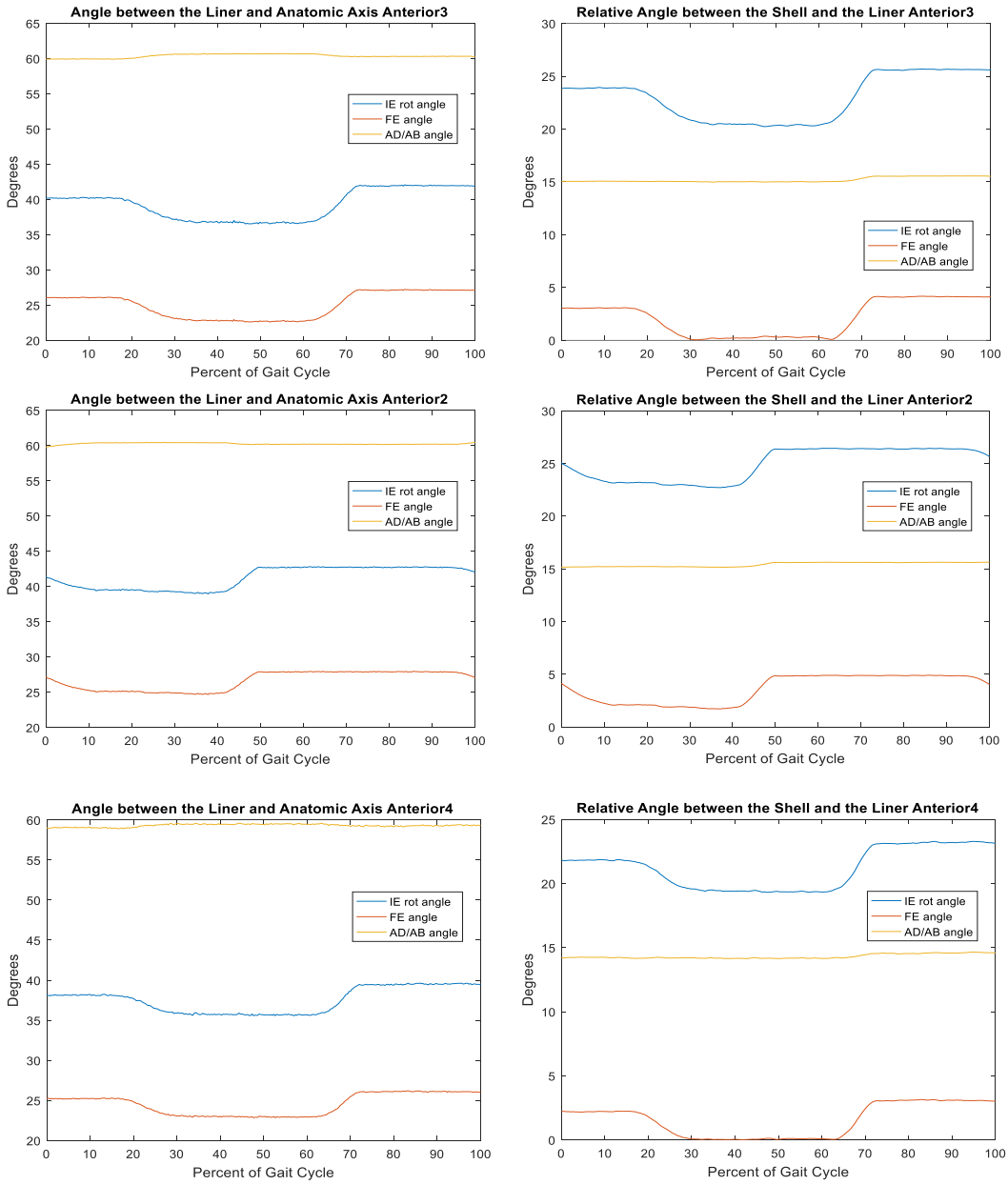

Figure A 3: Motion of the liner during on trial of a gait cycle, at 1- standard deviation compressive loading, with an anterior initial cup position. Three trials are shown (rows) with tow angles measured (columns) with the angle between the liner and the cup shown on the left with the relative angle between the shell and the liner calculated on the right.

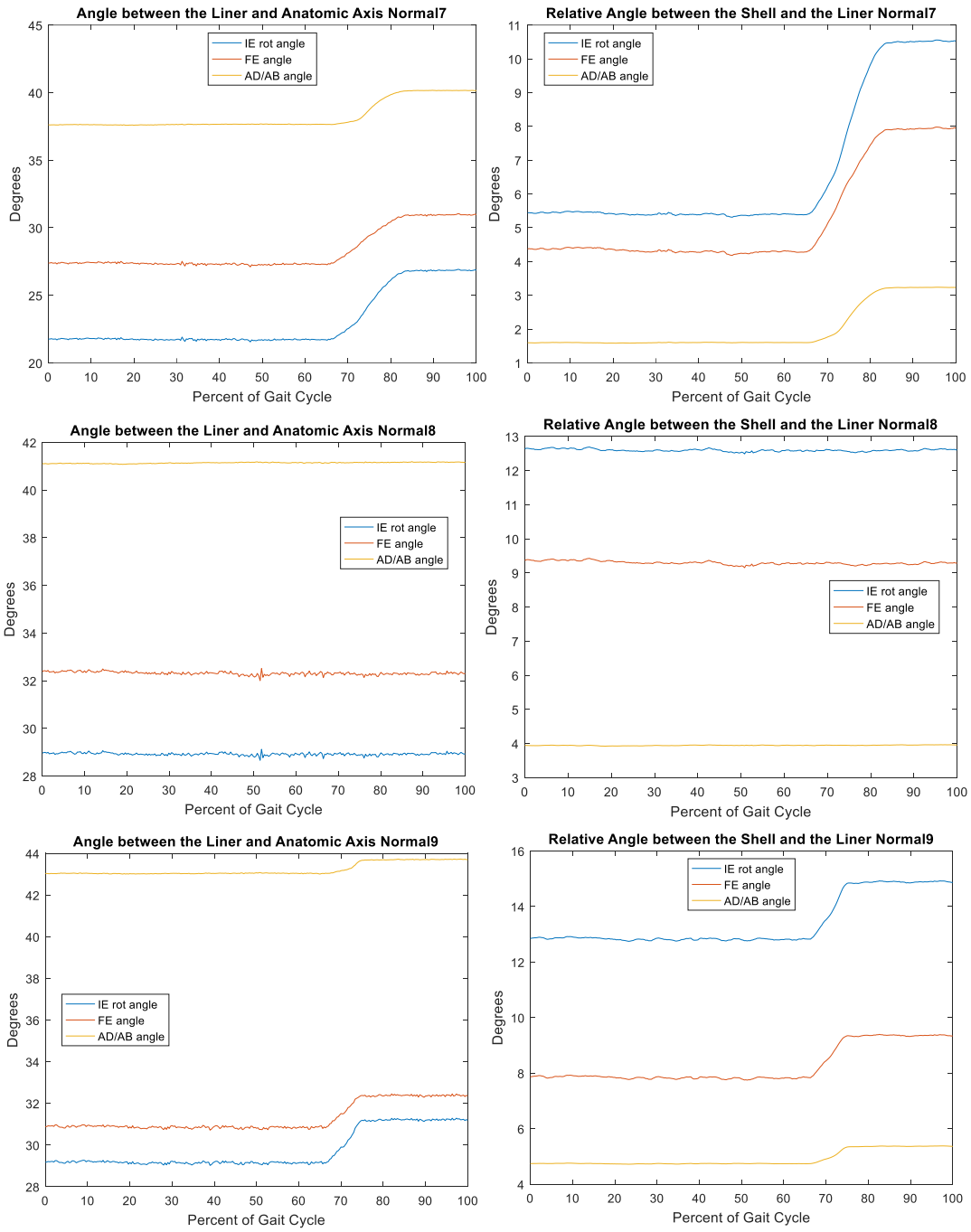

Figure A 4: Motion of the liner during on trial of a gait cycle, at mean standard deviation compressive loading, with a normal initial cup position. Three trials are shown (rows) with tow angles measured (columns) with the angle between the liner and the cup shown on the left with the relative angle between the shell and the liner calculated on the right.

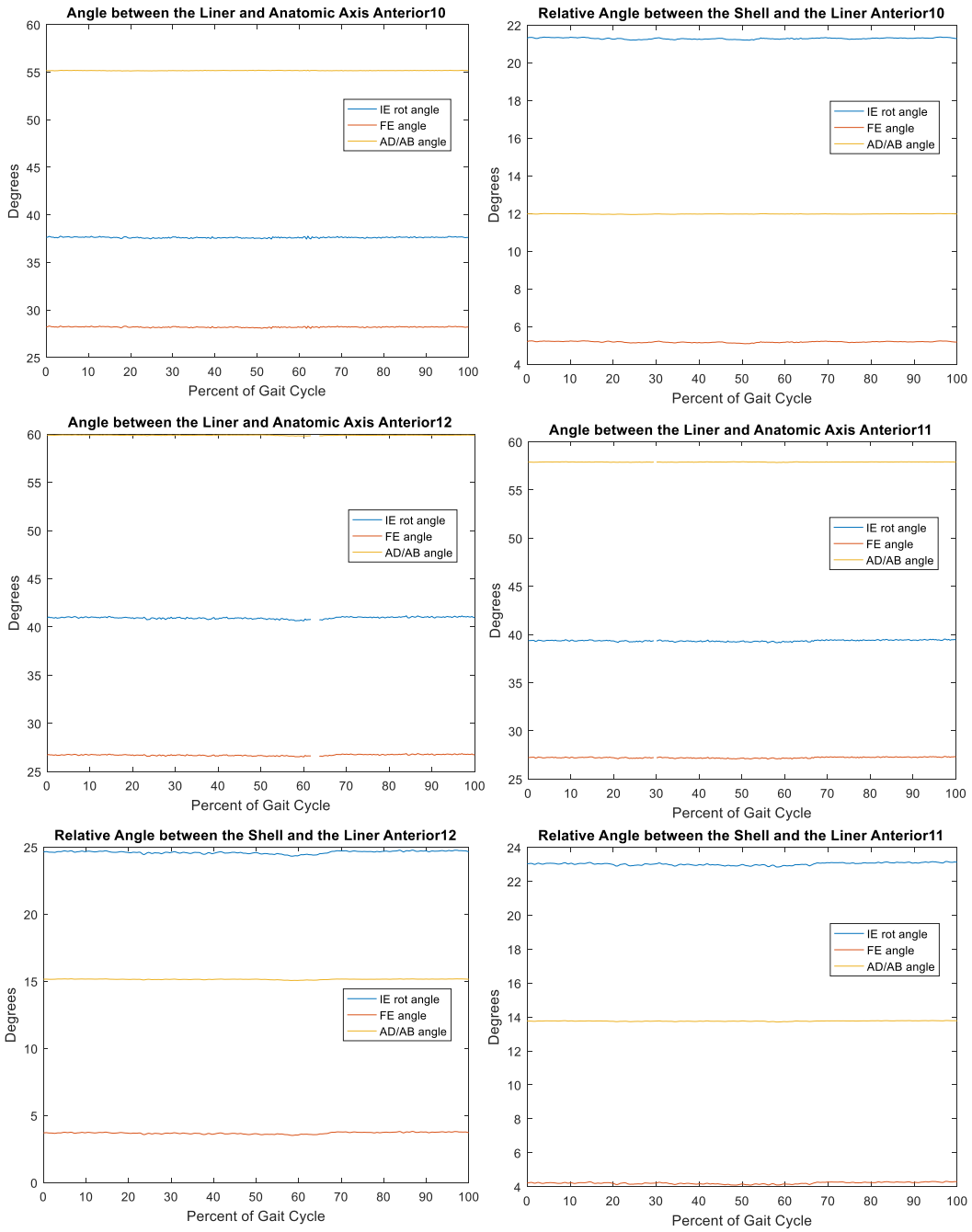

Figure A 5: Motion of the liner during on trial of a gait cycle, at mean standard deviation compressive loading, with an anterior initial cup position. Three trials are shown (rows) with tow angles measured (columns) with the angle between the liner and the cup shown on the left with the relative angle between the shell and the liner calculated on the right.

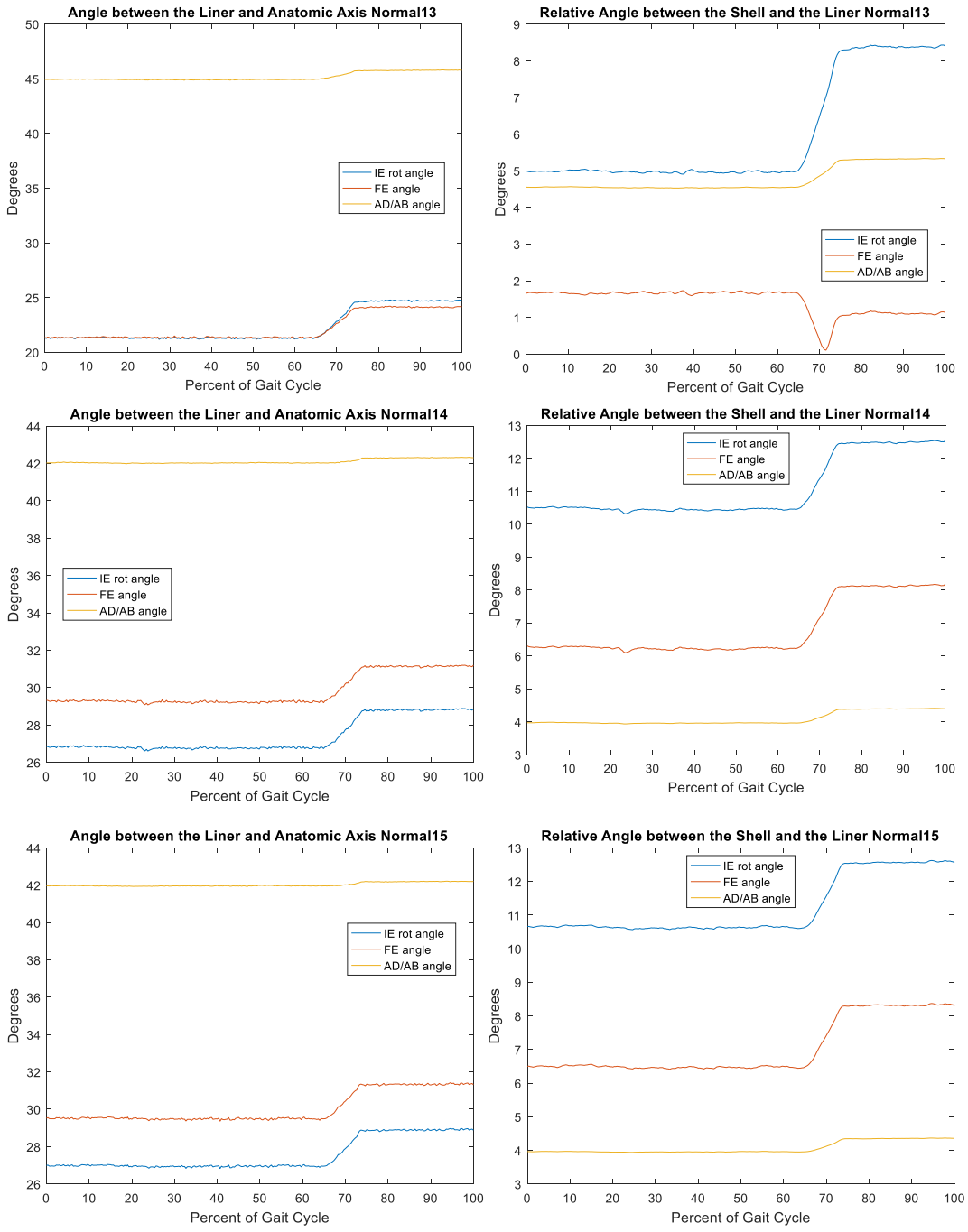

Figure A 6: Motion of the liner during on trial of a gait cycle, at 1+ standard deviation compressive loading, with a normal initial cup position. Three trials are shown (rows) with tow angles measured (columns) with the angle between the liner and the cup shown on the left with the relative angle between the shell and the liner calculated on the right.

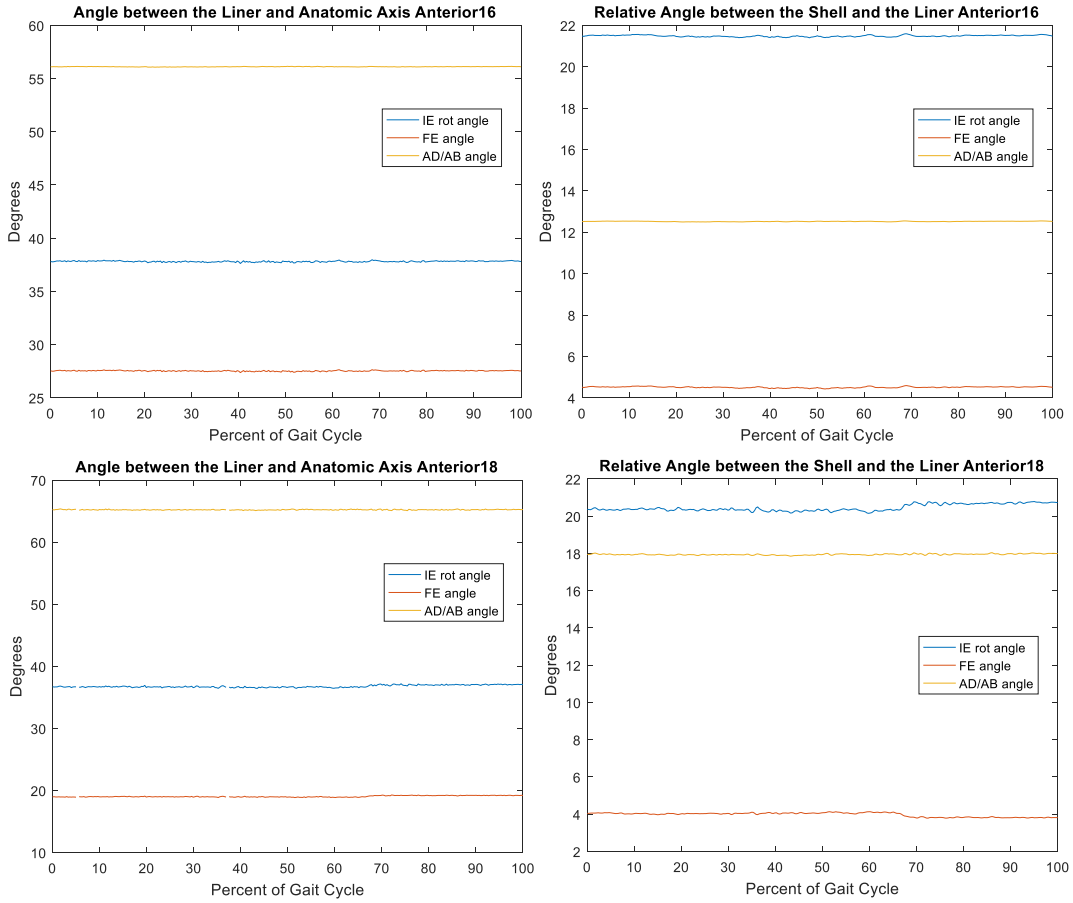

Figure A 7: Motion of the liner during on trial of a gait cycle, at 1+ standard deviation compressive loading, with an anterior initial cup position. Two trials are shown (rows) with tow angles measured (columns) with the angle between the liner and the cup shown on the left with the relative angle between the shell and the liner calculated on the right.

A.4: Additional Figures Associated with Chapter Four

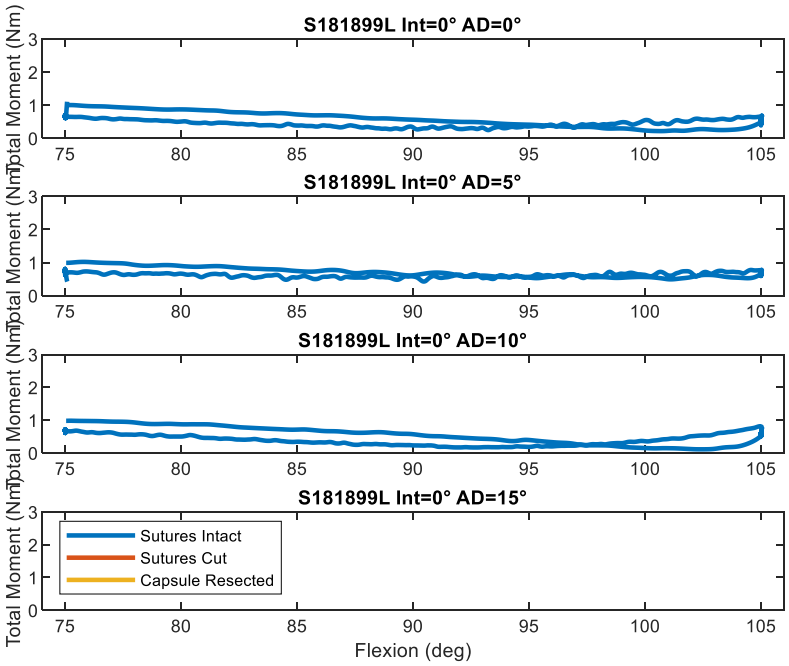

Figure A 8: Example set of graphs for one posterior approach for the complete cycle, plotting the total peak moment on the y axis. All plots are for internal rotation of 0 degrees. The sutures intact graph is the only one shown because the torque response was so small in these trials that the next set of tests was not even conducted.

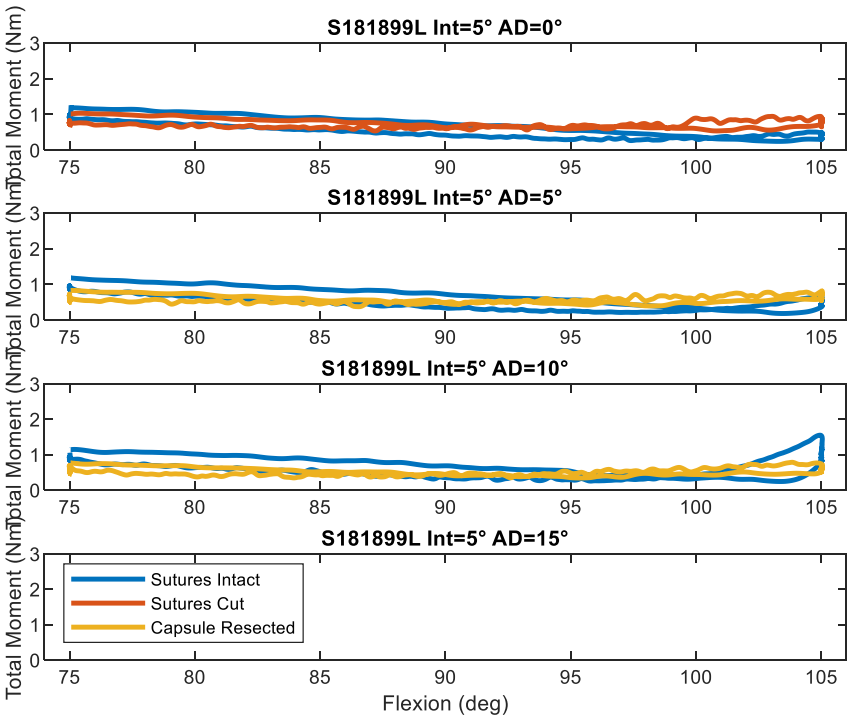

Figure A 9: Example set of graphs for one posterior approach hip for internal rotation angle of 5 degrees with varying adduction angles. Only a select few tests were run to test the torque response exhibited by each trial

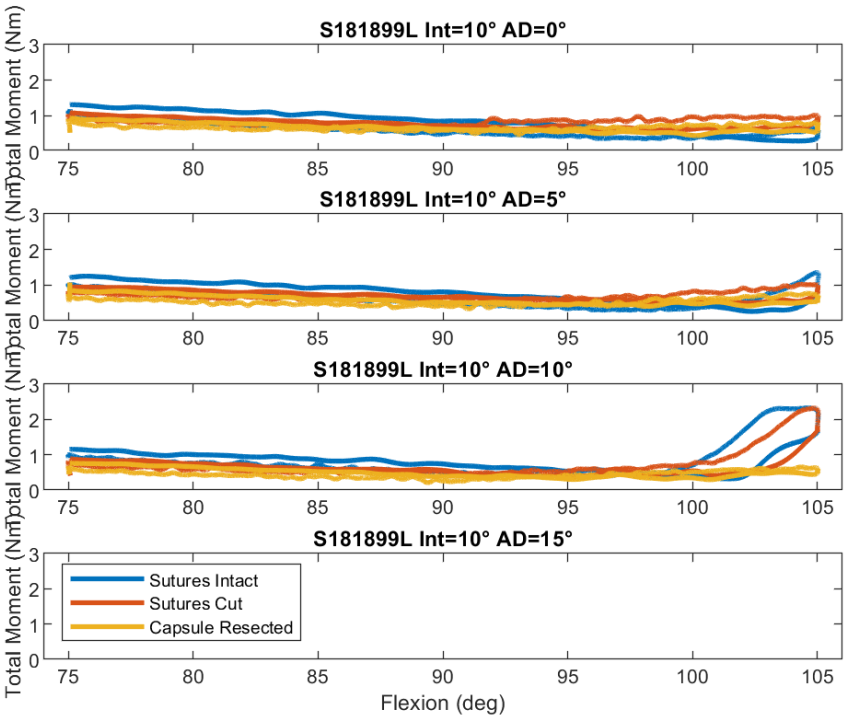

Figure A 10: Example set of graphs for one posterior approach hip for internal rotation angle of 10 degrees with varying adduction angles. The three suture conditions are shown

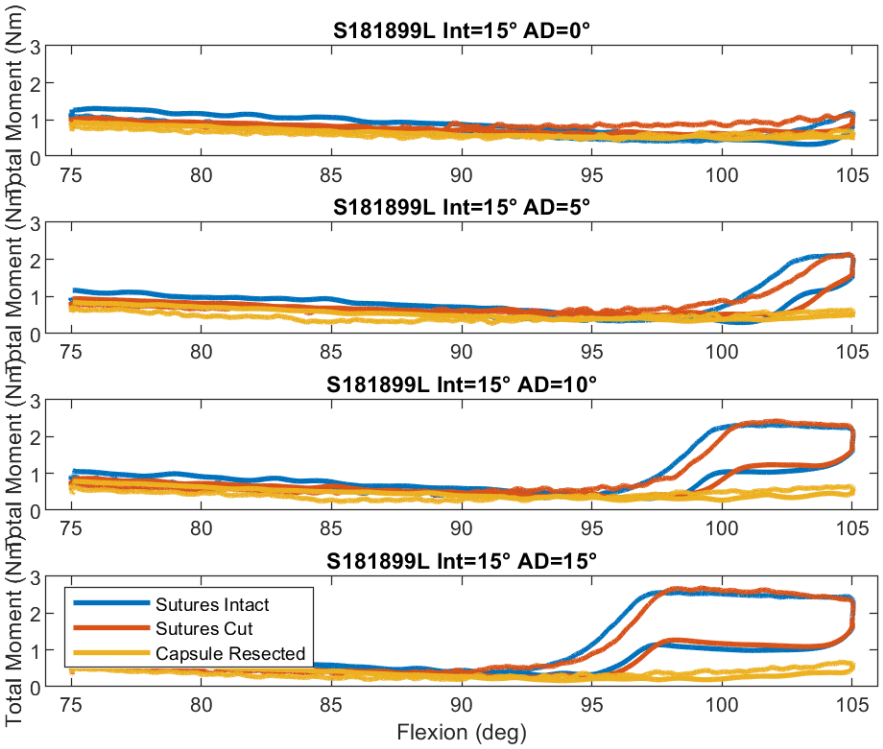

Figure A 11: Example set of graphs for one posterior approach hip showing the trials for internal rotation angle of 15 degrees with varying adduction angles. The three suture condition tests are also shown

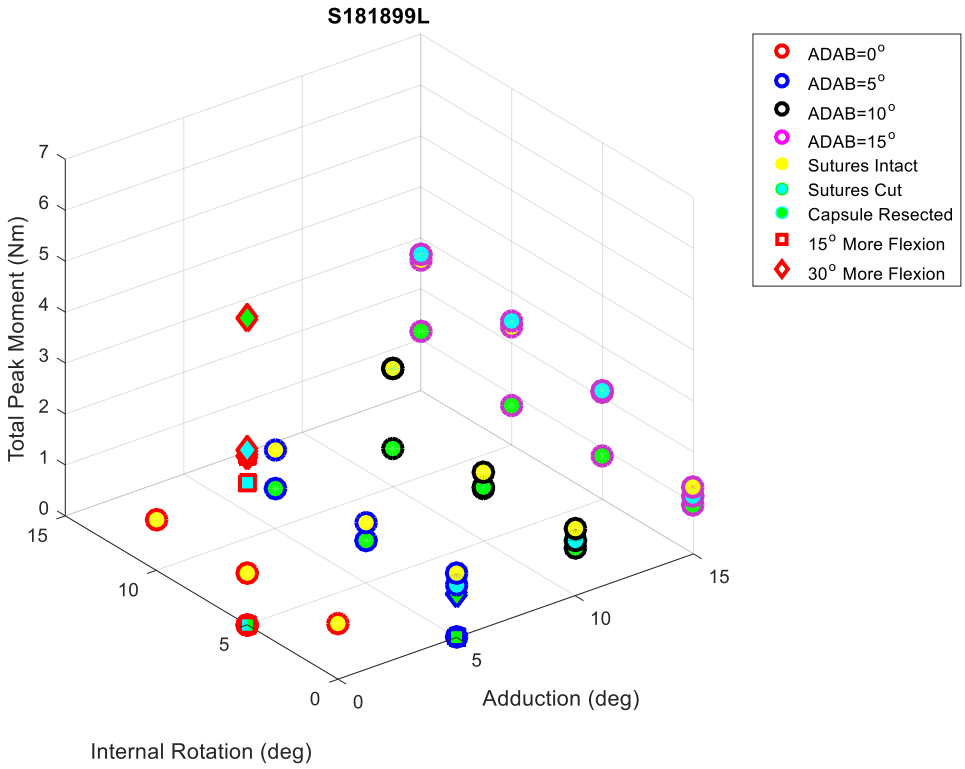

Figure A 12: Posterior approach left-side hip, 3D graphs plotting the internal rotation angle and adduction angle showing all suture contribution data plots

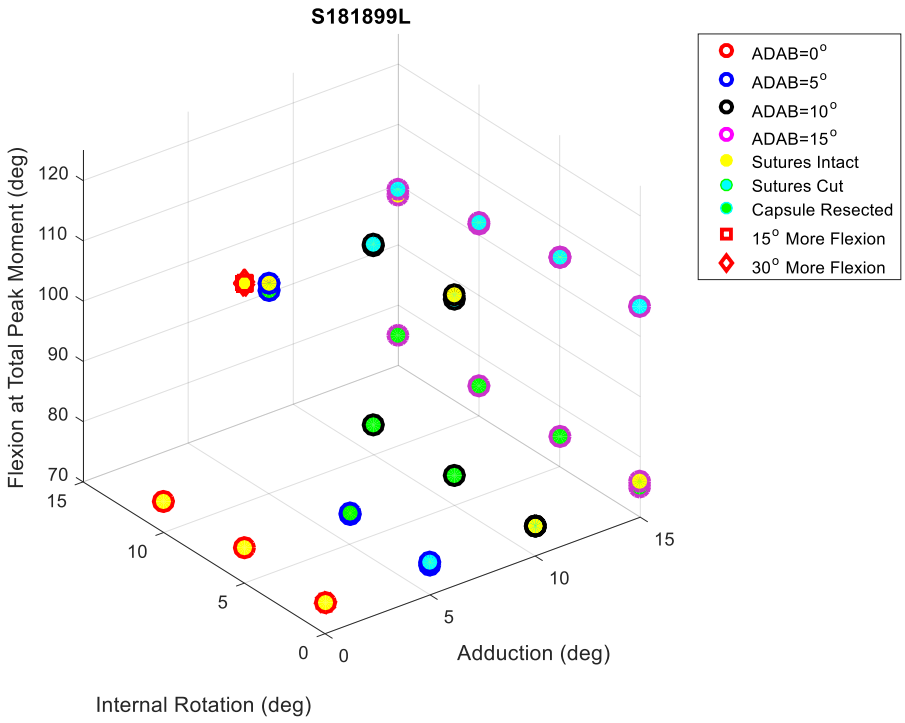

Figure A 13: Posterior approach left-side hip comparing the flexion degree angle, internal rotation angle, and adduction angle

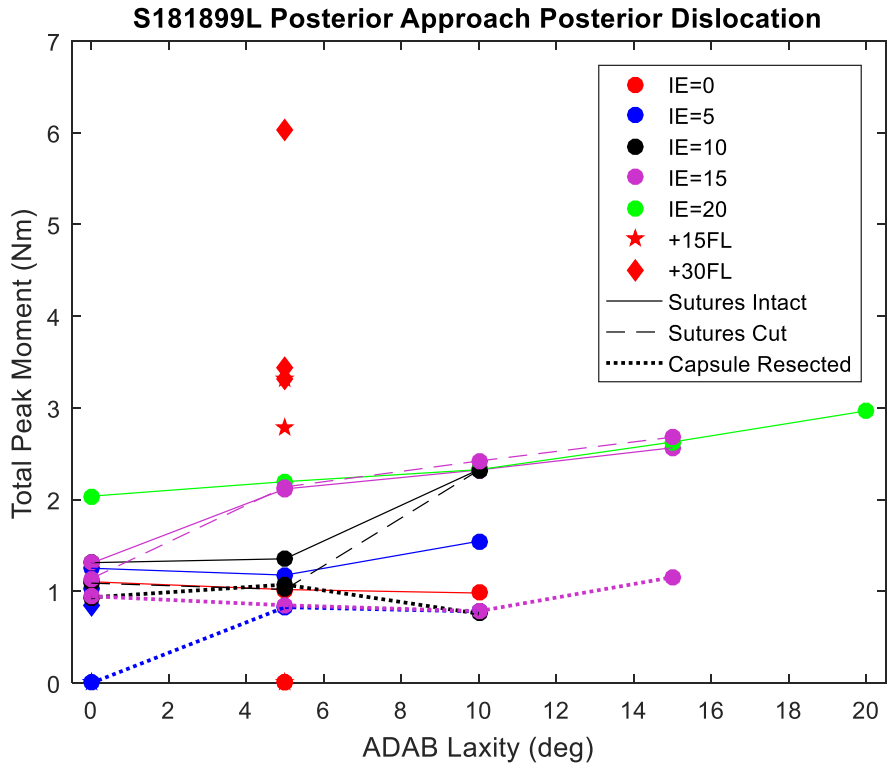

Figure A 14: 2D graph comparing the different suture conditions, the adduction rotation angle and the internal rotation angle

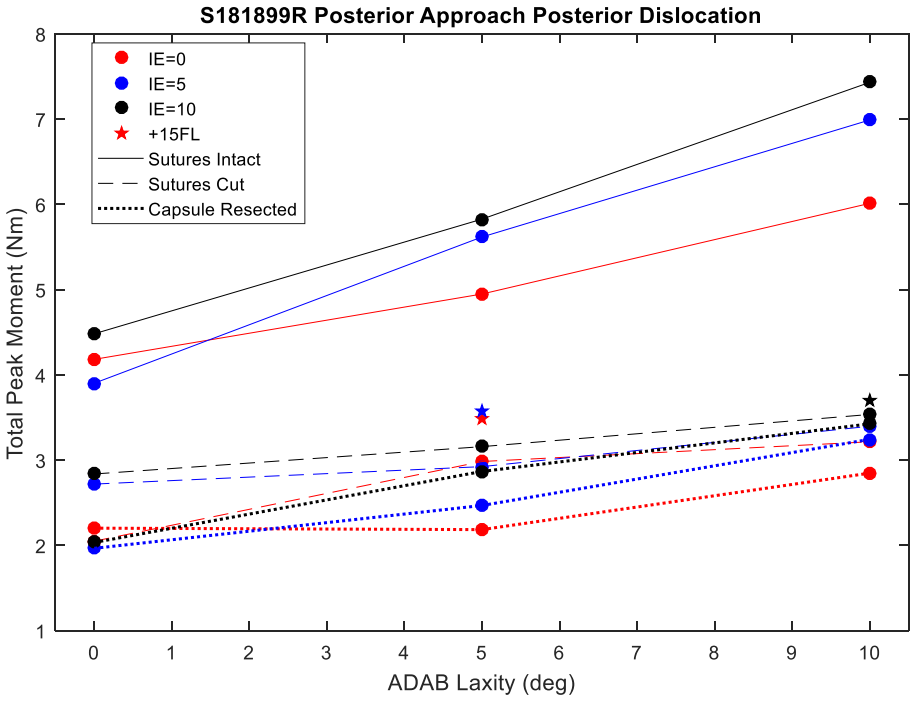

Figure A 15: 2D graph comparing the different suture conditions, the adduction angle, and the internal rotation angle

A.5: Additional Figures Associated with Chapter Five

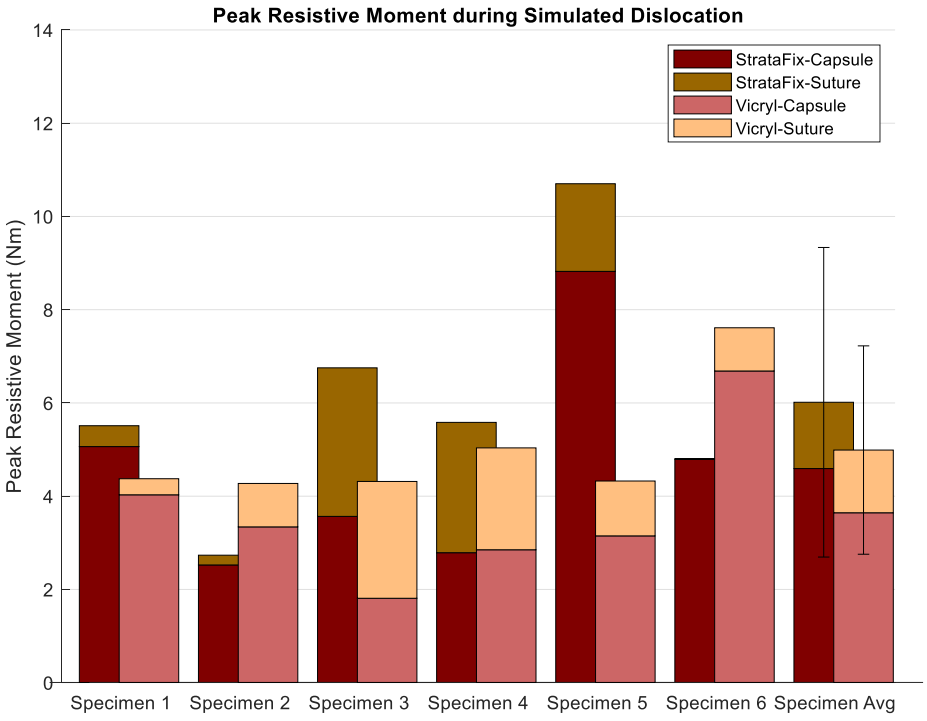

Figure A 16: Anterior dislocation simulation graph of hyperextension and external rotation plotting the peak resistive moment on the y axis and each specimen's results on the x axis

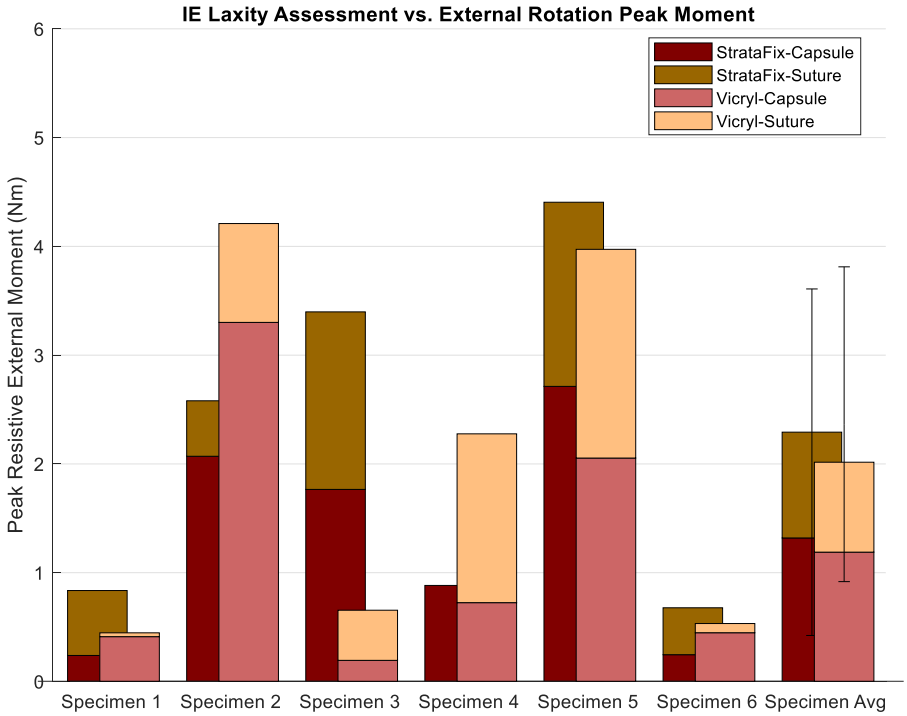

Figure A 17: Internal and External Rotation Laxity Assessment Test plotting the peak external moment on the y axis for each specimen

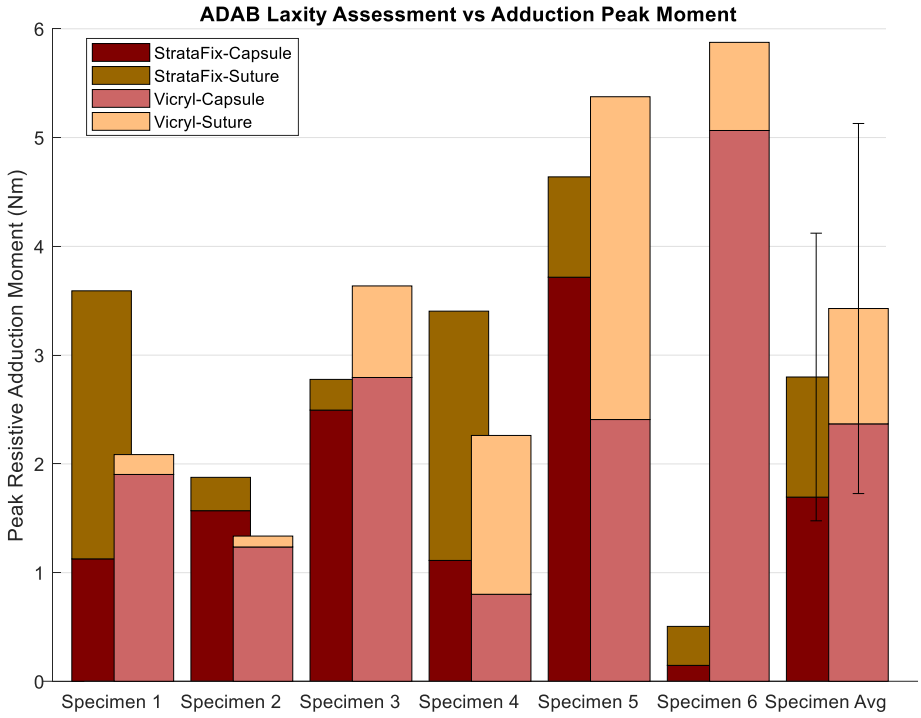

Figure A 18: The peak resistive adduction moment for the adduction and abduction laxity assessment tests plotting for each specimen

Anterior Dislocation Simulation Graphs of Moment Components for 1st Specimen:

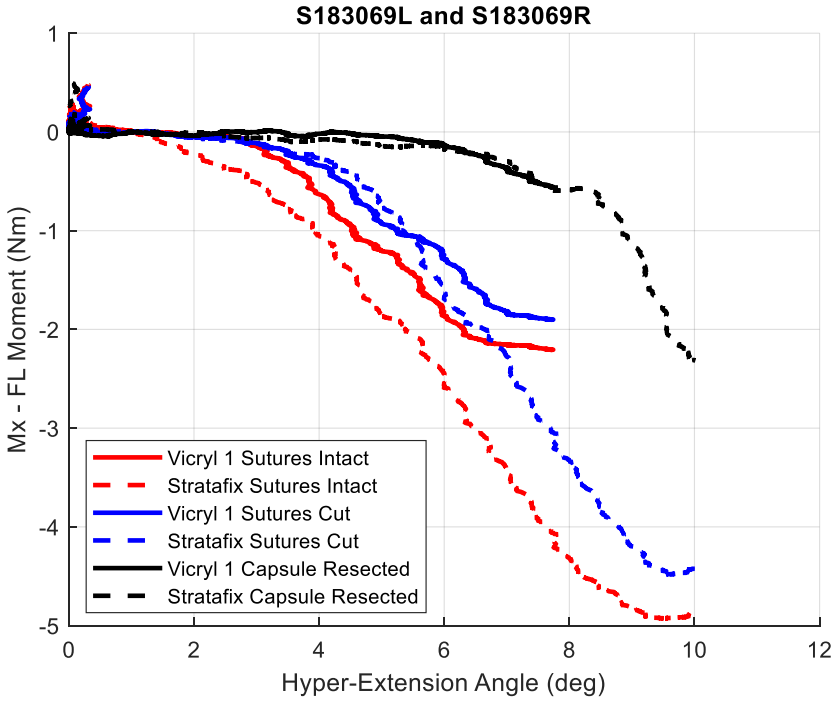

Figure A 19: One specimen example comparing the Vicryl and Stratafix plotting the flexion moment for the Hyper-Extension and External Rotation movement

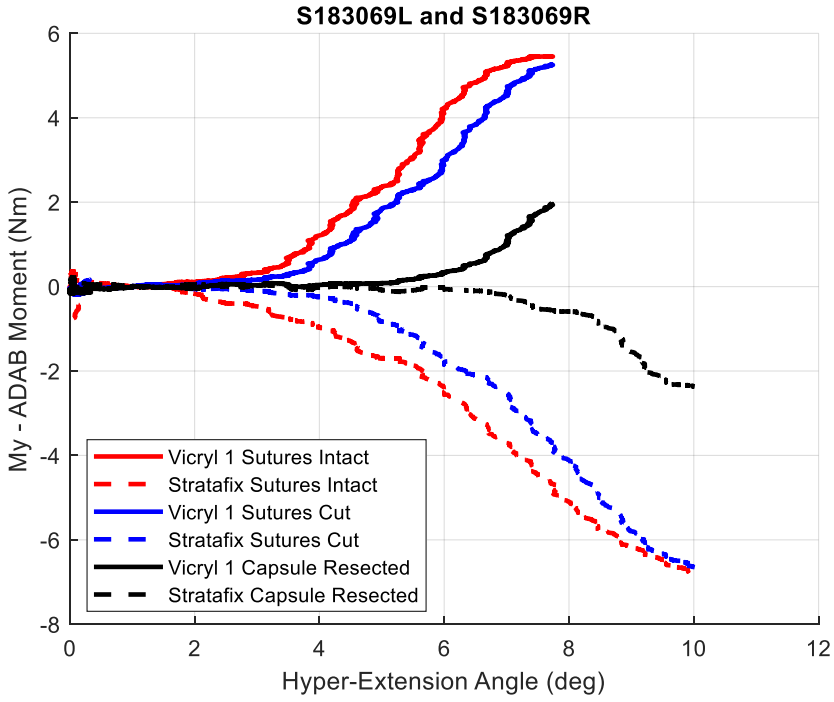

Figure A 20: One specimen example comparing the Vicryl and Stratafix plotting the adduction moment for the Hyper-Extension and External Rotation movement

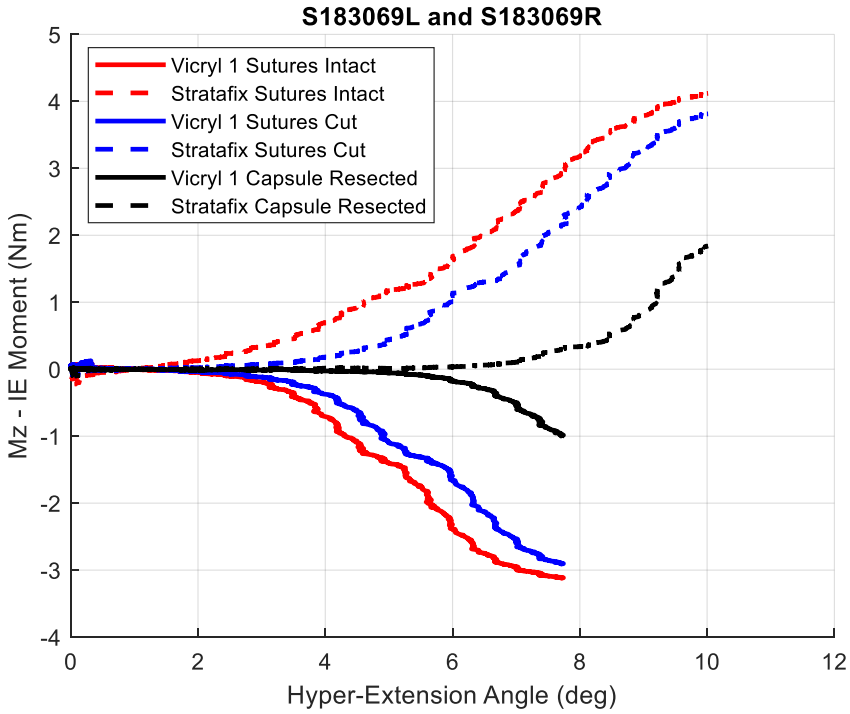

Figure A 21: One specimen example comparing the Vicryl and Stratafix plotting the internal rotation moment for the Hyper-Extension and External Rotation movement

Adduction and Abduction Laxity Graphs of Moment Components for 1st Specimen:

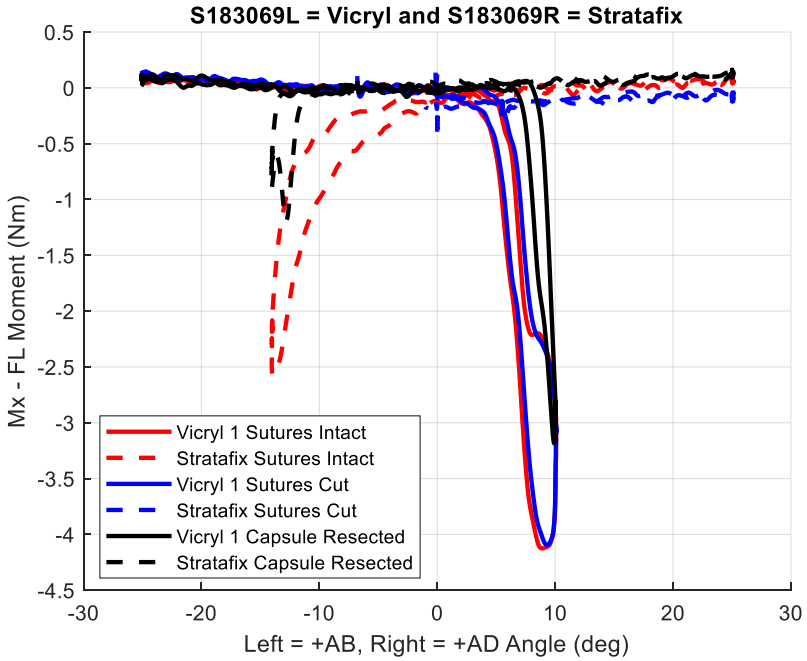

Figure A 22: One specimen example comparing the Vicryl and Stratafix plotting the flexion moment for the adduction and abduction laxity assessment

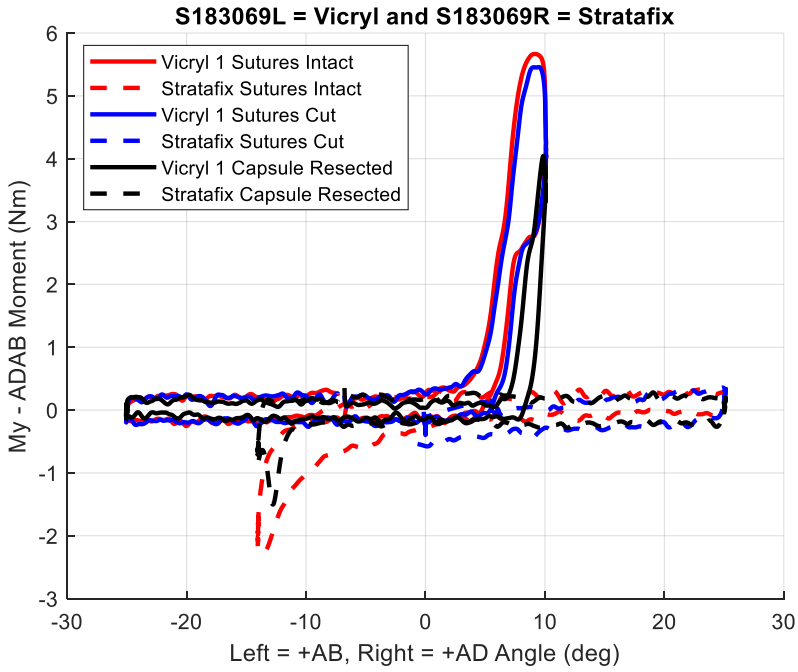

Figure A 23: One specimen example comparing the Vicryl and Stratafix plotting the adduction moment for the adduction and abduction laxity assessment

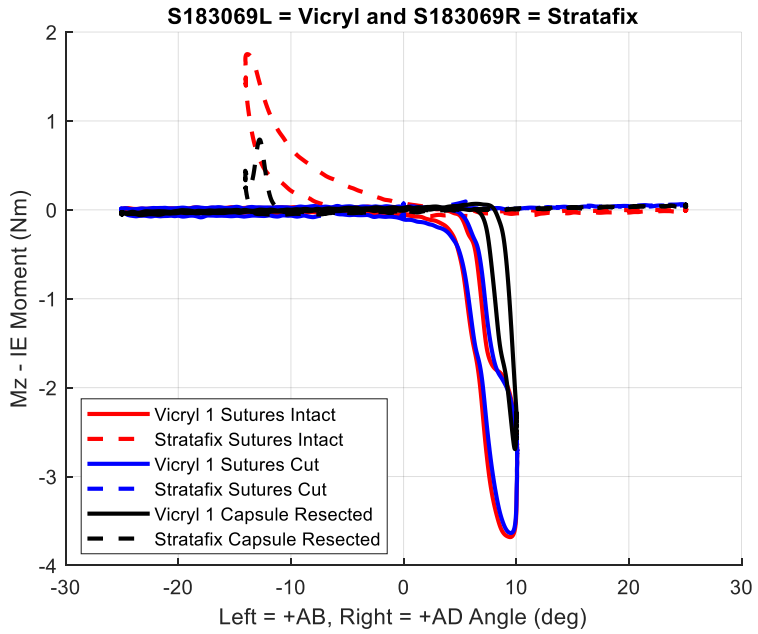

Figure A 24: One specimen example comparing the Vicryl and Stratafix plotting the internal rotation moment for the adduction and abduction laxity assessment

Internal and External Rotation Laxity Graphs of Moment Components for 1st Specimen:

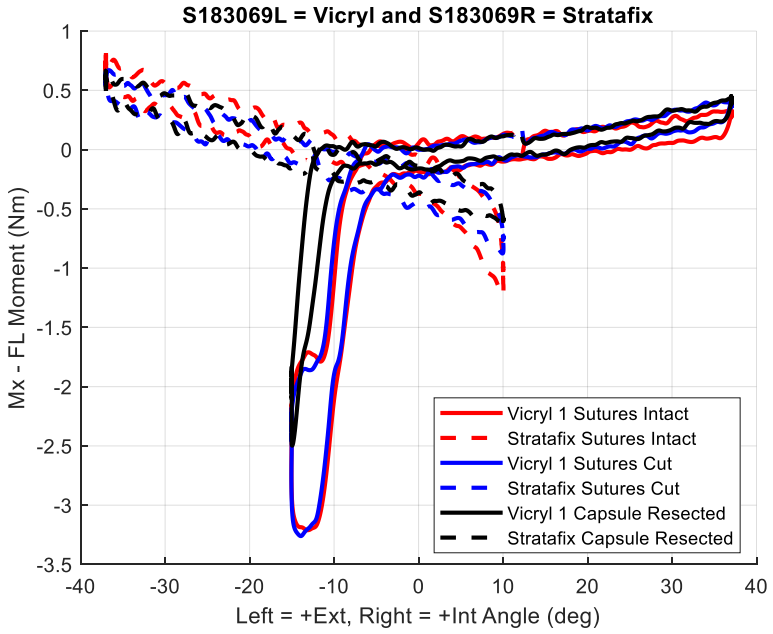

Figure A 25: One specimen example comparing the Vicryl and Stratafix plotting the flexion rotation moment for the internal and external laxity assessment

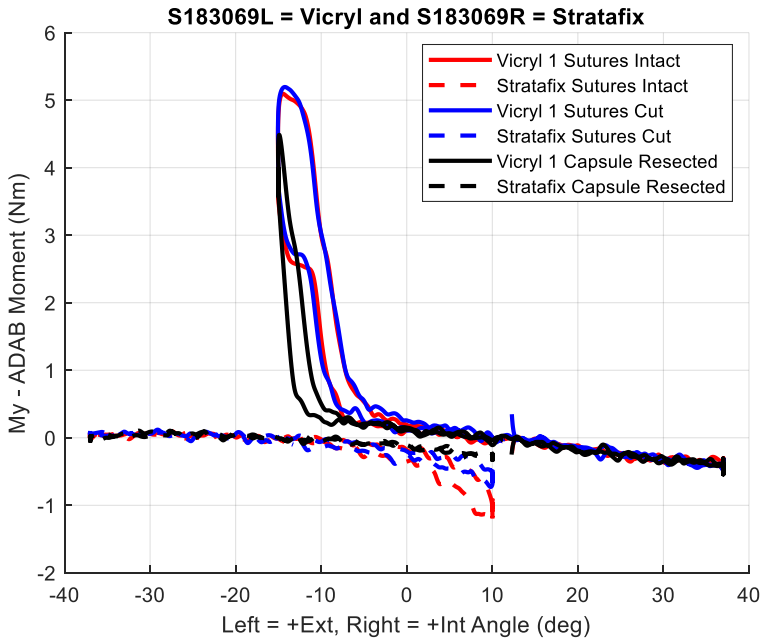

Figure A 26: One specimen example comparing the Vicryl and Stratafix plotting the adduction rotation moment for the internal and external laxity assessment

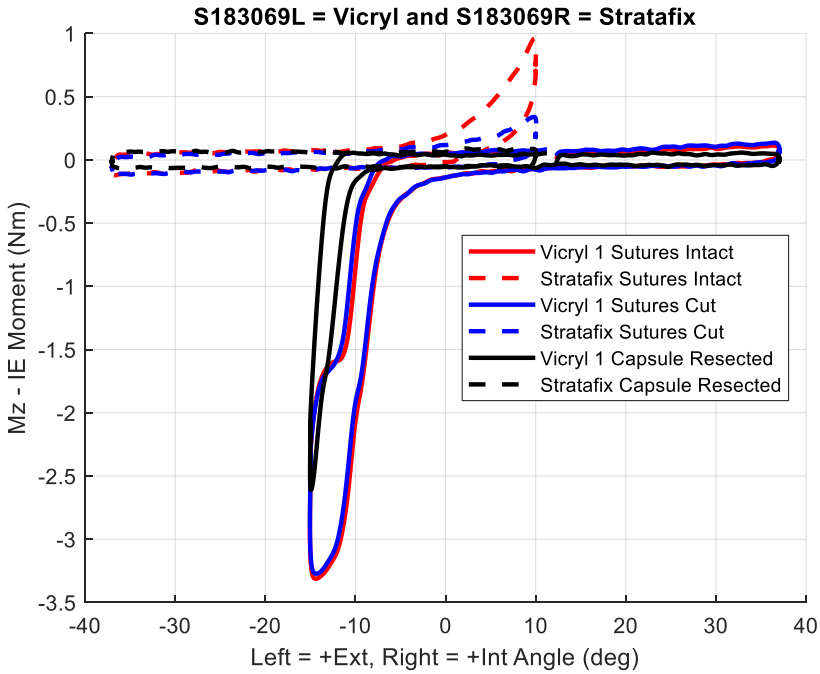

Figure A 27: One specimen example comparing the Vicryl and Stratafix plotting the internal rotation moment for the internal and external laxity assessment

Anterior Dislocation Simulation Graphs of Moment Components for 2nd Specimen:

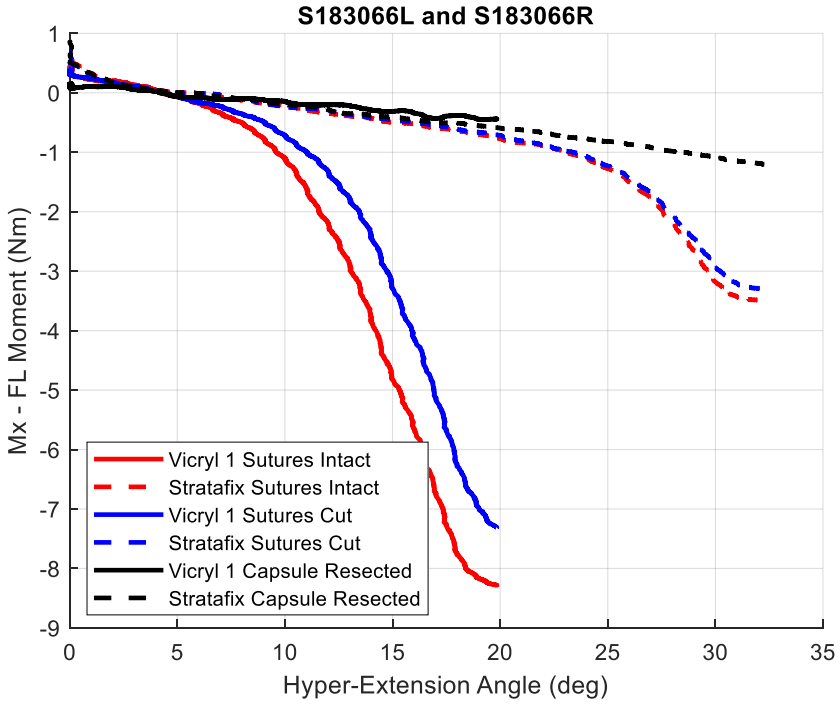

Figure A 28: A second specimen example comparing the Vicryl and Stratafix plotting the flexion moment for the Hyper-Extension and External Rotation movement

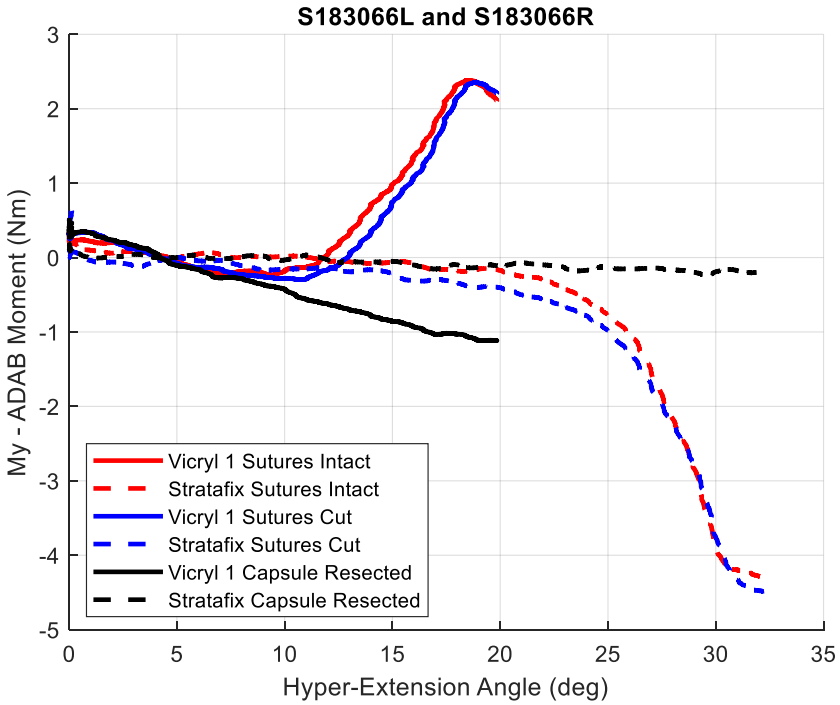

Figure A 29: A second specimen example comparing the Vicryl and Stratafix plotting the adduction rotation moment for the Hyper-Extension and External Rotation movement

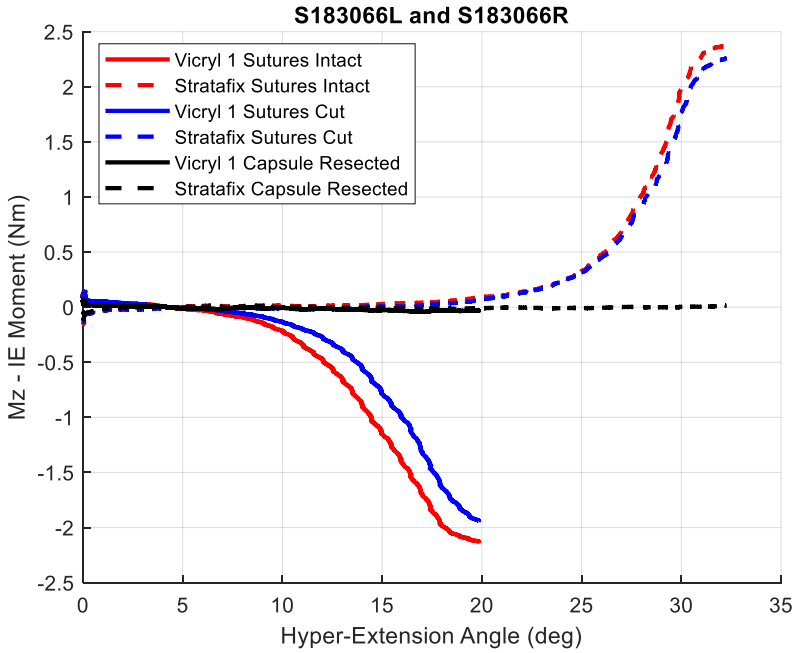

Figure A 30: A second specimen example comparing the Vicryl and Stratafix plotting the internal rotation moment for the Hyper-Extension and External Rotation movement

Adduction and Abduction Laxity Graphs of Moment Components for 2nd Specimen:

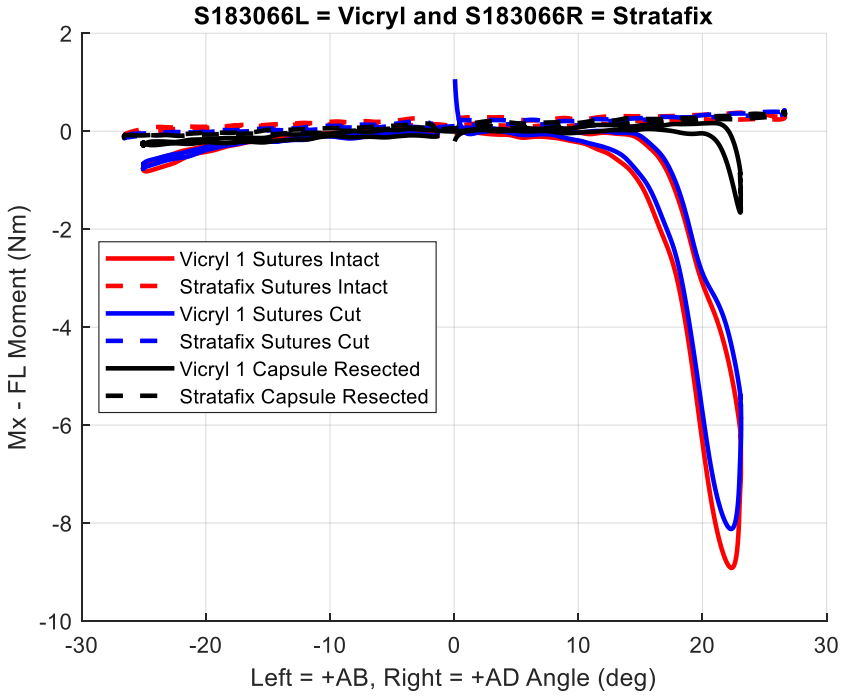

Figure A 31: One specimen example comparing the Vicryl and Stratafix plotting the flexion rotation moment for the adduction laxity assessment

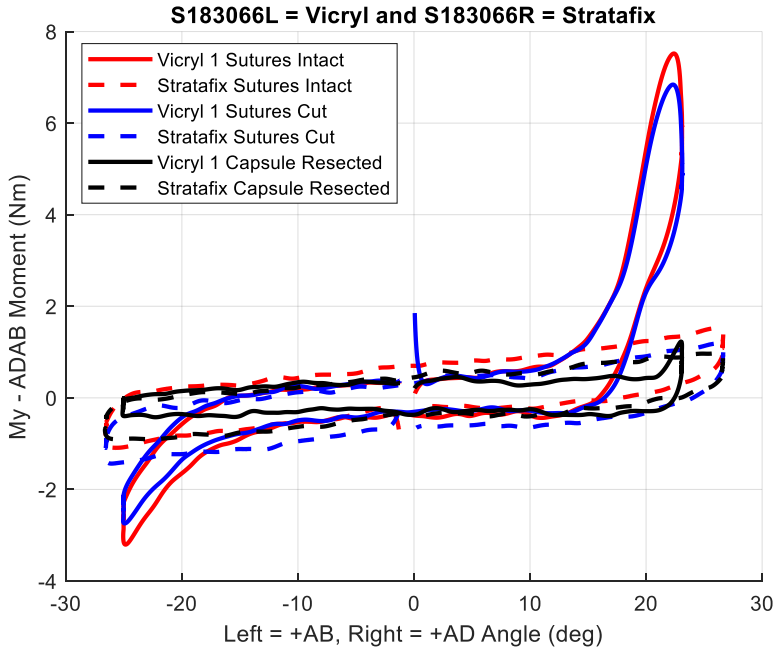

Figure A 32: One specimen example comparing the Vicryl and Stratafix plotting the adduction rotation moment for the adduction laxity assessment

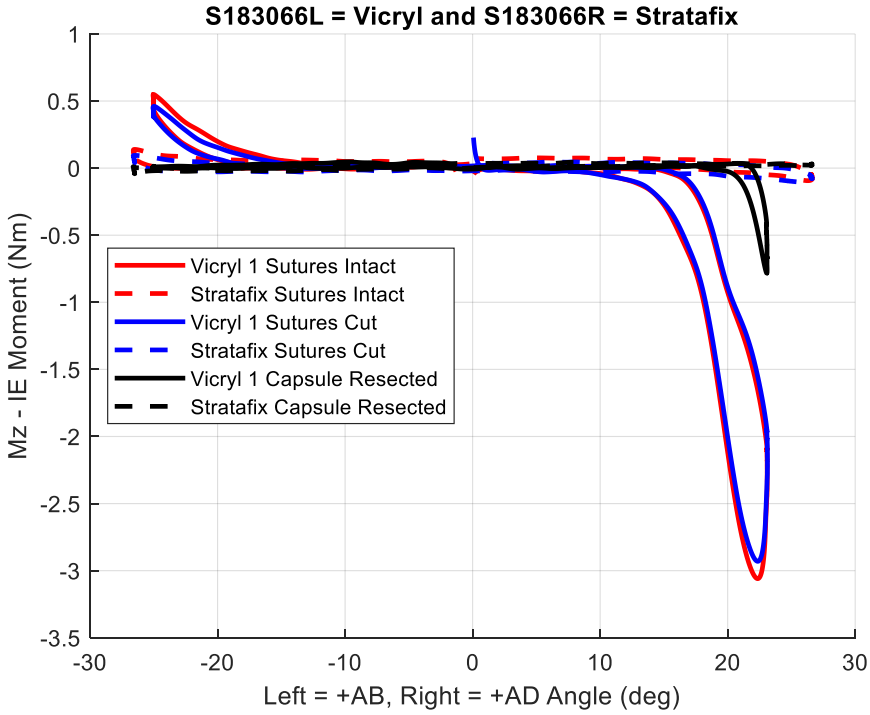

Figure A 33: One specimen example comparing the Vicryl and Stratafix plotting the internal rotation moment for the adduction laxity assessment

Internal and External Rotation Laxity Graphs of Moment Components for 2nd Specimen:

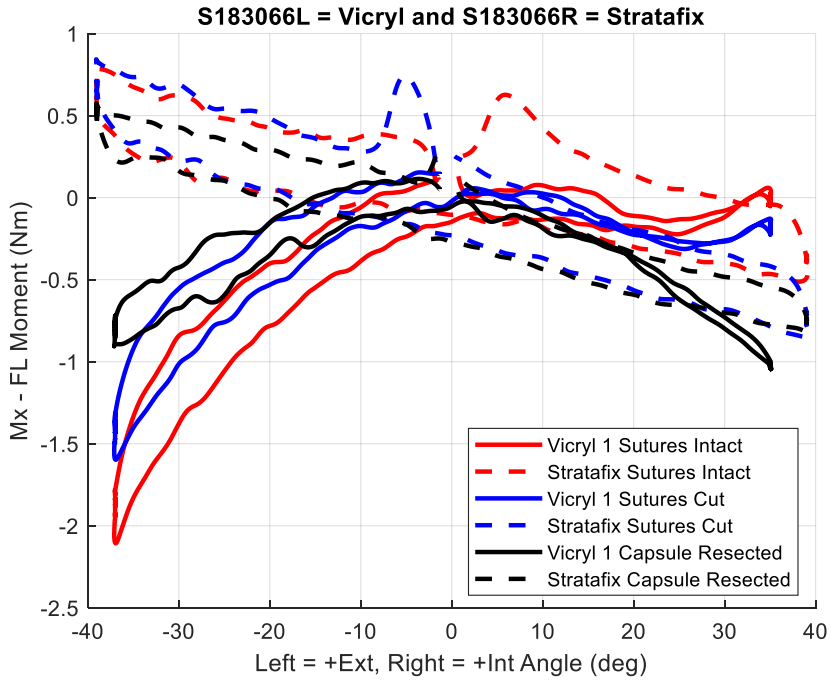

Figure A 34: Second specimen example comparing the Vicryl and Stratafix plotting the flexion rotation moment for the internal and external laxity assessment

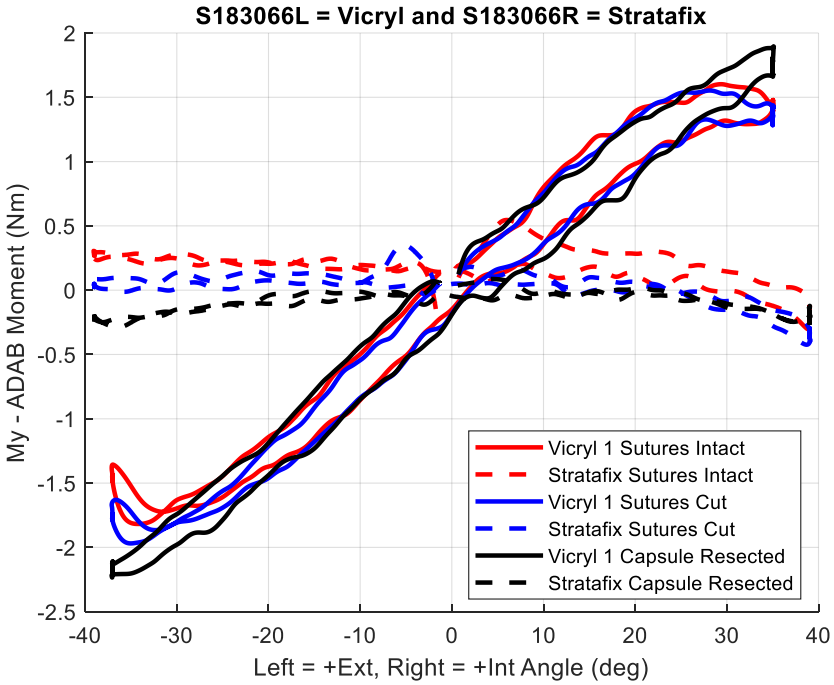

Figure A 35: Second specimen example comparing the Vicryl and Stratafix plotting the adduction rotation moment for the internal and external laxity assessment

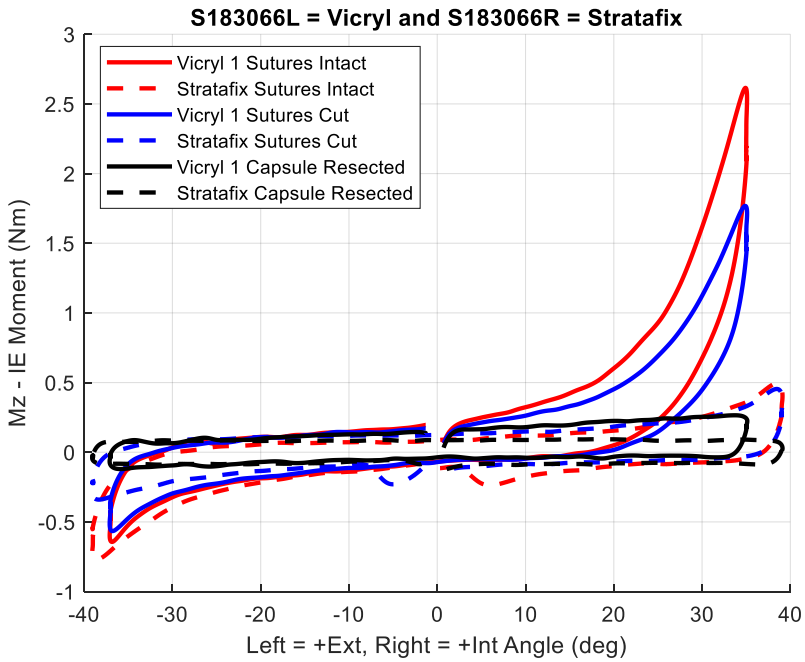

Figure A 36: Second specimen example comparing the Vicryl and Stratafix plotting the internal rotation moment for the internal and external laxity assessment

A.6: Additional Information Associated with Chapter Six

Specimen	Side	Approach	DM Liner	Stem Implant	Shell Implant	Poly Head	Femoral Head
C191002	Left	Anterior	58/49	Corail KA Sz 14	Pinnacle Gription 58mm	SERF 49/28	28 +1.5
	Right	Posterior	60/51	Summit Size 5 High Offest	Pinnacle Gription 60mm	SERF 51/28	28 +1.5
C191021	Left	Posterior	48/41	Summit Size 5 Std Offset	Pinnacle Gription 48mm	SERF 41/22.2	22.225 +4
	Right	Anterior	48/41	Corail KA Sz 10	Pinnacle Gription 48mm	SERF 41/22.2	22.225 +4
C191008	Left	Anterior	54/47	Corail KS Size 15 Std Offset	Pinnacle Gription 54mm	SERF 47/28	28 +8.5
	Right	Posterior	52/45	Corail KHO Size 14 High Offset	Pinnacle Gripion 52mm	SERF 45/22.2	22.225 +7
S192577	Left	Anterior	48/41	Corail KS size 10 Standard Offset	Pinnacle Gription 48mm	SERF 41/22.2	22.225 +4
	Right	Posterior	48/41	Corail KS size 10 Standard Offset	Pinnacle Gription 48mm	SERF 41/22.2	22.225 +4
L191570	Left	Posterior	54/47	Summit Size 2 High Offset	Pinnacle Gripiton 54mm	SERF 47/28	28 +8.5
	Right	Anterior	52/45	Corail KS Size 11 Standard Offset	Pinnacle Gription 52mm	SERF 45/22.2	22.225 +4
L191562	Left	Anterior	50/43	Corail KS Size 12 Standard Offset	Pinnacle Gription 50mm	SERF 43/22.2	22.225 +7
	Right	Posterior	50/43	Summit Size 5 High Offset	Pinnacle Gription 50mm	SERF 43/22.2	22.225 +4